공학박사학위논문

레이저 빔 및 전기화학 복합 가공을 이용한 텅스텐 표면의 마이크로 스트럭쳐링 기술

Tungsten Surface Micro Structuring Technology Using Laser Beam and Electrochemical Machining

2016년 8월

서울대학교 대학원

기계항공공학부

박 종 욱

A

Tungsten Surface Micro Structuring Technology

Using Laser Beam and Electrochemical Etching

Dissertation

SUBMITTED TO THE SCHOOL OF MECHINICAL AND

AEROSPACE ENTGINEERING AND THE COMMITTEE ON

GRADUATED STUDIES OF SEOUL NATIONAL UNIVERSITY

IN PARTIAL FULFILLMENT OF THE REQUIREMENTS FOR

THE DEGREE OF DOCTOR OF PHILOSOPHY

Jong Wuk Park

August 2016

B

Abstract

Jong Wuk Park

School of Mechanical and Aerospace Engineering

The Graduated School

Seoul National University

In this dissertation, surface structuring to implement various functions was carried out by using hybrid process composed to laser beam machining and electrochemical etching. The suggested method fabricated tungsten easily which had varied applications, and achieved high productivity with fast machining speed, improved surface quality and low cost process, and thus it resolved problems of previous researches to texture tungsten. As using laser beam machining in first step, various shapes of tungsten micro patterning were pre-textured in short time. Generated recast layer and burr were formed on the original core shape that was pre-determined by laser scanning path, and thus degree of precision was low. For this reason, electrochemical etching to improve surface quality was

carried out to dissolute recast layer into NaOH electrolyte, and thus pre-defined original micro pattern was revealed.

In this research, guide lines to texture tungsten surface for micro channel and pin were suggested by using new micro structuring method. As combining varied laser scanning path array, fabricated shapes of structures were analyzed, and the resulted tendencies with different laser parameter were studied. Moreover, the solutions to texture vertical micro channel with over 90 ° angles of slope and anisotropic angles were introduced by changing laser scanning direction and tilting procedure. The surface analysis of textured structure was achieved as control electrochemical etching time, and the etching conditions were chosen to eliminate recast layer efficiently. EDS analysis was also implemented finally, and thus the principle of the suggested micro hybrid structuring process was verified.

The textured tungsten micro channel was applied to lock each other mechanically, and directional locking force was also measured. The textured tungsten micro pin was used as micro needle for delivering drug, and thus various application areas using newly introduced hybrid structuring process were suggested.

Contents

List of Figures

control of textured surface

(a) 50 μm, (b) 100 μm and (c) 200 μm

tungsten micro needle

List of Tables

Chapter 1

Introduction

1.1 Research background

There are lots of micro scale textured surface for various functions such as thermal sink [1], wettability [2], mechanical locking [3] and penetration for drug delivery [4]. This functional surface for specific application suffers from relatively low material stiffness and poor mechanical strength, which generally is resulted from inherent material properties and structural weakness. The use of high strength metallic material can be considered as an alternative to improve these drawbacks.

Tungsten is a mechanically advantageous material due to its high strength and density. For this reason, it is used for cutting tool, tungsten carbide bite tip. Furthermore, it is used for weight balancing and vibration reducing [5]. Tungsten block is used to balancing of aerospace, automotive and even sport area such as fishing weight and golf club. Moreover, its high strength and density features can be applied to projectile of missile in military area [5].

The main issue of these areas using hard-to-cut material tungsten is a precision machining for reducing waste of material and useless overweight which is trade off problem. Tungsten has other advantages that attenuation properties make it ideal for radiation shielding such as X-rays and gamma radiation. These properties can be applied to medical area and nuclear industries. Additional property which is outstanding conductivity and relative chemical inertness can realize using it as an electrode. Last superior characteristic of tungsten is its high thermal resistance quality. Tungsten has the highest melting temperature among all metals. When product made of tungsten is exposed to high temperature, it has advantage for thermal cracking and heat corrosion phenomena [6]. The ITER (International thermonuclear experimental reactor) is a tokamak nuclear fusion reactor that is set up in the south of France [7]. An aim of the ITER is a suggestion to resolve energy problem without environmental problem. Plasma physics experiment for nuclear fusion phenomenon causes high temperature circumstance in ITER fusion reactor. This harsh condition with facing plasma causes thermal problem of each parts of fusion reactor. The divertor which is a parts of ITER, situated at the

bottom of the vacuum vessel, carries out extraction of heat and ash by-product from fusion reaction, minimizes contamination of plasma and protect a surrounding wall from heat and neutronic loads [8]. For this reason, the plasma facing components (PFC) of divertor is made of full tungsten. The main issues of full tungsten divertor are shape optimizing of tungsten PFC for improving resistance for thermal load and improvement for bonding between PFC and coolant tube.

In spite of versatility, however, tungsten is difficult to precision machine as its high stiffness. Proper machining method needs to texture with various structures for carrying out specific function on this hard-to cut material. MEMS technology based on the semiconductor process, which has been used in structuring micro structure, is not suitable any more due to the limitation of material property [9]. There are some surface structuring methods for dealing with tungsten high strength material. Electrical discharge machining (EDM) is known to non-traditional method for machining hard-to-cut material such as tungsten, titanium and stainless steel. It uses thermal energy which is generated by spark during potential discharging between tool and workpiece. A problem which is tool

3

wear, however, exists in EDM process [10]. Though resolving tool wear slightly, strip EDM that was studied recently have still same problem [11]. Moreover, micro scaled surface structuring and control of its various shapes are impossible as a limitation of size of strip tool. Electrochemical machining (ECM) is also a structuring method on tungsten surface. It has an advantage to fabricate without tool wear. When potential is added on between tool and workpiece, workpiece is eluted into electrolyte. ECM is atomic scale dissolution process that is used for surface treatment to achieving high surface quality [12]. Nevertheless, the machining time of ECM for various shape of structuring is relatively slow that causes a problem for productivity. As this time consuming limitation, ECM in micro scale is studied only in laboratory environment [13]. Laser beam machining (LBM) resolves these problems of previous method that are tool wear and productivity. In spite of high machining speed, it has some problem about surface quality. As LBM using thermal ablation energy, burr and recast layer which are made of aggregating dross are generated after machining. This by-product causes low surface quality for precision micro machining [14]. Though resolving recast layer and burr slightly as using pico and

femto second pulsed laser beam, cost problem of high quality machine can also be a limitation. Moreover, as the power intensity of LBM following Gaussian distribution, the shape of structure in vertical direction is not straight but tapered [15]. This limitation makes low quality for precision micro surface structuring. In case of tungsten cutting process, tool parts should be treated with additional surface coating for wear that causes cost consuming problem. Though improved tool wear by surface treatment, the burr generation after cutting is inevitable. Moreover, unnecessary heat is generated on machined region after cutting that causes property deformation of the basic tungsten [16]. Another surface structuring method focused on the beginning process of tungsten production. The sintering during metallurgy is a bonding process between material powders under high pressure and temperature conditions. The tungsten powders are formed as a mass product in shaped mold after sintering, which is treated with additional process such as cutting or polishing after sintering. The sintering process, however, is not suitable for various shapes of texture, as cost problem to manufacture varied shapes of mold, and the shrinkage during sintering can be an another problem for precision micro fabrication.

In addition, as implemented bonding phenomena under high pressure and temperature conditions, sintering process needs complex composited machining system, and thus it cannot promise efficient process [6, 17]. Table 1.1 shows the characteristics of various machining process to texture micro structure on tungsten surface [18].

Table 1.1 The characteristics of various machining process to texture micro structure on tungsten surface

	Characteristics	Limitation
EDM/Strip EDM	● Non-traditional / non-contact machining ● Thermal discharge energy ● Cratered surface	● Tool wear ● Improper to micro machine(strip EDM)
ECM	● Non-traditional / non-contact machining ● No tool wear	● Low machining speed (low productivity)

	• Atomic dissolution process • High surface quality	
LBM	• Non-traditional / non-contact machining • Thermal ablation process • High machining speed	• Low surface quality (recast layer, burr)
Cutting	• Traditional contact machining • High machining speed • Additional coating process on tool	• Tool wear • Cost consuming (coating) • Low surface quality (burr) • Property deformation (heat)
Sintering	• Traditional machining	• Low precision (shrinkage)

	• High productivity • Binding process under high temperature and pressure	• Cost consuming (Mold, temperature and pressure controller)

1.2 Research purpose

The purpose of this dissertation is to establish micro structuring and structuring process for various functions on tungsten surface. We propose new structuring technology to precisely control the shape of tungsten structure such as micro channel and micro pin array. For achieving this new functional structuring process, laser beam machining and electrochemical etching were carried out. First, rough shaping of micro structure via laser beam machining with predefined scanning path was implemented. The original shape of each structure was pre-determined by the designated laser scanning path in this step. Nevertheless, as using thermal energy for evaporating tungsten surface, recast layer and burr are generated on laser beam machined region. These by-products

8

cause low machining quality for precision machining as concealing the intended original shape of structure. Moreover, the machined region can be recrystallized due to thermal energy, and it makes mechanical strength of tungsten weaken [19, 20]. Second, electrochemical etching carried out to eliminate recast layer and burr after laser ablation. When electrochemical etching was carried out, the recast layer would be eluted into the electrolyte, and thus the original core structure could be revealed. As carrying out this hybrid machining, various structures with high surface quality were textured and controlled on tungsten surface. The principle of hybrid machining process was verified theoretically and experimentally as using specific analyzing method such as energy−dispersive spectroscopy (EDS). The textured and shape controlled surfaces using suggested new fabrication process were used for locking and medical needle applications. For verifying its performance, experimental test and discussion were also carried out.

In this dissertation, a novel method to texture tungsten materials is demonstrated at the micro sized scale. This new process has various advantages and improves the disadvantages of previous structuring method. The problems of previous structuring methods

due to the limitation of material were resolve by using high strength tungsten as workpiece. This hybrid machining, which achieves high machining speed as using laser beam machining and improves surface quality due to electrochemical etching, and thus it resolves complementary problem between two processes. Moreover, suggested structuring method, as a non-contact process, does not have tool wear problem of EDM and cutting process. If varied structures for specific function are required, the wanted shapes can be textured easily as changing laser scanning path in short time. This convenience is remarkable in comparison to previous sintering process that needs a specific shaped mold, and thus cost reduction and high throughput can be achieved. Moreover, the shrinkage problem of tungsten product by using sintering can be resolved as not using powder but bulk material.

1.3 Dissertation overview

In chapter 1, the main issues for dealing with previous method for structuring on tungsten were introduced. The new technology that was suggested in this study was compared with previous method. In

this chapter, the originality of the new micro hybrid machining method was introduced.

In chapter 2, principle of hybrid machining process for functional surface structuring was explained. The each basic principle of laser beam machining and electrochemical etching is present. Tungsten was chosen for workpiece material. As carrying out micro hybrid machining on tungsten surface, the principle of newly suggested machining process with tungsten workpiece was verified.

In chapter 3, the experimental set up was introduced. To carry out precision surface structuring, micro 3−axial linear stages with 0.1 μm resolution was set up. Laser beam machine was set on Z axial stages. The tungsten workpiece moved to intended position with X, Y stages. Electrochemical etching was carried out with pulsed potential system.

In chapter 4, fabrication of textured surface with various shapes is presented. Micro sized vertical channel, anisotropic channel and various shapes of micro pin were fabricated. In this chapter, the surface structuring sequences for specific structures were suggested by various laser scanning path. As changing the arrangement of laser scanning line, the machining tendencies of

textured structure were considered by comparing with SEM images and laser intensity distribution. As a second step, shape control of pre−textured surface was carried out by using electrochemical etching, and its parameter studies according to etching conditions were implemented. Energy−dispersive spectroscopy (EDS) analysis was carried out to verify distribution in textured structure between tungsten original core and oxide recast layer.

In chapter 5, mechanical application of micro textured surface for directional locking was introduced. Micro textured anisotropic channels were used for locking mechanism. In this chapter, to verify performance of textured structure, generated locking force was measured. Moreover, medical application of micro surface structuring for micro needle was introduced. Fabricated micro conical pin array was applied to needle application. This experiment was implemented with gelatin skin dummy and thick skin of poke. Penetration force was measured with load cell system and high speed video camera. Finally, the textured surface for various functions was verified as carrying out locking and needle functional measuring test.

In chapter 6, Conclusion of this dissertation are presented.

Chapter 2

Principle of tungsten surface structuring

2.1 Laser beam machining

In this research, laser beam machining with nano second pulsed was carried out for functional structuring on tungsten surface. Nano second pulsed laser beam machining is a non-contact machining process that has high speed material removal rate comparing with other precision machining process. These days pico and femto second pulsed laser beam are used for fabricating micro structure. However, it has disadvantages such as complex optical alignment, low productivity as low machining speed and high cost problem for maintenance of system [18]. For this reason, as using nano second pulsed laser beam machining in this study, the problems about cost of previous researches were resolved.

Tungsten is a hard-to-cut material and has high thermal melting

point with 3370 ˚ C. Moreover, as high thermal conductivity characteristic of tungsten with 163.3 W/m−K, absorbed energy during laser beam machining is rapidly transferred [5]. As this reason, relatively high thermal energy comparing with other metal material during laser beam machining is needed.

In general laser beam machining process, dross of origin material is generated on machined area due to thermal melting process. This generated dross forms to recast layer and burr. This by−product should be eliminated for precision machining quality of workpiece. However, in previous research, micro pin array was fabricated by pilling recast layer. S. W. Lee used 304 stainless steel as a material that relatively generated lots of recast layer during laser beam machining [14]. In this previous research, micro pin array that was made of chromium oxide recast layer was fabricated for interlocking on vertical wall. However, the sample of stainless steel has weak mechanical strength for interlocking due to combination with pilling of oxidation recast layer. In this study, however, tungsten was used as a material for functional surface structuring. It generates relatively little recast layer that covered original inner shape slightly. Tungsten that has characteristic about generating little

recast layer is a proper material for locking or other various applications such as needle and hit transfer due to having sufficient mechanical and thermal property comparing with stainless steel [14]. Figure 2.1 shows the difference between previous stainless steel and tungsten micro machining which was used in this research. As repeating laser scan with intended scanning path, in case of stainless steel, recast layer was piled on original core shape. For this reason, height of the generated stainless steel structure was higher than original workpiece. In case of tungsten that was used this study, however, as carrying out laser beam machining, it was removed from top of the workpiece to end of laser beam. Generated dross was almost evaporated into air that relatively thin recast layer comparing with stainless steel covered on inner original shape. Figure 2.2 shows textured micro pin structure after laser beam machining. As shown in this Figure 2.2 (a), in case of tungsten, its tip radius was sharper than stainless still as a characteristic about thin recast layer. Moreover, surface roughness of tungsten structure is rough than stainless steel, because material removal rate is faster than pilling rate of recast layer. In case of stainless steel in Figure 2.2 (b), it has relatively round tip [14]. The height

of fabricated pin is higher than workpiece as pilling of recast layer.
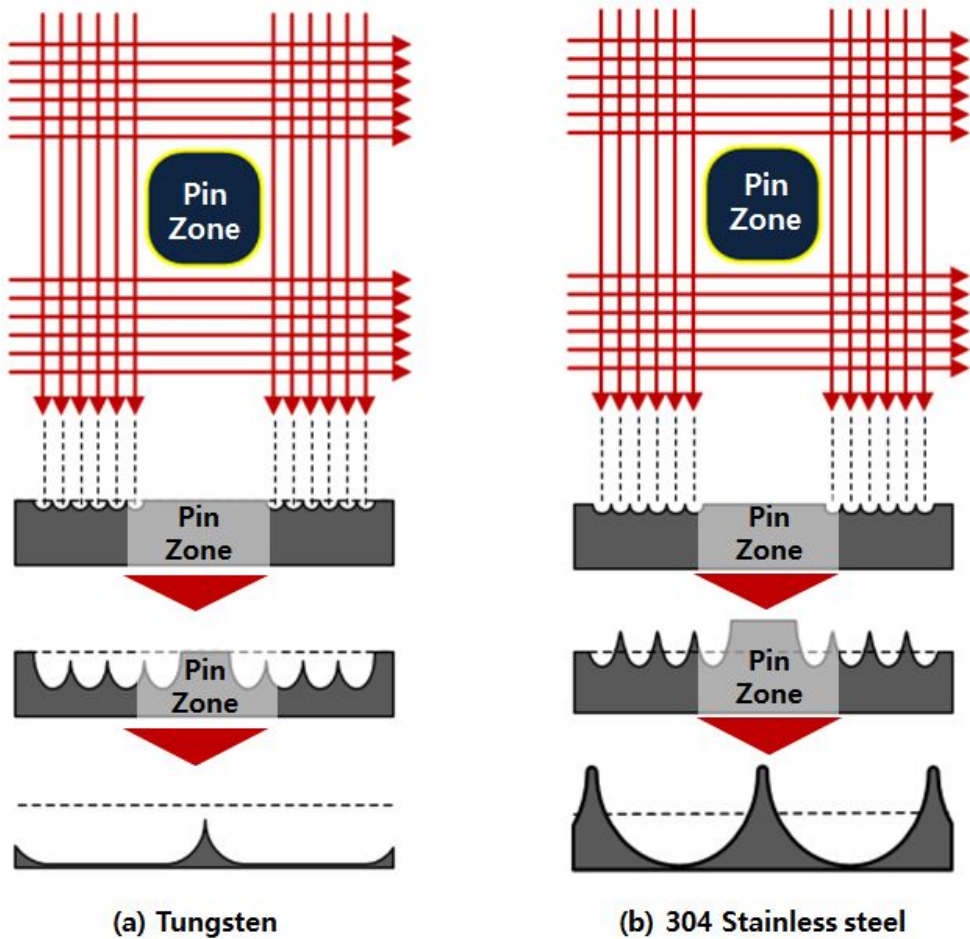
Figure 2.1 Principle of laser beam machining for surface structuring

on (a) tungsten and (b) 304 stainless steel
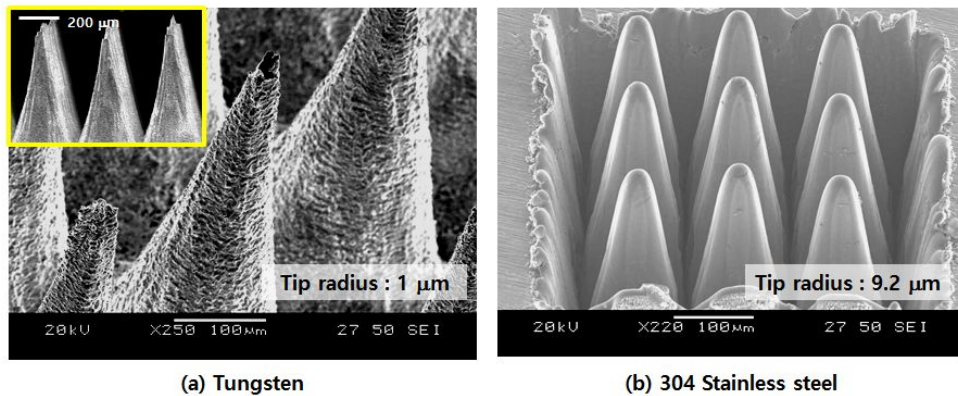
Figure 2.2 SEM images of textured structure that were fabricated by using laser beam machining (a) Tungsten and (b) 304 stainless steel [14]

There are some previous researches about fabrication tungsten with laser beam machining. As using nanosecond pulsed−ND:YAG lase, Y. Kawakami fabricated micro conical structure. This process could fabricated unintended structure about under 100 μm scaled [21]. T. Sano also fabricated microspike−arrays on tungsten surface using femtosecond laser [22]. Although the shape of structure could not be precision fabricated, these studies showed possibility about fabricating on tungsten surface using laser beam machining. Figure 2.3 shows fabricated tungsten structure of previous studies by using laser beam machining. Figure 2.3 (a)

shows micro conical structure [21] and (b) shows microspike－array [22].

In this dissertation, precision micro structure for functional surface was textured on tungsten by using laser beam machining. As changing laser scanning path, textured structure was formed with predefined shape that was covered with generated recast layer. This generated recast layer and burr was an obstacle for precision machining. It should be eliminated for machining quality and functional structuring.

(a) Micro conical structure   (b) Microspike-array
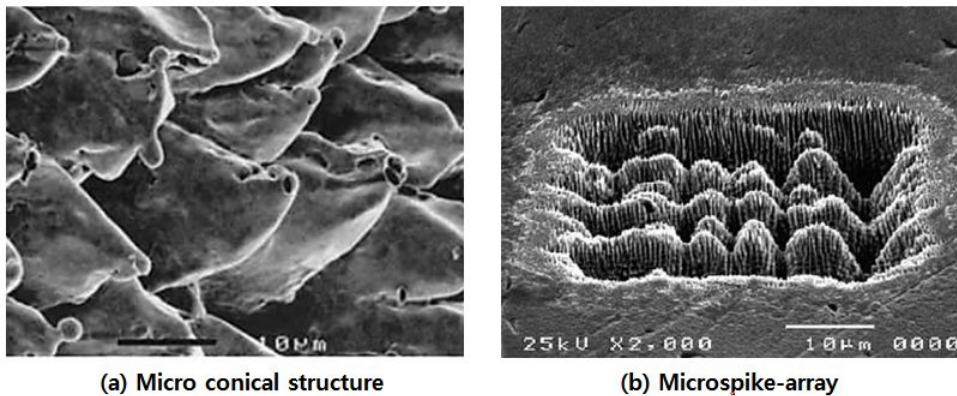
Figure 2.3 Fabricated tungsten structures of previous studies by using laser beam machining (a) micro conical structure [21], (b) microspike－array [22]

Laser ablation is a thermal diffusion process during machining. The

ablation is braking process of coupling between electron and lattice. Figure 2.4 shows the principle of laser ablation and two-temperature diffusion model. This new thermal explained model distinguishing between lattice grid and electron system of metal material becomes necessary to comprehend thermal diffusion phenomenon. As shown in this figure 2.4, the absorption of thermal energy is followed by a fast thermal energy relaxation within the sub-electron system, thermal diffusion, and a heat energy transfer to the lattice due to the electron and lattice coupling. The lattice thermal conductivity can be neglected, because heat diffuses much faster through the sub-electron system. Finally, transferred thermal energy braking the coupling between electron and lattice, and thus the material can be ablated by laser beam.
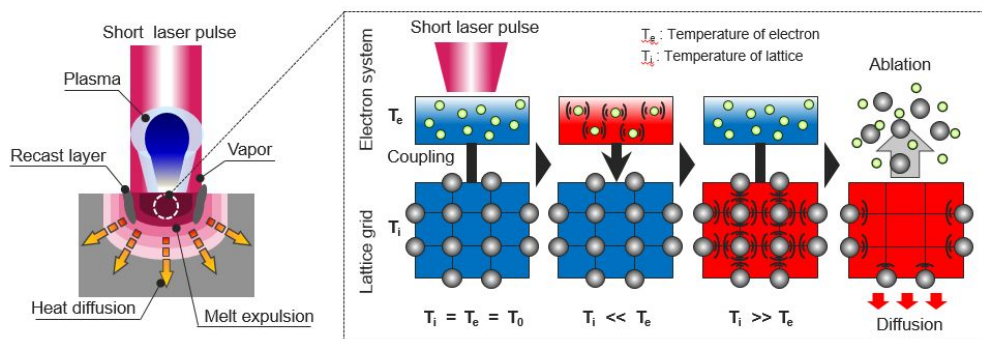
Figure 2.4 Principle of laser ablation and two-temperature diffusion model

$$C_e \frac{\partial T_e}{\partial t} = -\frac{\partial Q(z)}{\partial z} - \gamma(T_e - T_i) + S \qquad (2.1)$$

$$C_i \frac{\partial T_i}{\partial t} = \gamma(T_e - T_i) \qquad (2.2)$$

$$Q(z) = -k_e \frac{\partial T_e}{\partial z} \qquad S = I(t)A\alpha e^{-\alpha z} \qquad (2.3)$$

As following this phenomenon, the spatial and the temporal reaction of the lattice and sub−electron system temperature (T_e and T_i) can be explained by two−temperature diffusion model in one directional dimension. In these formulas, z is the direction perpendicular to the surface of ablated material. Q(z) is heat flux and S is the laser thermal energy source term, I(t) is the laser power intensity, A and α are the surface absorptivity and material absorption coefficient. C_e and C_i are the heat capacities of the electron system and lattice sub system, r is the parameter that is characterized about coupling between lattice and electron sub system. And k_e is the thermal conductivity of electron. All these terms follows the principle of the conservation of energy.

2.2 Electrochemical etching

Electrochemical etching is a chemical melting process for fabricating metal workpiece. This machining process can fabricate all electrical conductor and relatively wide area of workpiece into submerged electrolyte. Electrochemical etching can be carried out in room temperature condition that thermal deflection and stress can be prevented. Moreover, there are some subsidiary advantages such as the tool non-wears in spite of hardness of the material because electrochemical etching is a non-contact surface manufacturing method. Moreover, it has other advantages such as increase of corrosion resistance, surface gross and removing residual stress on the surface [23]. Figure 2.5, shows the principle of electrochemical etching. Workpiece is connected to anode and electrode should be connected to cathode. If electrical potential or current is added on, electrochemical reaction would occur. This electrochemical reaction is atomic scaled dissolution phenomenon, and thus workpiece is eluted into electrolyte.
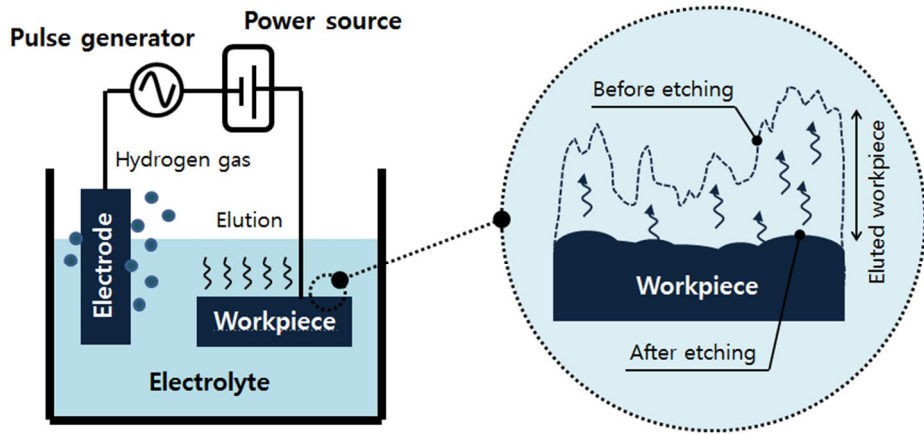
(a) Principle of electrochemical etching   **(b) Enlarged view**

Figure 2.5 (a) Principle of electrochemical etching, (b) enlarged view

on the machined workpiece

Electrochemical etching, however, fabricates all area of workpiece which is immersed into electrolyte. In addition, acute point or sharp edge is reacted preferentially during etching that causes shape error of textured structure. For this reason, in this study, ultra short pulsed power was added on during electrochemical etching. In general etching process, electrochemical reaction arises on entire workpiece into electrolyte that it is not proper for micro area machining. For this reason, Schuster used ultra short pulse for micro etching [24]. When short pulsed potential is added,

electrochemical machining area can be localized on near the electrode [25]. For explaining this reaction, electrical double layer theory can be used.

In case of electrochemical machining system, when a metal electrode is submerged into electrolyte, difference of electrical property can be generated on interface between metal electrode and electrolyte. This interfacial region is called to electrical double layer [26-28].

Some researcher proposed proper solution models for explaining this complicated double layer region. Figure 2.6 shows the model for electrical double layer that was suggested by Bockris-Devanathan-Müller [28]. In this model, various anions have a tendency about contact with electrode surface. The plane which is composed of center line of absorbed anion is called inner Helmholtz plane (IHP). Moreover, fully solvated ion can be connected on metal electrode with some distance that is almost twice of water molecule diameter. The plane which is composed of center line of fully solvated ion is called outer Helmholtz plane (OHP). As crossed this layer, electrical potential property has difference [28].

23
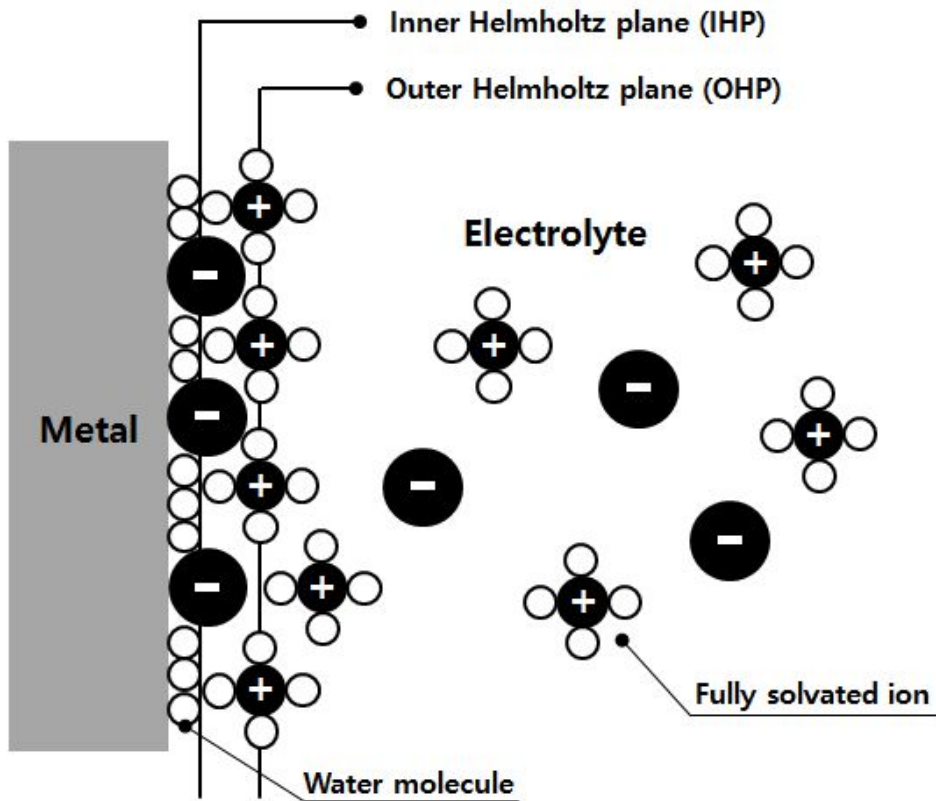
Figure 2.6 Bockris-Devanathan Müller electrical double layer model

[28]

Because this double layer in the transient range has similar properties of electrical capacitor, electrical model of the machined area can be explained as approximation with parallel circuit that is composed to capacitor and resistance. Figure 2.7 shows this concept for explanation double layer model for localizing [29].
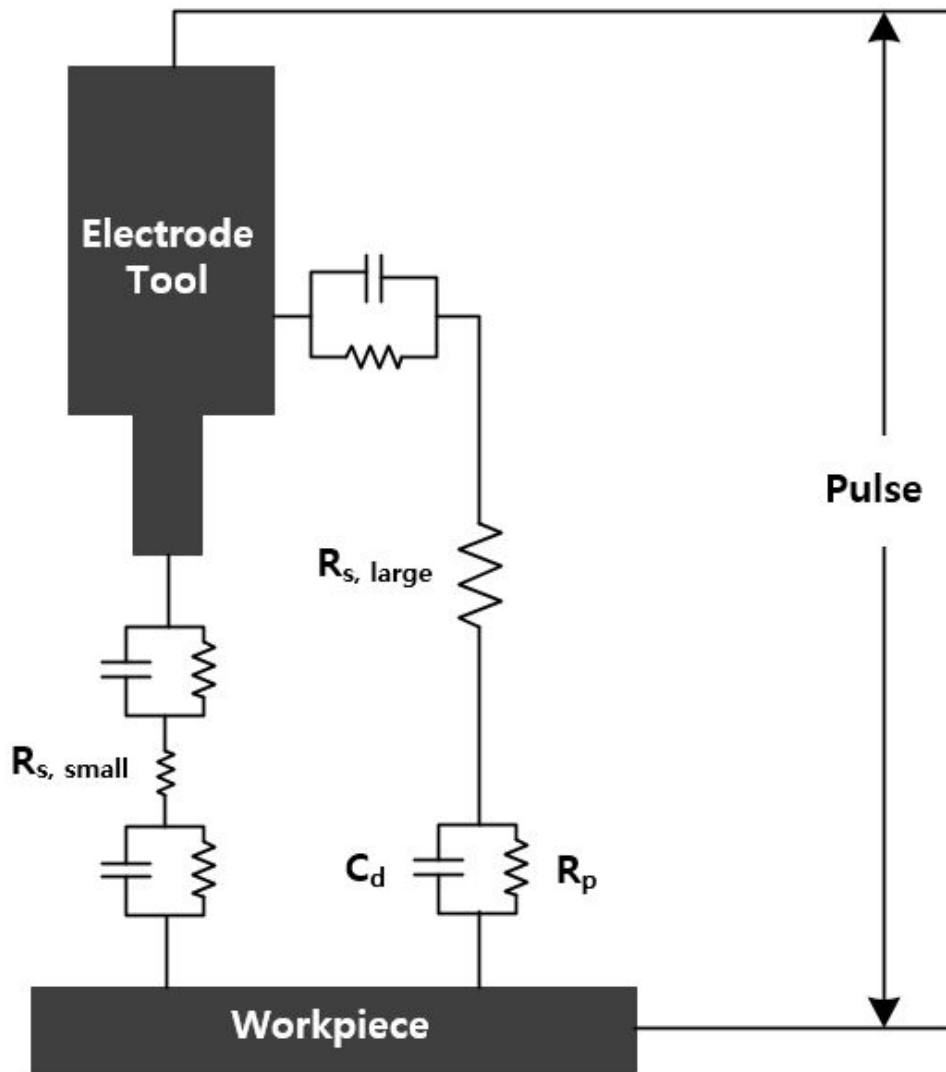
Figure 2.7 Double layer electrical model around electrode and

workpiece

Capacitance of double layer per unit area is C_d. R_p is polarization

resistance and R_s is solution resistance. The resistance of solution

(R_s) increases proportionally as the distance between electrode and

workpiece. When ultra short pulse is added on reaction region, the

area of workpiece far from electrode has large $R_{s,large}$ that this area

has large $\tau = RC_d$ value. $\tau = RC_d$ value means the charging time

constant in the double layer model. On the other hand, the area of

workpiece near from electrode has relatively small $R_{s,small}$ that this

area has small $\tau = RC_d$ value. As mentioned before, the charging time

values of τ are defined as distance from electrode to workpiece. In

case of small distance, the charging time for reaction is smaller than

the case of large distance. τ_S is the time constant value of near

distance from electrode and τ_L is the value of far distance case.

$$\tau_S = R_{s,small} \times C_d \qquad\qquad (2.1)$$

$$\tau_L = R_{s,large} \times C_d \qquad (2.2)$$

If pulse width (on time) value T is smaller than τ value, polarization

and electrolysis could not arise because of short time for the charging. As shown in Figure 2.8, if pulse width value between τ_S and τ_L ($\tau_S < T < \tau_L$) is added on electric cell, the charged potential of short distance region between electrode and workpiece could be enough to electrochemical react. On the other hand, in case of long distance, the charged potential is insufficient to reach reactive potential level due to short charging time. For this reason, as using pulsed potential system, localized micro chemical etching can be carried out on intended region with micro meter scaled gap [28].
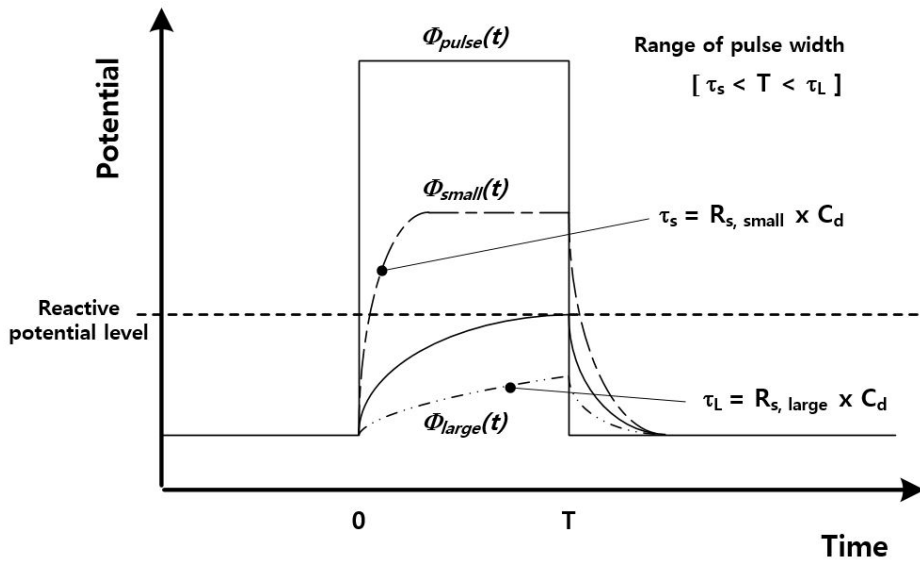
Figure 2.8 Graph about difference in charged potential [$T_S < T < T_L$]

There are some previous researches that use electrochemical etching for tungsten electrode. Z. W. Fan fabricated cylindrical tungsten microelectrode with NaOH solution [30]. Y. M. Lim also fabricated cylindrical micro pin that was made from tungsten rod [31], however, these previous research were implemented to fabricated only conical electrode structure. In this dissertation, as using electrochemical etching, various shapes of surface structuring were carried out around tungsten plate workpiece. It is not used tungsten rod but plate to fabricate functional micro array that has difference with previous studies. In electrochemical etching process, a metal workpiece is eluted into electrolyte when electrical potential is added on electrical cell. In case of tungsten (W), generally NaOH electrolyte that is relatively less hazardous than other chemical solution was chosen for electrochemical etching. As pulsed potential was applied, electrochemical reactions with tungsten workpiece and NaOH electrolyte could be explained as following formulas.

$$W + 6OH^- \rightarrow WO_3 + 3H_2O + 6e \quad (2.3)$$

$$WO_3 + 2NaOH \rightarrow Na_2WO_4 + H_2O \quad (2.4)$$

$$W + 2NaOH + 6OH^- \rightarrow Na_2WO_4 + 4H_2O + 6e \quad (2.5)$$
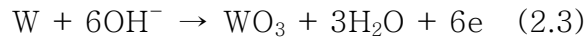
Anode (Tungsten workpiece)

$$6Na^+ + 6H_2O + 6e \rightarrow 6NaOH + 3H_2 \quad (2.6)$$
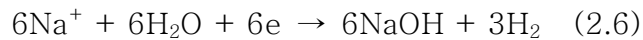
Cathode (Platinum electrode)

$$W + 2NaOH + 2H_2O \rightarrow Na_2WO_4 + 3H_2 \quad (2.7)$$
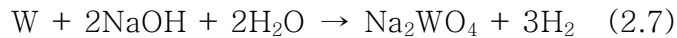
Total reaction equation

In this electrochemical reactions, the formulas (2.3~2.5) explain
the phenomena on tungsten workpiece which is connected to anode.
As shown in formulas (2.3) and (2.4), tungsten workpiece is eluted
into electrolyte. Formula (2.5) shows combined chemical reaction of
(2.3) and (2.4). In this reaction, for dissolving 1 mol of tungsten, 6
mols of hydroxide ions should be need. Formula (2.6) shows the

electrochemical reaction on cathode with platinum electrode. In this cathode region, hydrogen gas is generated as electron gathering. Formula (2.7) shows total electrochemical reaction between tungsten and NaOH electrolyte during etching.

2.3 Hybrid process for surface structuring

Nano second pulsed laser beam machining that was used in this dissertation has some characteristics such as high machining speed and low precision machining quality due to wide heat affected zone and recast layer. Generated recast layer and burr has rough surface and micro crack which cause low durability of functional textured surface. For this reason, some post machining method for improving degree of shape precision and surface quality of product as removing recast layer, burr and heat affected zone were studied, for example thermal process [32], under water process [33] and laser cleaning method [34]. Electrochemical etching process with pulse system that could remove selectively bump area such as heat affected zone and recast layer from laser beam machining is useful

relatively compared with other machining process for fabricating precision micro structure.

In this study, newly suggested micro hybrid machining process combined with laser beam machining and electrochemical etching is a complementary fabrication process that has high machining speed as using laser beam machining and can improve low surface machining quality from nanosecond laser beam machining as carrying out electrochemical etching. Figure 2.9 shows this principle of micro hybrid machining process. In other words, as shown in figure 2.9 (a), pre-structuring process was carried out quickly as using nano second pulsed laser beam machining. After this process, electrochemical etching (figure 2.9 (b)) was carried out for removing generated recast layer and burr on pre-textured surface by laser beam machining. In this process, pre-determined inner original textured shape that was scanned on purpose during laser beam machining process could be revealed finally as removing outer recast layer and burr.

This newly suggested hybrid machining process has many advantages. It is a non-contact machining process that never has wear of tool which is disadvantage of all cutting and EDM process.

31

In this respect, cutting tool cost problem can be resolved. Moreover, previous machining process such as rolling, cutting, die-sinking EDM and sintering have disadvantage for fabricating various shaped structures, because proper machining tools or molds for structuring various shapes with different angle and aspect ratio should be prepared. In case of MEMS process, for achieving various shaped structures, proper masking process should be need [9]. On the other hand, novel suggested hybrid process would not need masking process for achieving various shaped structures because the original core shape of textured structure can be controlled easily as changing pre-determined laser scanning path on purpose. It is efficient process as saving mask making cost and reducing machining time due to non-masking process. Table 2.1 shows the advantages of newly suggested hybrid micro machining process.

(a) After laser machining　　(b) After electrochemical etching
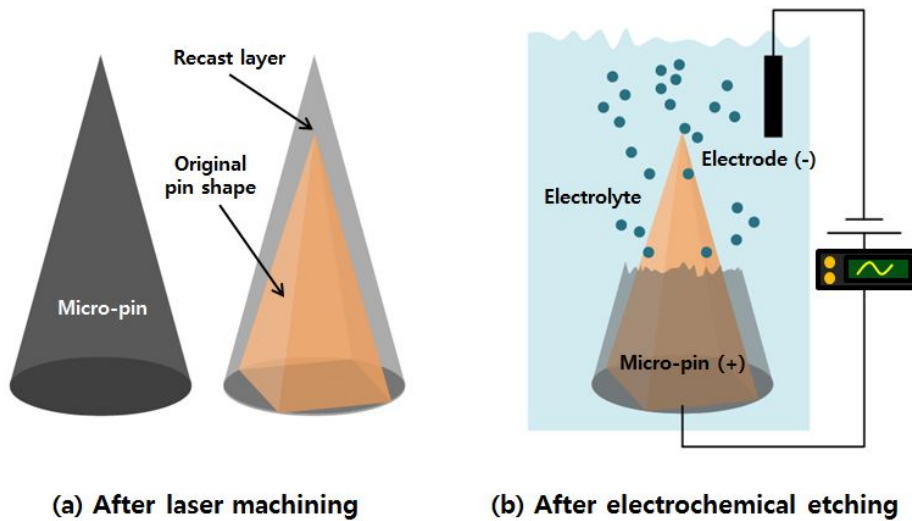
Figure 2.9 The principle of hybrid micro machining process for

control of textured surface

Table 2.1 The characteristics and advantages of newly suggested

hybrid micro machining

	Characteristic and advantage
Hybrid micro machining (LBM + ECE)	● Non-contact machining (No tool wear) ● Low cost problem ● High machining speed ● Easy shape control of textured structure (No masking, molding) ● High surface quality (No recast layer, burr, heat- affected zone)

Chapter 3

Experimental set up

3.1 Laser beam machining system

There are many lasers that can be divided by kind of active medium, power density and its wavelength. Solid state laser is generally used for machining metal efficiently. Also, fiber laser that has optical glass fiber with ytterbium (Yb) can generate efficient power than solid state laser due to the improved cooling property [35].

In this study, the ytterbium pulsed fiber laser (YLP-C series, IPG photonics) with 1064 nm wavelength and galvanometer scanning system was used. The galvanometer scanning system (SCANcube 10, SCANLAB AG) was set on Z axis stage. The linear stepping motor (ZETA 57-83 stepping motor) of Z axis stage has 0.1 μm/count resolution. It was controlled by using optical limit/home switching sensor. All the machining area using laser beam system was focused by using this Z axial stage. X, Y axial stages were used for moving workpiece on laser focal spot. The peak power range of this pulsed fiber laser could be selected from 2 W to 20 W. The

range of pulse repetition rate was from 20 kHz to 80 kHz. The scan speed of the galvanometer could be controlled from 58.6 mm/s to 458.6 mm/s. Moreover, the calculated spot size of the laser beam was about 40 μm diameter [20]. Table 3.1 shows various specifications of the fiber laser beam machine that was used in this dissertation. In all experimental process, micro structuring on tungsten metal surface using hybrid machining was implemented in air condition. Figure 3.1 shows the laser beam machining system that was used in this study. Moreover, Table 3.2 shows the specification of positioning system.
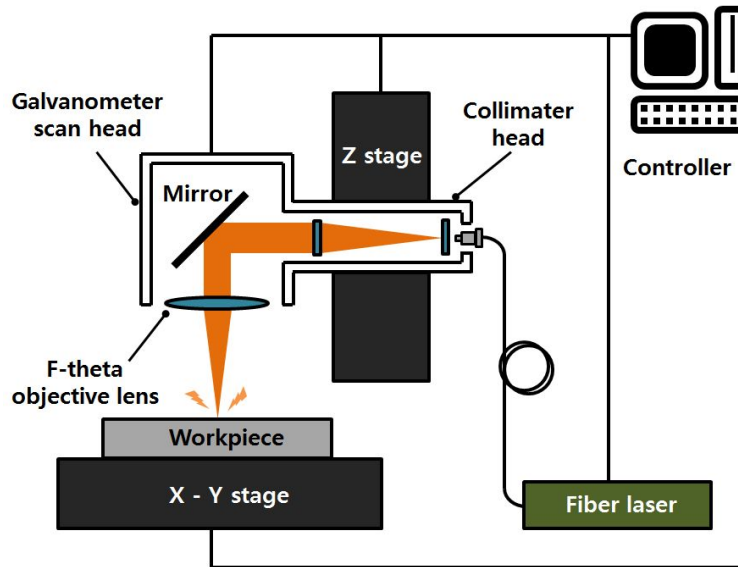
Figure 3.1 Experimental set up for pre−surface structuring on tungsten using laser beam machining

Table 3.1 Specification of pulsed fiber laser

Characteristics	Minimum	Typical	Maximum	Unit
Mode of operation	Pulsed mode			
Maximum pulse energy		1		mk
Nominal average output power	19	20	21	W
Output power adjustment range	10		100	%
Nominal pulse repetition rate		20		kHz
Pulse duration	80	100	120	ns
Central emission wave length	1055	1064	1075	nm
Pulse repetition rate	2		80	kHz
Beam quality, M^2		1.5	2.0	
Output beam diameter	6		9	Mm

Table 3.2 Specification of positioning stage system

	X, Y axial stage	Z axial stage
Motor	ZETA 57-83 stepping motor	ZETA 57-83 stepping motor
Travel	150mm respectively	150 mm
Resolution	0.1 μm/count	0.1 μm/count
Positional repeatability	3 μm	3 μm
Limit, home switch	Optical sensor type	Optical sensor type

3.2 Electrochemical etching system

After controlling of textured structure using laser beam machining with predefined scanning path, electrochemical etching was carried out for precision surface structuring. Figure 3.2 illustrates the Experimental set up for electrochemical etching. The electrochemical etching system consists of the electrolyte water tank, oscilloscope, optic vision camera (Focus 100H, SNU precision)

and electrolyte circulation system and pulse generator. Table 3.3 shows the specification of pulse generator. An X, Y axial linear stage moves with 0.1 μm resolution step. The electrolyte tank was made of polycarbonate material that does not react with chemical solution. In this study, NaOH was used as an electrolyte for tungsten etching. Platinum rod was used as an electrode. To remove recast layer on tungsten after laser beam machining, pulsed voltage was applied on etching unit. Applied pulsed voltage was 15 V, and pulse on time was 5 μs for 10 μs period time. Gap between electrode and workpiece was set to 100 μm. The concentration of NaOH was 2 wt% and etching time was controlled with intended range during test. Table 3.4 shows electrochemical etching conditions.
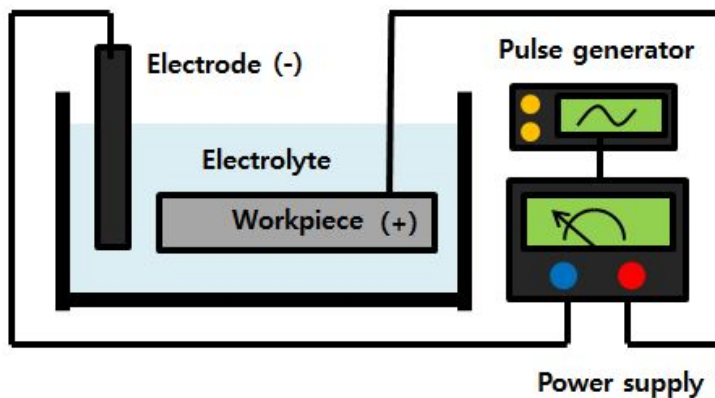
Figure 3.2 Experimental set up of electrochemical etching for

removing recast layer of pre-surface structuring on tungsten

Table 3.3 Specification of pulse generator that was used during electrochemical etching

Model	8551, Tabor electronics
Pulse width	10 ns ~ 999 ms
Amplitude	−8 V ~ 8 V
DC offset	−8 V ~ 8 V
Pulse repetition	~ 50 MHz
Output impedance	50 Ω
Rise and fall time	T_r ≤ 6 ns, T_f ≤ 6 ns

Table 3.4 The condition during electrochemical etching

Electrolyte	NaOH
Concentration	2 wt%
Applied voltage	15 V
Pulse duty	5 µs / 10 µs
Electrode	Platinum

Gap between tool and workpiece	100 μm

Chapter 4

Surface structuring of various micro structures

In this section, various shapes of surface textured structures were fabricated by using laser beam machining and electrochemical etching. Some parameters of laser beam machining were previously analyzed to texture various structures. This process follows Gaussian distribution, and thus the initial conditions such as spot size, machined depth and width should be verified in advance. As using this data, fabrication aspects were analyzed by changing arrangement of laser scanning path with different parameters. When electrochemical etching was carried out, resulted structures were verified with different etching time. Etching time is important parameter for precision structuring and surface treatment of resulted structure, this step should be considered in detail.

In this chapter, the surface structuring methods for determined

shape of structures were suggested. As following suggested a series of procedures, micro channel and pin were textured precisely. Moreover, fabricated tendencies were verified by changing machining parameters.

4.1 Parameter test

Laser beam machining follows Gaussian distribution mode for power intensity. For this reason, the spot size and machining tendency of used laser machine should be prior to main surface structuring. Figure 4.1 illustrates graph which explains power intensity of laser beam machining versus radial distance from center of beam. Formula 4.1 shows the Gaussian distribution of laser power intensity. Parameter I_0 is maximum power intensity, r is a radial distance from center of beam, and w is a radius of spot size. Formula 4.2 shows the calculated spot size of laser beam [19]. Parameter f is a focal length, d is a diameter of released beam, λ is a wavelength, and M^2 is a quality factor of laser. As following this formula, the spot size (d_0) of used laser was about 40 μm. The practical width of fabricated structure (d_T, diameter at threshold power intensity), however, is narrower than the spot size, because necessary minimum machining power intensity (I_T, threshold power

intensity) for ablating tungsten is higher than idle spot size condition. As shown in Figure 4.1, the power intensity is I_0/e^2 at spot size, however, the value for practical ablation machining in case of tungsten is I_T ($I_T > I_0/e^2$). As following Gaussian distribution, for this reason, the resulted diameter of fabricated tungsten is narrower than original spot size ($d_T < d_0$) [19].
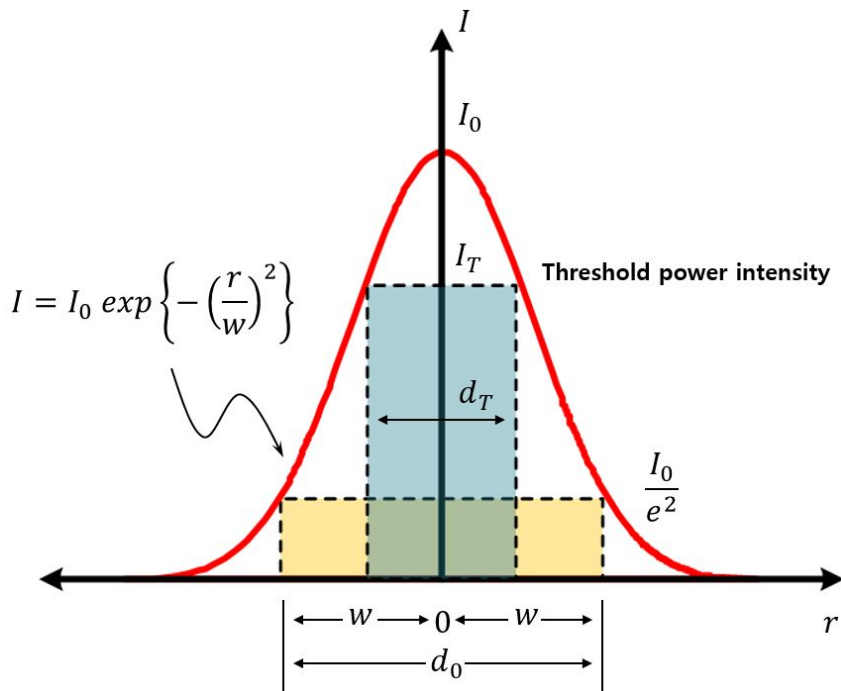
Figure 4.1 Power intensity graph of laser beam with Gaussian distribution mode

$$I(r) = I_0 exp\left\{-\left(\frac{r}{w}\right)^2\right\} \quad\quad (4.1)$$

I_0 : maximum power intensity at center of beam

r : radial distance from center of beam w : radius of

spot size

$$d_0 = \frac{4}{\pi}\frac{f}{d}M^2\lambda \qquad\qquad (4.2)$$

d_0 : spot size f : focal length d : diameter of released beam

M^2 : quality factor of laser λ : wavelength

Figure 4.2 shows the fabricated result with 10 W power densities, 350 numbers of scanning and 1 line scanning path. As shown in this SEM picture, the resulted width of textures structure with 1 line scanning path was about 19.23 μm and the depth was 66.67 μm. This result (figure 4.2 (a)) verifies the principle of figure 4.1, which the width of practical fabricated result is narrower than spot size. Figure 4.2 (b) illustrates the composition of textured surface after laser beam machining. Fabricated surface was composed of micro groove, recast layer and heat affected zone.
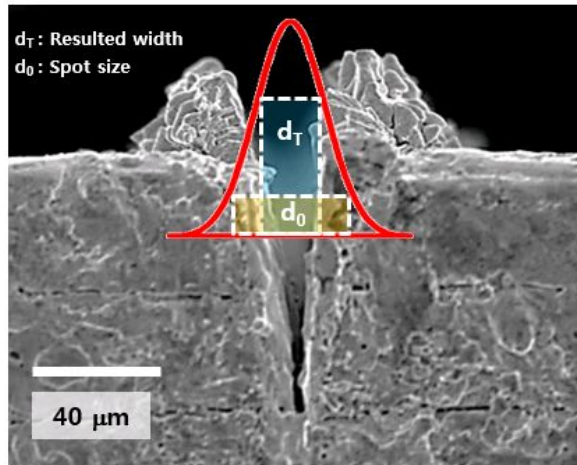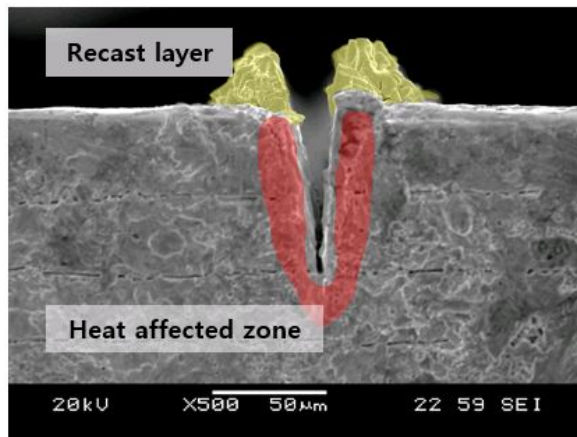
Figure 4.2 Fabricated groove with 1 line scanning path (10 W, 350 numbers of scanning) (a) enlarged image with Gaussian distribution. (b) overall image

As I mentioned before, laser ablation phenomenon follows two-temperature model and Gaussian distribution. For this reason, the resulted profiles of ablated groove can be calculated from these formulas. Formula 4.3 shows two-temperature diffusion model, and it follows the principle of energy conservation.

$$C_e \frac{\partial T_e}{\partial t} = -\frac{\partial Q(z)}{\partial z} - \gamma(T_e - T_i) + S \qquad (4.3)$$

$$C_i \frac{\partial T_i}{\partial t} = \gamma(T_e - T_i)$$

$$\mathrm{Q(z)} = -k_e \frac{\partial T_e}{\partial z} \qquad \mathrm{S = I(t)A\alpha e^{-\alpha z}} \qquad \mathrm{I(t)} = I_0 e^{\frac{t}{t_L}}$$

And thus, finally calculated temperature in z direction (perpendicular to surface of material) can be explained to formula 4.4

$$T_i \cong \frac{\alpha F_a}{C_i} e^{-z\alpha} \qquad (4.4)$$

$$F_a \cong I_0 A t_L$$

As following this phenomenon, the spatial and the temporal reaction of the lattice and sub-electron system temperature (T_e and T_i) can be explained by two-temperature diffusion model in one directional dimension. In these formulas, z is the direction perpendicular to the surface of ablated material. $Q(z)$ is heat flux and S is the laser

thermal energy source term, I(t) is the laser power intensity, A and α are the surface absorptivity and material absorption coefficient. C_e and C_i are the heat capacities of the electron system and lattice sub system, r is the parameter that is characterized about coupling between lattice and electron sub system. And k_e is the thermal conductivity of electron. To evaporate material during laser ablation, the energy of lattice should be over the heat of evaporation. Formula 4.5 shows this condition. C_iT_i is energy of lattice and ρσ of evaporation, and F_{th} is threshold laser fluence and σ s specific heat of evaporation per unit mass of material.

$$C_iT_i \geq \rho\sigma \qquad (4.5)$$

$$F_a \geq F_{th}e^{z\alpha} \qquad F_{th} \cong \frac{\rho\sigma}{\alpha}$$

Moreover, the threshold laser fluence can be changed according to multiple laser shot (N). This value is related to incubation coefficient S of material. Finally, calculated depth of ablated groove is explained to formula 4.6

$$L \cong \alpha^{-1}\ln(\frac{F_a}{F_{th}N^{S-1}}) \qquad (4.6)$$

Width of ablated groove can be calculated from Gaussian distribution equation. Formula 4.7 shows applied laser fluence

according to Gaussian distribution. r is distance from beam center, w_0 is beam radius in $I=I_0/e^2$, t_L is laser pulse duration, N is number of laser scanning, and S is incubation coefficient of material.

$$F_a(r) = F_0 e^{-2(\frac{r}{w_0})^2} \qquad (4.7)$$

$$D = w_0 \sqrt{2\ln(\frac{F_a}{F_{th}N^{S-1}})} \qquad (4.8)$$

Finally, ablated diameter (width) of groove is resulted from Gaussian distribution. Figure 4.3 shows the estimated profiles of ablated groove according to applied laser peak power and number of laser scanning. As shown in this figure, the profiles increases logarithmically, but resulted width was converged according to increase peak power. For this reason, laser ablation using only single scanning line cannot achieve width control, and thus cannot fabricated wide channel structure. Laser ablation using single scanning line is suitable for cutting and drilling.

$$L(depth) \cong \alpha^{-1}\ln\left(\frac{F_a}{F_{th}N^{S-1}}\right) \qquad D(width) = w_0\sqrt{2\ln\left(\frac{F_a}{F_{th}N^{S-1}}\right)}$$
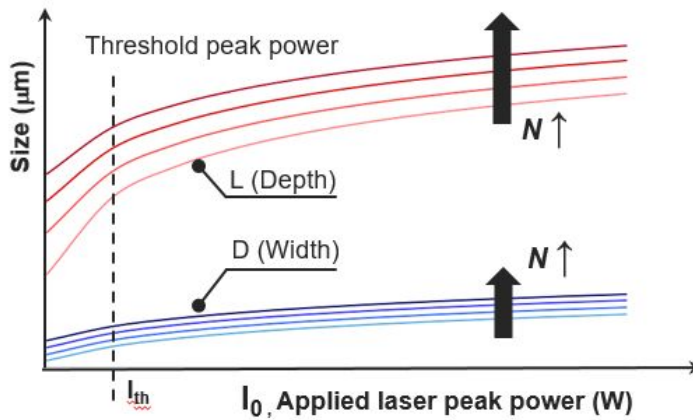
Controlled parameters for micro structuring

I_0 : Applied laser peak power

N : Number of laser scanning

Figure 4.3 Tendency of profile of ablated groove according to applied laser peak power and number of laser scanning

Peak power intensity

As following previous analysis, in this section, parameter test of laser beam machining such as peak power and number of scanning were carried out. All parameters tests during laser beam machining were implemented with 1 scanning line. Figure 4.4 shows the

results as changing peak power of laser beam with same number of scanning time (2000 number of scanning, 258.6 mm/s scan speed). In case of 2 W peak power condition, practical machining did not occurred due to lack of thermal energy. To fabricate tungsten, peak power intensity should be over the threshold condition. However, the machining condition of figure 4.3 (a) was too insufficient to machine. As increasing peak power condition from 6 W, tungsten groove was textured on surface with 1line laser scanning path. Though fabricated depth was deeper as increasing peak power, the textured width results was narrow compared between 6 W and 10 W conditions. This result was come from generation of recast layer as increasing power. Generated recast layer was formed on side wall of groove, and its quantity was high as increasing power condition, and it was pilled on the surface beside groove. Figure 4.5 illustrates the principle of this phenomenon that width expansion as increasing power. TEM 00 mode of laser beam is following Gaussian power distribution. I_1 and I_2 is each power distribution with different quantity. I_2 is higher than I_1, and thus peak of distribution was also higher, however, the released beam diameter from laser source was same. As mentioned previous, minimum peak

49

power should be over the threshold power intensity. For this reason, the reactive diameter d_2 of I_2, over the threshold power, is higher than the diameter $d_1$of I_1 case, and thus resulted width of groove was also wider as increasing peak power.
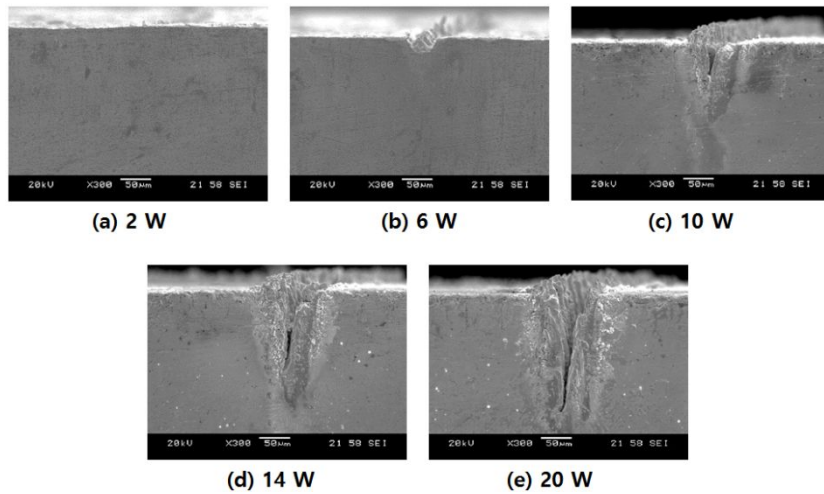
Figure 4.4 Fabricated grooves with 1 line of laser scanning path as changing peak power of laser beam (2000 number of scanning, 258.6 mm/s scan speed)
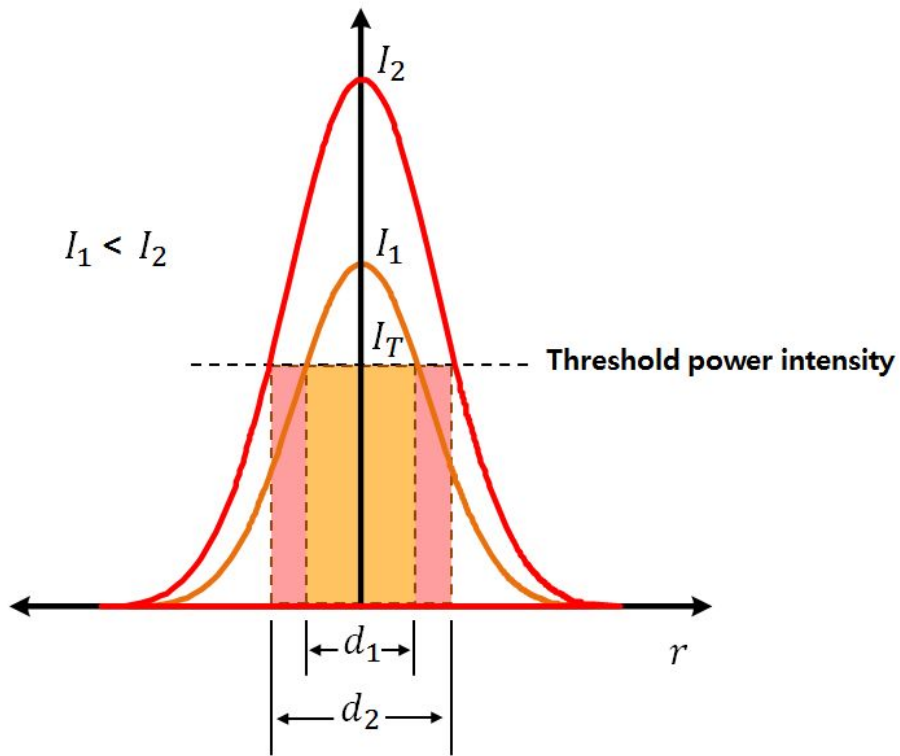
Figure 4.5 Principle of width expansion as increasing peak power condition with Gaussian distribution

In general laser beam machining process on metal, thermal ablation rate is related to reflectivity and absorptivity, and these characteristics are related to temperature of metal. If temperature of metal is high, the resulted electrical conductivity will be low, and thus relative reflectivity of metal is also low by Hagen−Rubens equation [19]. As decreasing reflectivity, relative absorptivity of

metal finally increases, and thus thermal ablation rate during laser beam machining can be high as increasing temperature of metal.

As following previous mention, practical reflectivity and absorptivity can be different as peak power of laser beam due to thermal energy. In case of low peak power condition, laser beam is almost reflected on metal surface, and thermal heat energy from absorbing laser beam is also rapidly conducted to other area of material, and thus the resulted total ablation rate is low. On the other hand, high power condition causes low reflectivity of laser beam, and thus total thermal ablation late is surely low.

Figure 4.6 shows the resulted depth and width of groove according to changing peak power conditions. In case of depth, the resulted value was higher as increasing peak power, however, change rate of width values were relatively low. This phenomenon was come from characteristic of laser beam Gaussian distribution. Resulted beam size to machine tungsten surface is directly correlated to textured width, however, generated initial beam size from laser source was same, because initial beam size could be only decided from wavelength of used laser. Formula 4.9 shows the size of beam and verifies this reason. For this reason, though peak power of laser

beam increased, changing rate of machined width was not much high

[36].

$$w = w_0 \left[1 + \left(\lambda\frac{z}{\pi w_0}\right)^2\right]^{0.5} \qquad (4.9)$$

w : radius of released beam w_0 : beam waist

λ : wavelength z : displacement in z direction
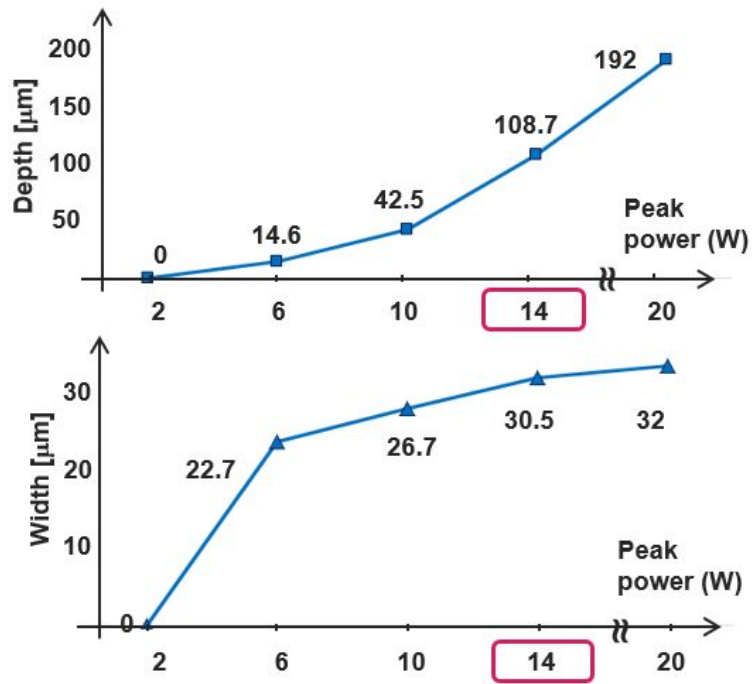
Figure 4.6 Measured depth and width values of textured groove according to changing peak power of laser beam

Number of scanning

In this section, other parameter test of laser beam machining was carried out to verify tendencies. Number of scanning during laser beam machining can be another important parameter to texture structure on tungsten due to control total thermal ablation energy. Figure 4.7 illustrates the resulted groove as changing number of scanning during laser beam machining. Applied peak power was 14 W and scan speed was 258.6 mm/s. As shown in figure 4.7, textured tendencies had high ablation quantity as increasing number of scanning. This phenomenon was come from increase of total thermal energy, and multiple absorption and replication in machined area. If a surface has rough wedge, multiple absorption and replication of laser beam will occurred. Figure 4.8 shows this principle about multiple reactions on wedged surface during laser beam machining. As shown in this figure, wedged surface causes multiple reflection and absorption, and thus it has an advantage to laser beam machine. For this reason, repeat of laser scanning has advantageous aspect not only increase of total thermal energy but also multiple reaction of ablation [19]. Figure 4.9 illustrates the measured depth and width of groove as increasing the number of

scanning. In both results, 10000 numbers of scanning results show the highest values. However, excessive number of scanning time could not applied to texture wide textured groove, due to limitation of overall thickness (1t) of tungsten material. Because many number of scanning make not only width but also depth ablation.
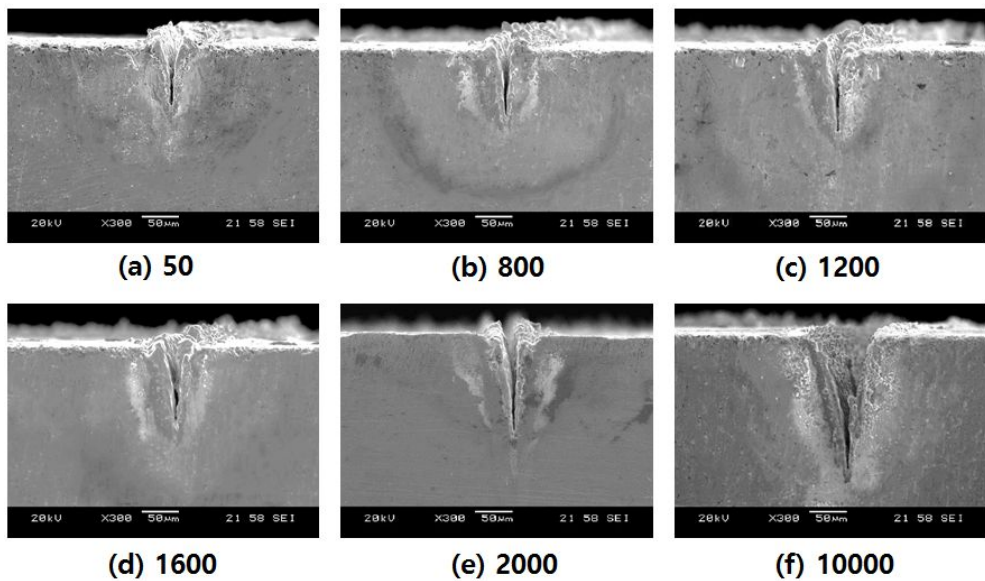
Figure 4.7 Fabricated grooves with 1line of laser scanning path as changing number of scanning (14 W peak power, 258.6 mm/s scan speed)
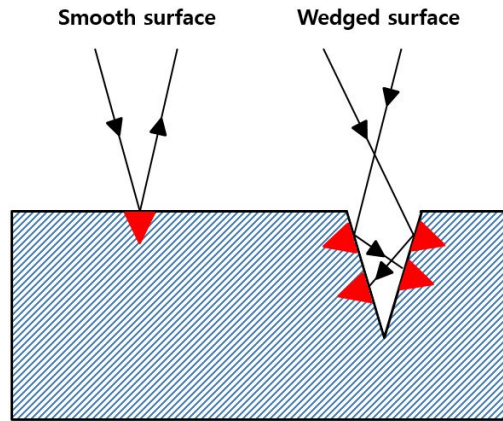
Figure 4.8 Principle of multiple reflection and absorption due to wedged surface
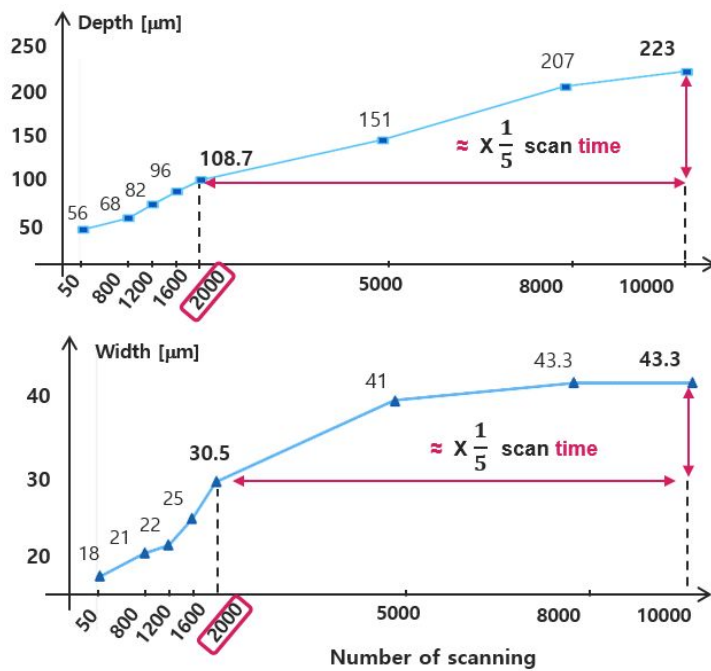
Figure 4.9 Measured depth and width values of textured groove according to changing number of scanning

Scan speed

Pulsed laser generates laser beam with pulsed shape and it makes high peak power intensity. For this reason, structuring process of material is carried out by repeating pulsed beam, and thus textured result is affected by overlapping of pulse from movement of laser beam or workpiece. Scan speed can be an important factor during laser beam machining due to previous mentioned reason. Figure 4.10 illustrates the principle of overlapping of laser beam as changing scan speed. As increasing scan speed, distributed beam shape is changed from circle to ellipse, and degree of overlap is also low. It means that laser ablation rate is low due to short accumulation time of thermal energy. On the other hand, low scan speed causes high ablation rate due to long accumulation time of heat. Although scan speed was different, applied power intensity of laser beam was same, and thus power distribution also occurred. In case of low scan speed, relative power around circle beam shape was high that textured width was wide. On the other hand, in case of high scan speed, relative power around elliptic beam shape was low, and thus textured width of groove was narrow [19].

57
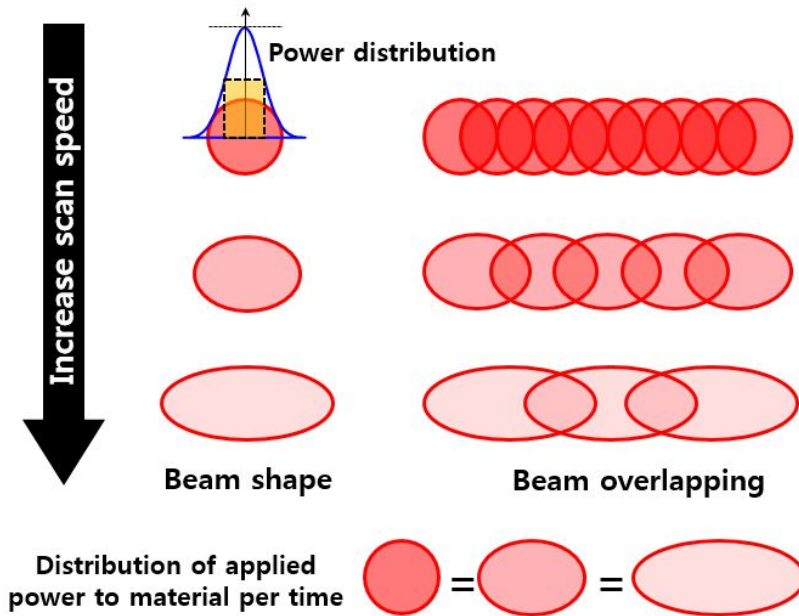
Figure 4.10 Beam shape and overlapping as changing scan speed

Figure 4.11 shows the textured groove on tungsten as changing scan speed of laser beam. As mentioned previously, low scan speed case (figure 4.11 (a)) had the highest ablation quantity, on the other hand, high scan speed condition (figure 4.11 (e)) had relatively low. Scan speed is an important trade-off factor that decides productivity. Low scan speed causes high laser ablation and wide width of groove due to long staying time on machined area, but makes productivity low. On the other hand, high scan speed causes low laser ablation and narrow width due to short staying time, but

58

makes productivity high. For this reason, proper scan speed to texture structure on tungsten should be selected.

(a) 58.6 mm/s   (b) 158.6 mm/s   (c) 258.6 mm/s

(d) 358.6 mm/s   (e) 458.6 mm/s
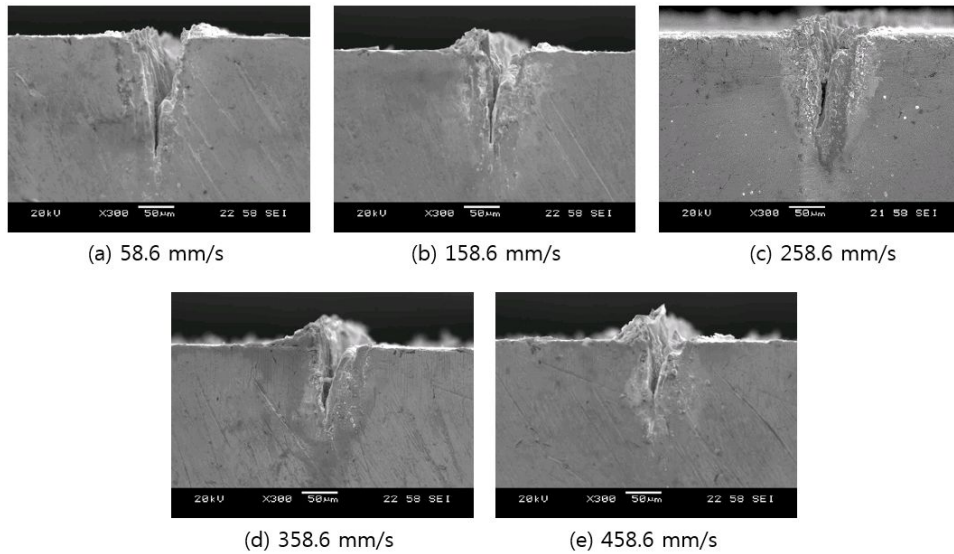
Figure 4.11 Textured grooves as changing scan speed during laser beam machining

Figure 4.12 shows the measured profile of ablated groove according to scan speed. In case of 58.6 mm/s, the largest depth and width of groove were fabricated due to long thermal ablation time. However, its size of groove, low scan speed makes low productivity, and thus 258.6 mm/s condition was selected to texture various shape of structure.
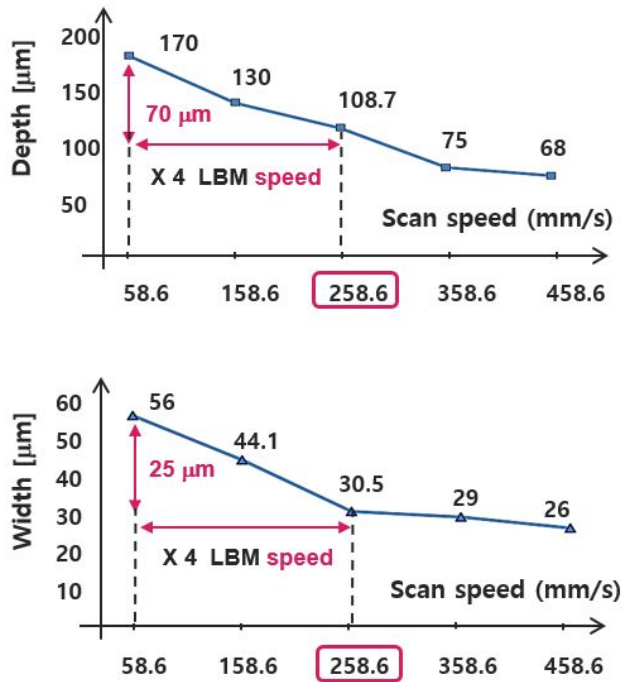
Figure 4.12 Measured depth and width values of textured groove according to changing scan speed

In this section, parameter studies of laser beam machining using single laser scan were carried out. However, it is impossible to control width size to achieve various shape of structure such as wide channel in single line laser beam machining. Figure 4.13 shows this tendency of resulted shape of groove according to various parameters. Profile (a) was came from high peak power and number of scanning conditions, and (b) shape was resulted from low scan speed.
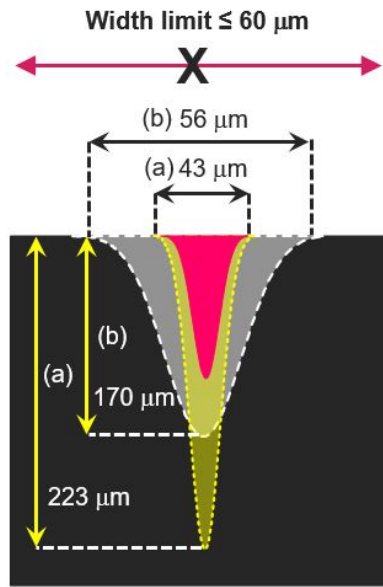
Figure 4.13 Tendency of shape of the groove according to various parameters of laser beam machining

As mentioned previous, some parameters such as peak power, number of scanning and scan speed tests were implemented to verify structuring tendencies. Although 1 line of laser scanning path was useful to control depth of micro groove as combining various laser parameters, the width of groove was not controlled easily. Tough excessive peak power and number of scanning could widen the texture width, practical growth of the width was little. Moreover, thickness of tungsten (1t) made a limitation of total quantity of

thermal energy from excessive peak power and number of scanning. For this reason, laser beam machining using 1 line of scanning path is not suitable to texture various structures with wide width, and thus it is not suitable for micro milling but drilling to fabricating micro hole or cutting process. Figure 4.14 shows textured grooves as changing number of scanning path under same total energy condition. Applied total energy constant during laser beam machining was calculated by formula 4.10. Thermal energy is proportional to peak power, number of scanning and number of scanning path. Textured grooves were fabricated with same 16800 energy constant value conditions. In case of figure 4.14 (a), scanned path had just 1 line, and thus overall thermal energy was used to texture depth direction. On the other hand, 3 lines and 6 lines scanning path cases had relative wide width and short depth compared to figure 4.14 (a). As following these results, textured shapes with same total thermal energy could be different as combining number of scanning line.

$$E = P \times N_s \times N_{sl} \qquad (4.10)$$

P: peak power of laser beam N_s: number of scanning

N_{sl}: number of scanning line

In this research, various structures for specific functions should be textured quite freely on tungsten. For this reason, not only laser beam machining parameters control but also combination of laser scanning path such as number of scanning line should be needed.

(a) 1 line 14 w 1200 (NS)   (b) 3 lines 14 w 400 (NS)   (c) 6 lines 14 w 200 (NS)
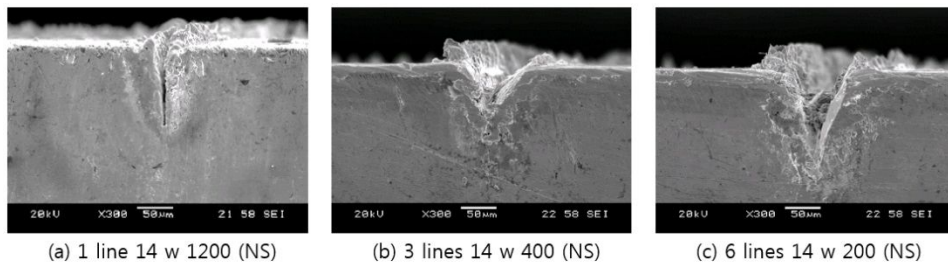
Figure 4.14 Textured grooves as changing number of scanning path under same total energy condition

4.2 Micro channel

Laser beam machining

As following results and analysis of previous section, to find suitable arrangement of laser scanning path is necessary for surface structuring with various shapes. Moreover, the parameter test as changing arrangement of scanning path during laser beam machining should be carried out for apprehending surface structuring tendencies. Figure 4.15 shows the parameters of laser scanning path that were controlled during laser beam machining.
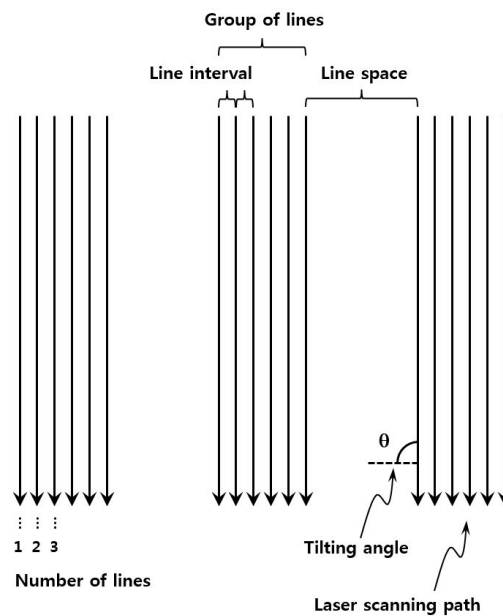
Figure 4.15 Determined parameters of laser scanning path

Number of lines

Number of lines means the arranged number of scanning path in grouped area. This parameter can affect to width and depth of the textured groove, as relating to overall laser machining quantity of tungsten. Practical width of textured groove is narrower than calculated width by combining spot size, and thus the affection of number of lines should be verified during laser beam machining. Figure 4.16 shows resulted SEM images of varied number of scanning path. These results were implemented under 14 W power density, 350 times number of scanning, 10 μm line interval, 200 μm line space and no tilted conditions.
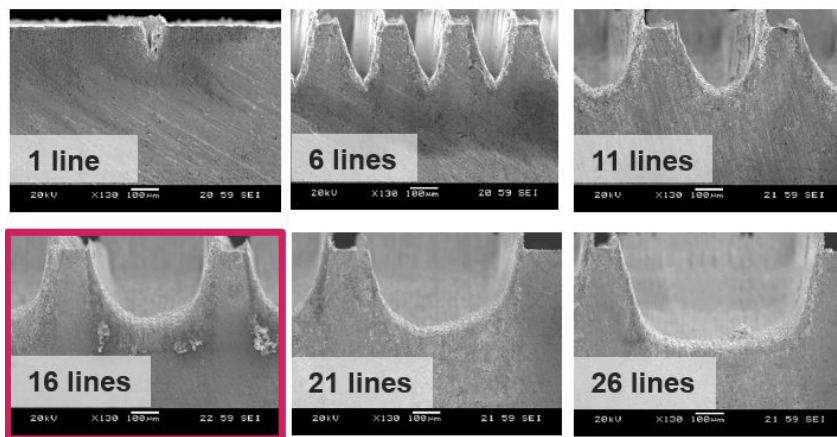
Figure 4.16 Textured results as changing the number of laser scanning path

The fabricated groove was roughly wider as increasing number of laser scanning path as shown in figure 4.16. The resulted depth was similarly deeper, and the slope of groove was gentler due to increasing scanning line. These results were come from difference of laser ablation rate due to thermal transfer and laser beam absorption [19]. As shown in figure 4.17(a), when a lot of laser scanning path were applied to workpiece, thermal energy at the center of scanned area was accumulated due to continuous supplement before heat transfer into remained area, and thus ablated quantity was higher. In case of metal, thermal laser beam absorption is generally related to its temperature, electrical conductivity and reflectivity. As increasing thermal temperature on metal surface by laser beam machining, the electrical conductivity is generally lower, and thus the resulted reflectivity on surface becomes also lower as mentioned in Hagen-Rubens formula (formula 4.11). It makes directly absorption of laser beam on metal high, and thus total machining quantity is higher [19].

$$R = 1 - 2\sqrt{\frac{\nu}{\sigma}} = 1 - \frac{2}{\sqrt{\frac{\sigma\lambda}{c}}} \qquad (4.11)$$

R: reflectivity of metal λ: wavelength of laser beam σ:

Electrical conductivity of metal c: speed of light

On the other hands, in case of few number of laser scanning path (figure 4.17 (b)), though high thermal energy intensity at the center of scanned area as Gaussian distribution, accumulated heat energy quantity was relatively low due to easy heat transfer, and thus the ablated quantity was small.
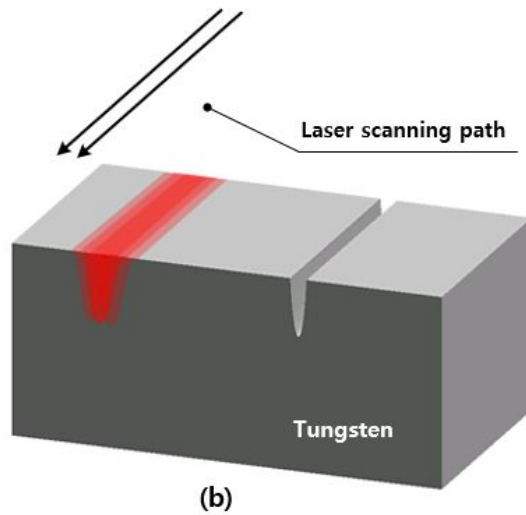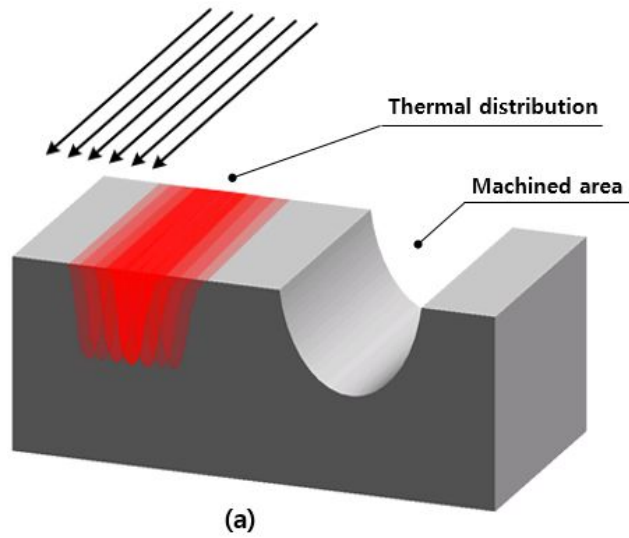
Figure 4.17 Difference of thermal ablation rate as changing the number of scanning line, (a) a lot of laser canning path, (b) few number of scanning path

Figure 4.18 is graphs that compare the measured and calculated results as changing number of scanning line.
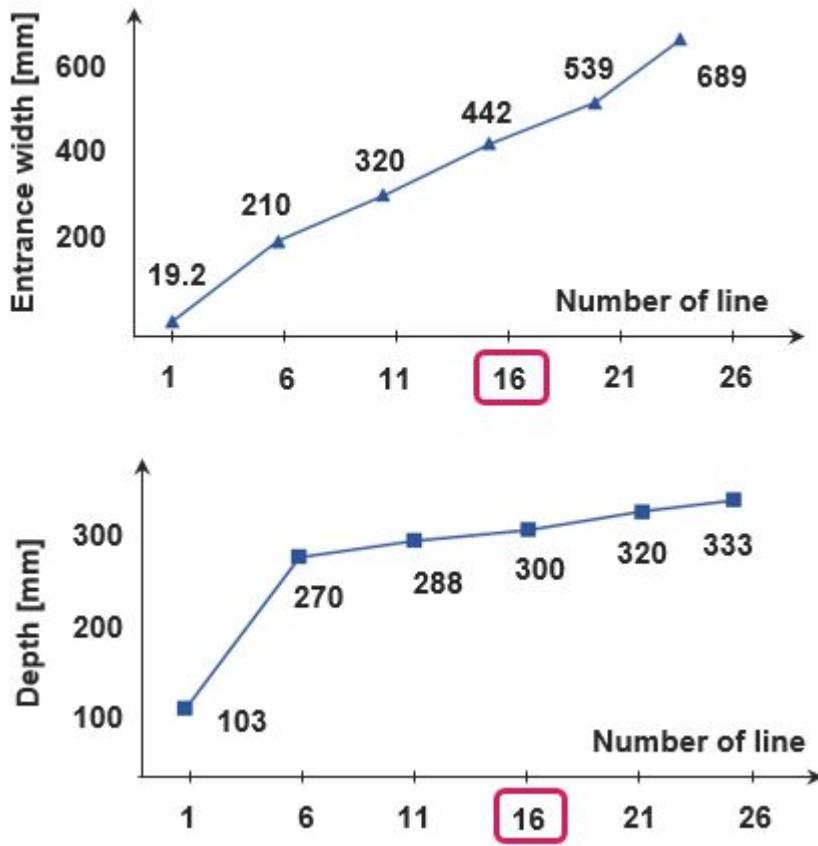
Figure 4.18 Measured width and depth of fabricated groove as changing the number of line path

The width (figure 4.18(a)) and depth (figure 4.18(b)) of fabricated groove was wide and deep as increasing the number of scanning path. As shown in this figure, the resulted width increased according to increase number of scanning line, because number of overlapped beam increased. On the other hand, depth was converged according to number of scanning line. Though the applied

multiple laser beam were accumulated, total accumulated thermal energy had limitation. In this section, laser beam machining with multiple laser scanning path was carried out, and thus thermal energy accumulation should be considered to achieve surface structuring. Formula 4.12 explains the resulted profile of ablated groove by using multiple laser scanning path. This phenomenon is related to thermal accumulation and laser beam overlapping. I_{sum} is accumulated laser intensity, and it follows sigma summation. For this reason, applied laser fluence also follow this accumulation phenomenon. In case of width, number of scanning line and line interval also relate to resulted value. Figure 4.19 shows this phenomenon and principle of overlapping and accumulation.

$$L(\text{depth}) \cong \alpha^{-1} \ln\left(\frac{F_{a,sum}}{F_{th}N^{s-1}}\right) \qquad (4.12)$$

$$D(\text{width}) \cong (M-1)l + w_0 \sqrt{2\ln\left(\frac{F_{a,sum}}{F_{th}N^{s-1}}\right)}$$

$$I_{sum} \cong I_0 \sum_{i=0}^{M-1} -\frac{2\{x-(l\times i)\}^2}{w_0{}^2}$$
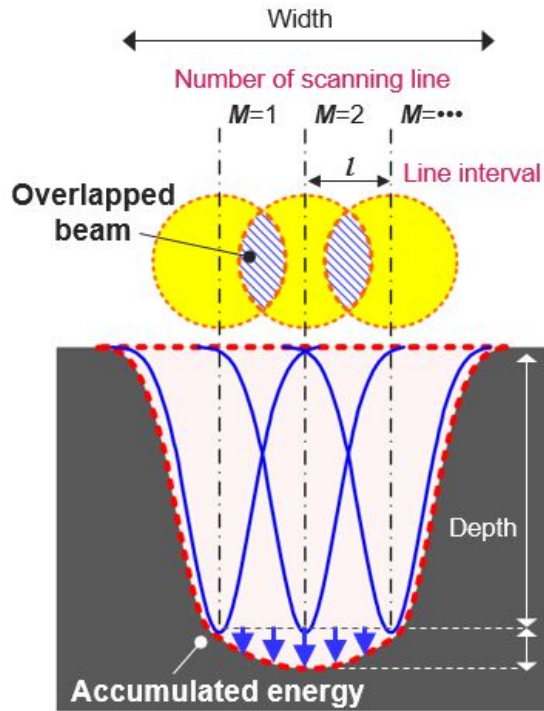
Figure 4.19 The principle of overlapping and accumulation by using
multiple laser scanning path

In this research, laser scanning path control was carried out to
fabricate various shapes of structures. To fabricate micro channel,
tilting process was carried out (tilt, reverse tilt section). This tilting
process was implemented vertical side wall of groove. At this point,
narrow bottom width of groove is more efficient. Figure 4.20 shows
this phenomenon. In case of wide bottom width, resulted side wall
cannot achieve vertical angle, and thus 16 number of lines was
selected as a condition (refer to figure 4.16). To achieve large

micro channel, many number of scanning lines, large laser beam machining conditions (high peak power, large number of scanning) should be applied, and thus deep depth and narrow bottom width of groove can be fabricated.
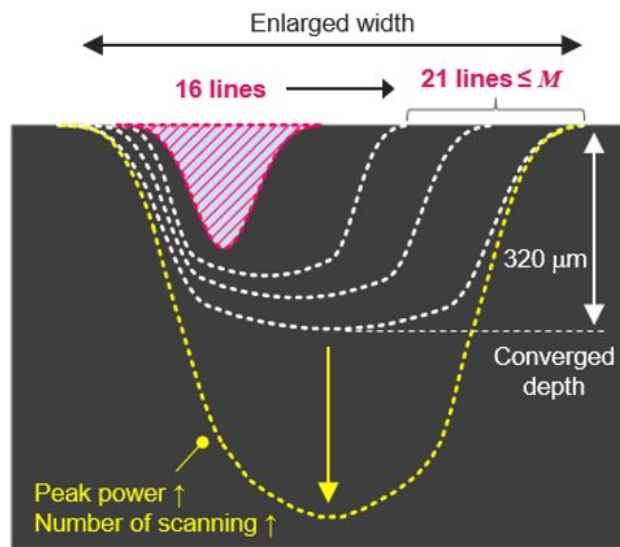
Figure 4.20 Tendency of fabricated groove according to number of scanning and resulted shape of tilted groove according to bottom width

Line interval

Line interval means the gap between each line in group of lines (figure 4.15). As mentioned previous section, line interval is related to overlapping of laser scanning line, and thus various values of line interval can causes different laser structuring tendencies. Figure 4.21 shows the resulted SEM images as changing line interval during laser beam machining. These structuring results were carried out under 14 W power density, 350 times number of scanning, 200 μm line space, 16 number of scanning line and no tilted conditions. Fabricated tendencies were generally wider due to increasing gap between each line in group. The fabricated structure with 5, 10 μm line interval condition was similar to edged valley, and had steep linear slope. This phenomenon was come from heat concentration on center area, because thermal ablating scanning lines were overlapped tightly. On the other hand, resulted structure with 15, 20 μm line interval has round edge at bottom of groove, and had gradual curved slope. As heat concentration phenomenon was lower than 5, 10 μm line interval case due to relative wide interval between thermal ablating scanning lines, and thus thermal energy distribution followed curved valley shape. In case of 25, 30

μm line interval, however, surface structuring was incomplete. As shown in case 25, 30 μm, many micro sized conical structure were generated by laser ablation, which is connatural characteristic of tungsten. Wide line interval caused remained region without laser beam machining, and thus this region and generated recast layer and burr composed the conical array. Moreover, in this case, thermal energy was not accumulated during laser structuring, because overlapping between near lines was not occurred. Though the resulted width was wider than narrow line interval cases (5, 10, 15, 20 μm), fabricated depth of machined structure was shallow due to heat dispersion without accumulating to thermal energy.
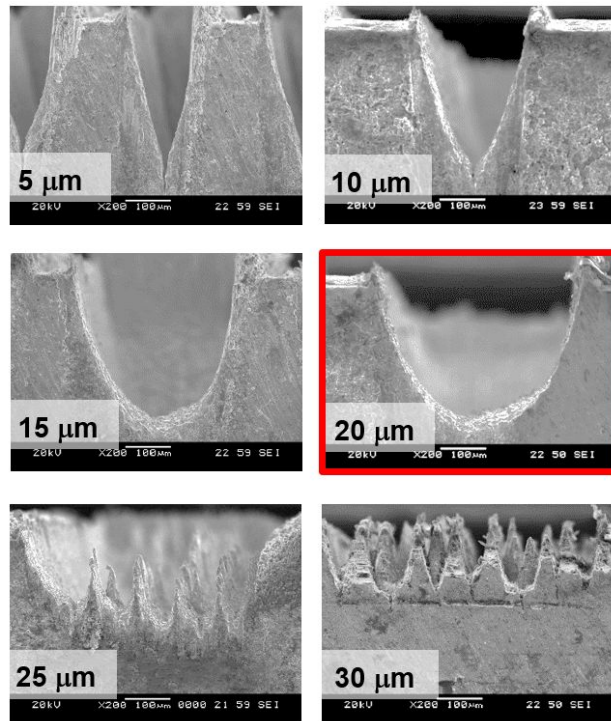
Figure 4.21 Textured structures with various line interval conditions

These phenomena can be explained laser beam overlapping. Figure 4.22 shows this principle, and the tilting efficiency was compared. In case of steep shape of groove, tilting angle in tilt process should be higher than gradual shape of groove. And volume of peak (that should be removed in trimming process) structure from gradual shape of groove case is smaller than steep shape of groove. However, the sharpness of groove edge in steep shape of groove case is sharper than gradual shape of groove case.

75
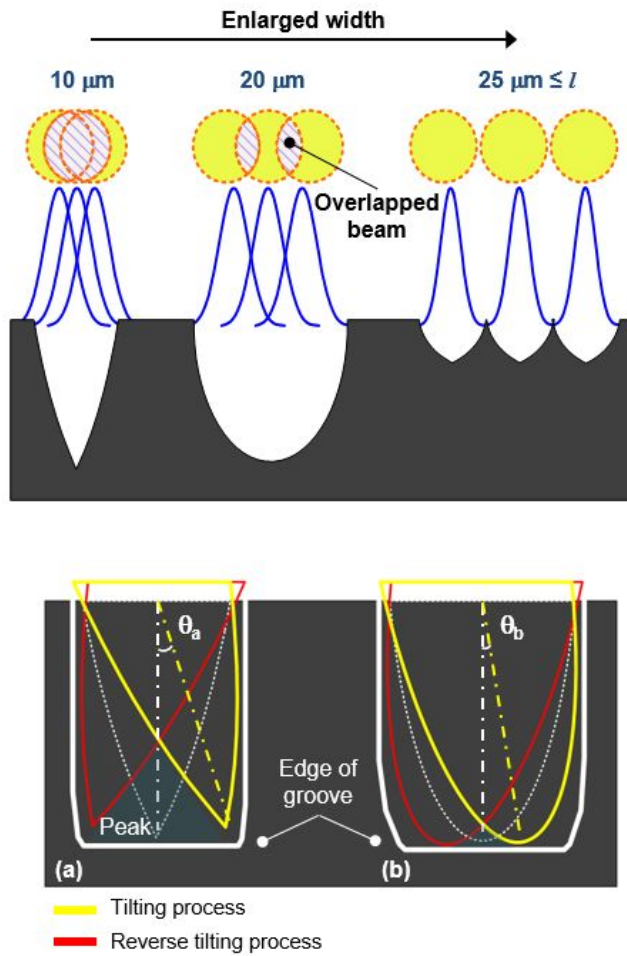
Figure 4.22 Principle of overlapping according to line interval and the resulted shape of groove according to slope shape of groove

Figure 4.23 illustrates the resulted width and depth of textures structures with various line interval conditions. The results that fabricated width were wide as increasing the line interval due to the

76

total width was determined by summation between practical ablated diameter and line interval with pre-defined number of line. In case of depth, however, the results of textured depth were similar from 5 μm line interval to 20 μm line interval case. On the other hand, as increasing interval gap, overlapped thermal ablation area was narrow contrastively, and thus practical fabricated depth was shallow. For this reason, this resulted total depth of 25, 30 μm line interval case was not much difference compared to single scanning line ablation depth.
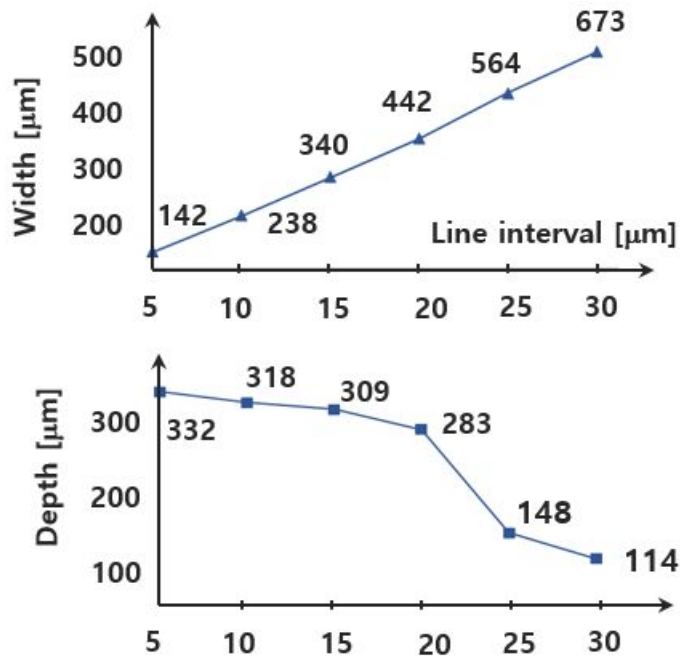
Figure 4.23 Measured width and depth results according to changing line interval during laser beam machining

Line space

Line space is an empty region between group of lines and it determines the remained size of fabricated structure without laser machining. This parameter is not related to the accumulated thermal energy due to overlapping of laser scanning. Figure 4.24 shows the fabricated results as changing line space values. Theses fabricated results were implemented under 14 W power intensity, 350 times number of laser scanning, 16 line the number of scanning path and 20 μm line interval conditions. As illustrated in figure 4.24, structural width of fabricated was wide as increasing the line space values. Moreover, the fabricated groove during laser beam machining was same, because other parameters related to thermal energy overlapping were not changed during structuring. Generated recast layer after laser beam machining was piled on the top of the structure. In case of 50 μm line space, the generated recast layer of each side wall was combined, and thus conical shape was fabricated in side view. Other conditions with 100 μm and 200 μm had not conical shape but only piled recast layers on side wall. This generated recast layer should be eliminated for precision shape control with post treatment. As following these results and analysis,

line space parameter can control the remained size of structure, is

not related to shape of groove and width and depth.
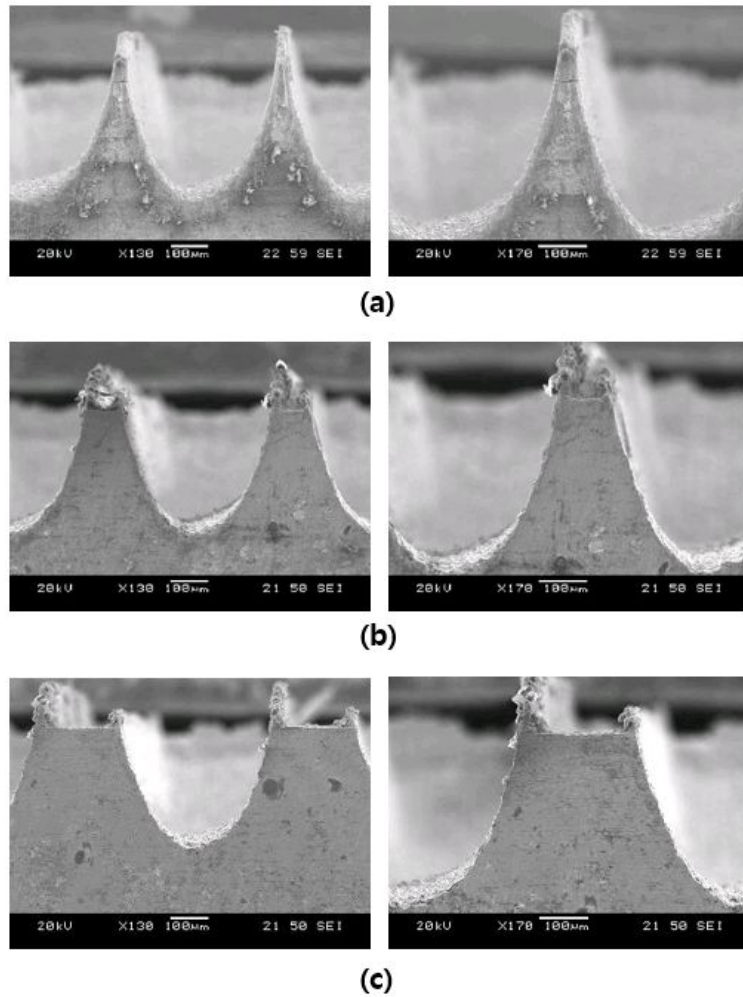
Figure 4.24 Textured structures on tungsten as changing line space,

(a) 50 μm, (b) 100 μm and (c) 200 μm

Tilt

Tilting motion during laser beam machining makes the shape of structures various with different angle and edge. The applied laser beam fabricates tapered structure as following Gaussian distribution. For this reason, to fabricate vertical side wall channel, special laser beam machining process should be need. In these sections, various tilting process were carried out, and then the results by changing tilt parameter and analysis were implemented for structuring vertical and anisotropic direction channel.

Figure 4.25 shows the principle of tilting motion method during laser beam machining. As applied laser beam vertical direction for determined focusing, tungsten workpiece was set on the tilting stage that was controlled angle from $+40°$ to $-40°$ degree. As shown in figure 4.25 (a), tilted angle θ from stage was reflected to the tungsten workpiece, and thus textured structure and groove were finally tilted from horizontal plane. As illustrated in figure 4.25 (b), defined angle parameter α is the slope angle of the textured channel, was measured to find proper angle for vertical wall channel.
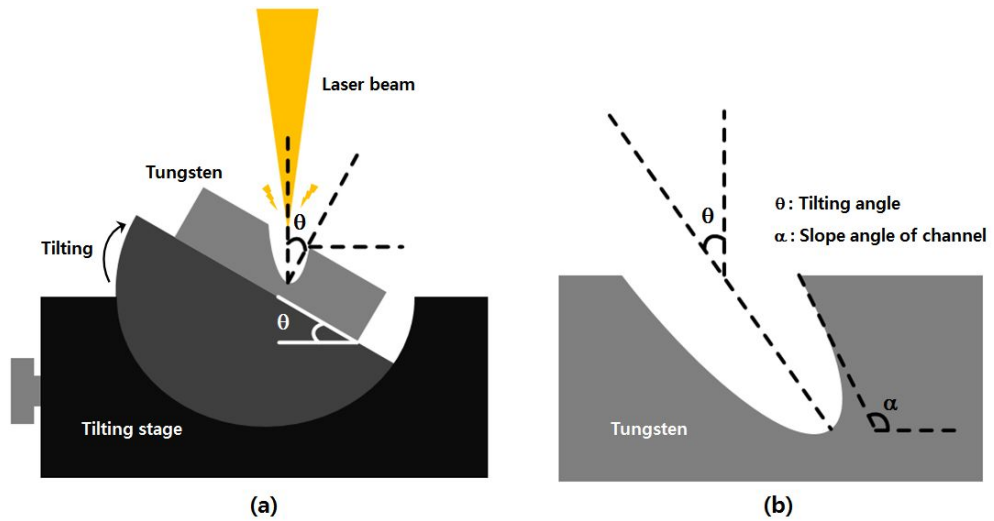
Figure 4.25 Principle of tilting process during laser beam machining
(a) overall view, (b) textured structure with tilting process

Figure 4.26 illustrates the fabricated structure by using tilting process with various angle θ. All the textured tungsten was textured under 14 W laser beam power intensity, 400 the number of scanning time, 20 μm line interval, 200 μm line space and 16 lines the number of scanning path. In case of 0° , the shape of textured groove was nearly symmetry, and the resulted slope of groove was tapered due to symmetric Gaussian distribution characteristic of laser beam machining. The shape of textured groove gradually was tilted to left side from 5° θ angel, and thus it was not symmetry

81

anymore. The slope angle of textured channel α was still an acute angle at 0° and 5° θ angle. In case of 15° θ angle, the resulted slope angle α was nearly vertical (92°), and thus this condition was chosen for structuring vertical channel for various function. As increasing the tilted angle θ (20° ~), however, angle range of the resulted slope α at the side wall was an obtuse angle. Figure 4.27 shows the resulted angle α slope at side wall as changing tilted angle θ. Each the resulted angle α was measured at the points marked with red line in figure 4.26 (e). In this section, various angled structure was textured by using tilting laser beam machining, and thus we found that the vertical angled (α) wall could be achieved at 15° θ angle. Moreover, all the shapes of textured results with tilting process were directionally anisotropic structures.
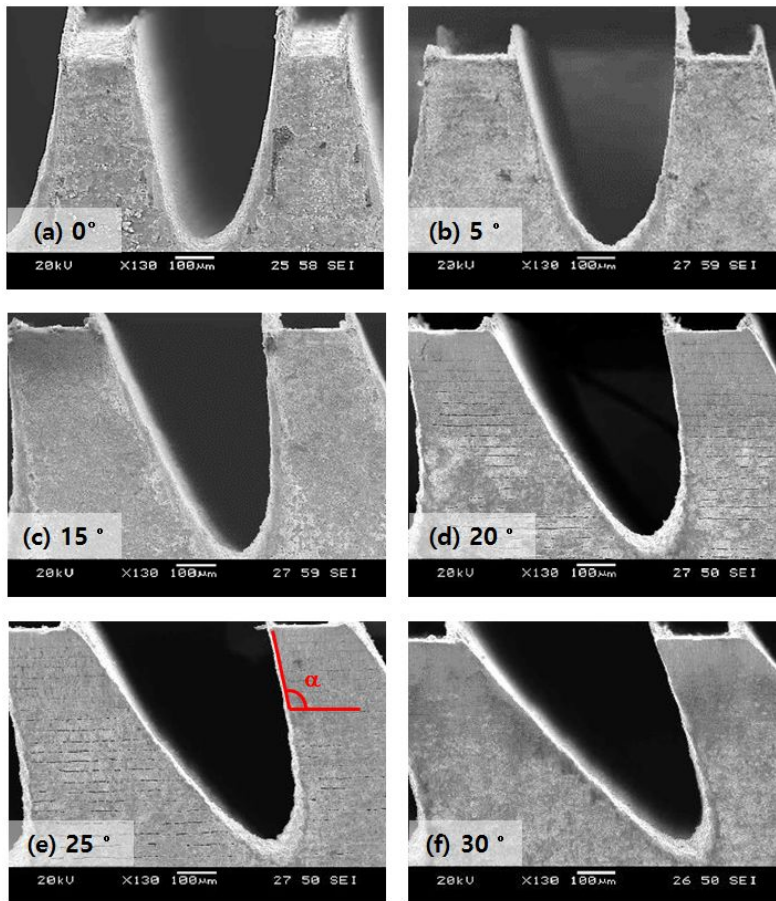
Figure 4.26 Textured structure with varied tilted angle θ, (a) 0°, (b) 5°, (c) 15°, (d) 20°, (e) 25° and (d) 30°
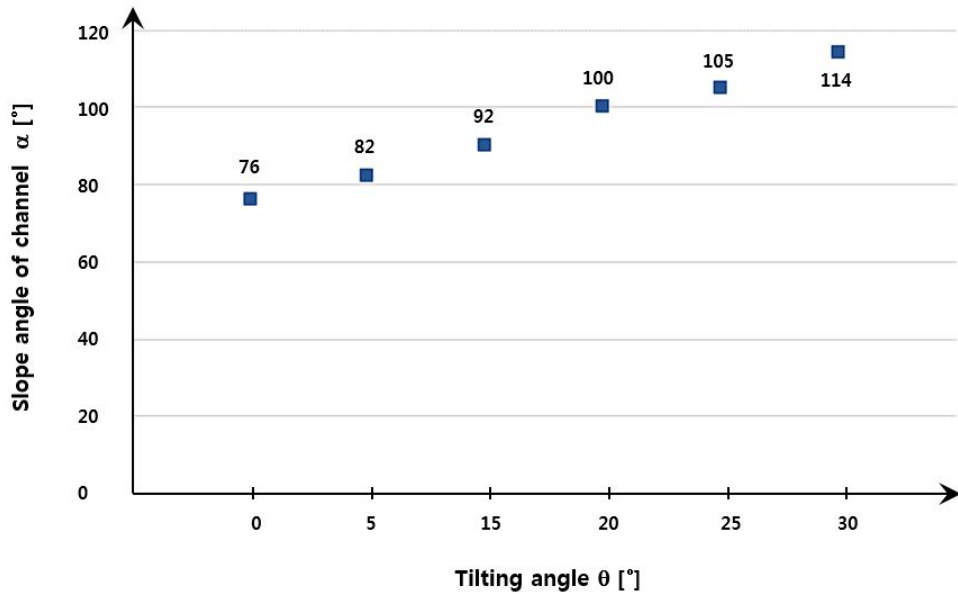
Figure 4.27 Resulted slope angle α of channel as changing tilting angle θ of applied laser beam

Reversal tilt

As analyzed previous section, to get an angle α for achieving vertical channel, laser beam machining process was carried out on tilted tungsten workpiece, and thus angle α can achieve nearly vertical structure at 15° tilting angle. However, the textured surface in this process had only vertical angle at partial side wall

84

like anisotropic structure. For this reason, to achieving micro channel with vertical at both side walls, reversal tilting process was carried out as a next step. Figure 4.28 shows the principle of reversal tilting process after only tilting laser beam machining. As shown in this figure, anisotropic textured surface with generated recast layer and burr was made from only tilting process, and then, to achieving fully vertical micro channel, reversal laser beam machining was implemented. In this process, small number of laser scanning path was chosen due to applying little quantity of thermal energy. In general laser beam machining, ablation rate is related to thermal energy transfer and aggregation, which are affected to total amount of workpiece [19]. In case of first tilting process to get anisotropic structure, laser beam machining was implemented on un-textured whole tungsten workpiece. On the other hand, second process, reversal tilting laser beam machining was carried out on pre-textured tungsten workpiece after first tilted structuring process. For this reason, in this reversal tilting process, total volume of the pre-textured workpiece could be easily ablated due to rapid heat transfer and aggregation, and thus small number of laser scanning path should be applied. The textured structure after

85

reversal process had finally w-shaped micro channel array.
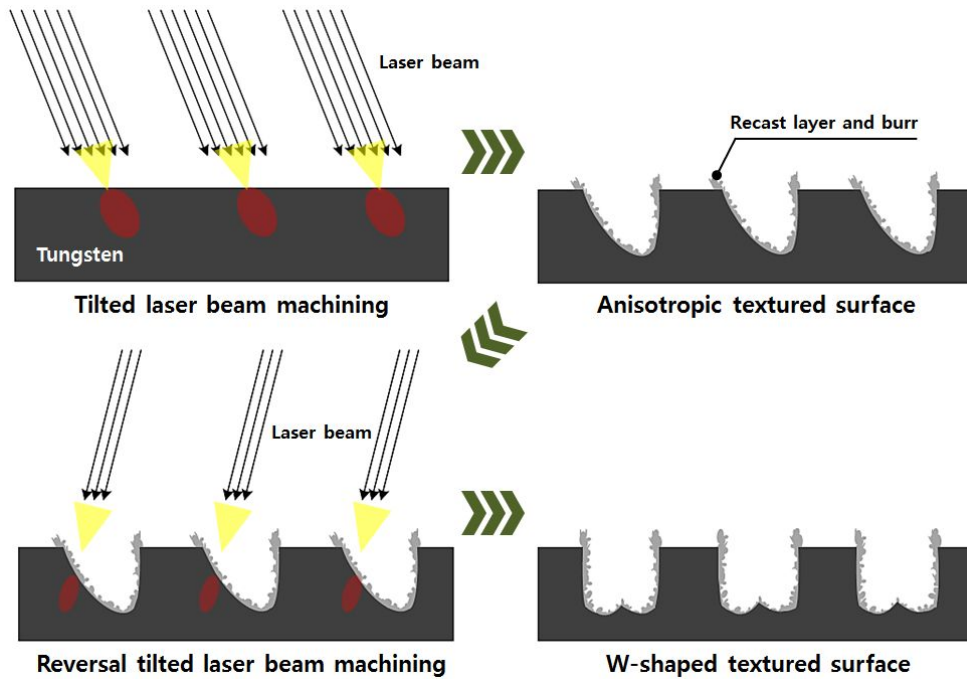
Figure 4.28 Principle and process of tilting and reverse tilting machining for vertical channel

In this process, positioning of pre-textured workpiece is the most important to achieving precision w-shape. Figure 4.29 illustrates the various fabricated w-shaped micro channel arrays with various positioning of pre-textured workpiece. To achieving these results, reversal tilted laser beam machining was implemented under 14 W power intensity, 300 the number of scanning time, 20 μm line

interval, 11 lines the number of scanning path, 350 μm line space and 15° tilting angle θ. Figure 4.29 (a) shows a precisely complete textured w-shaped micro channel. In this case, secondary laser beam was applied with symmetric direction. Figure 4.29 (b) illustrates an imbalanced textured w-shape micro channel due to secondary laser beam was leaned to left side from symmetric center line, and thus secondary grooved region was positioned upper side of pre-textured slope. In case of figure 4.29 (c), laser beam during reversal tilting process was applied to right side of symmetric center line, and thus pre-textured vertical side wall was collapsed. In this section, to fabricate symmetric vertical side wall micro channel, reversal tilted laser beam machining was carried out. As a result, w-shape textured structure array was resulted.
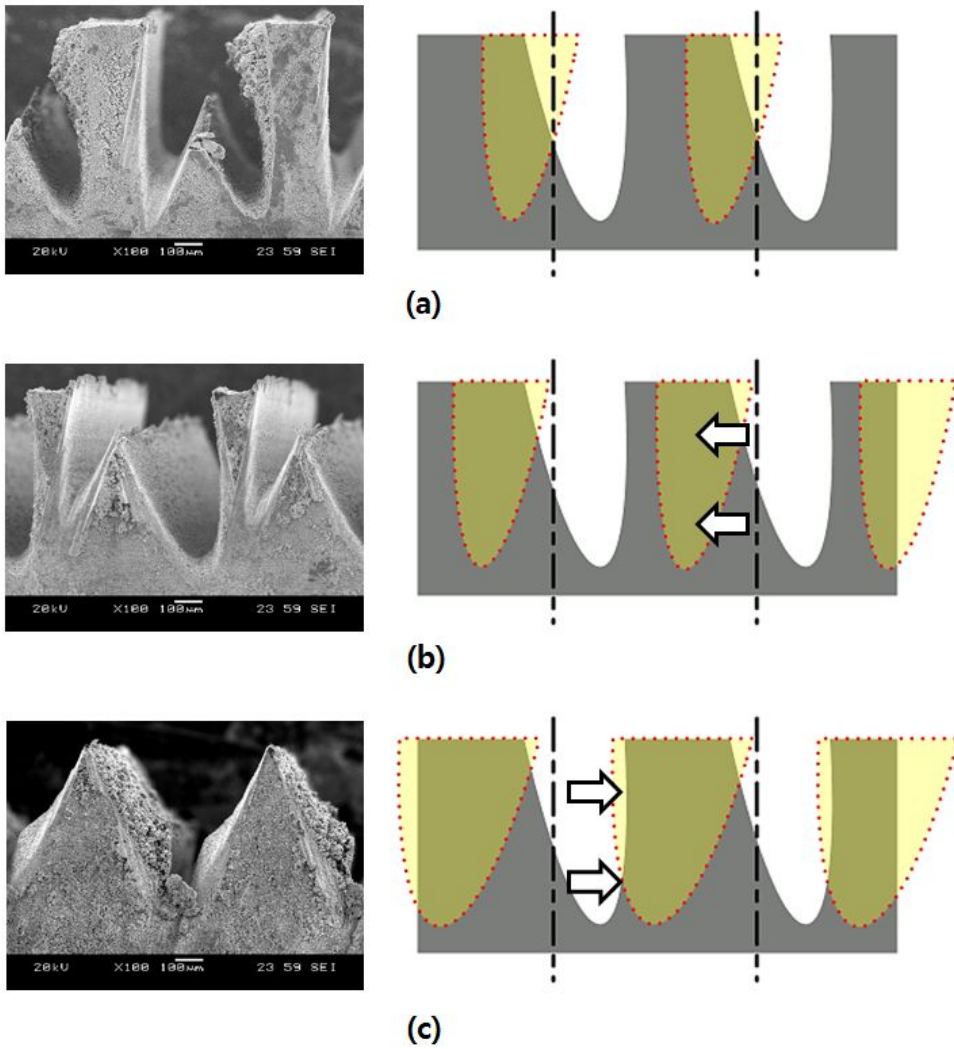
Figure 4.29 Textured micro channels after reversal tilting laser beam machining, (a) precisely complete w−shape, (b) imbalanced w−shape, (c) collapsed w−shape of micro channels

Trimming

In previous section, w−shaped micro channel array was textured by using reversal tilted laser beam machining. However, peak structure was still remained between each vertical side wall, and thus additional trimming process should be implemented to achieve complete vertical micro channel. This process should be carried out in vertical direction without tilting motion.

Figure 4.30 shows the principle of trimming process to eliminate peak on the middle of channel. In this process, precision positioning of pre−textured workpiece is also the most important. As mentioned previous section, pre−textured workpiece (w−shaped) has rapid heat transfer and aggregation due to lack of tungsten volume, and thus small number of laser scanning path should be applied to precision elimination of peak [19]. If the trimming process is finished, vertical micro channel with generated recast layer will be remained.
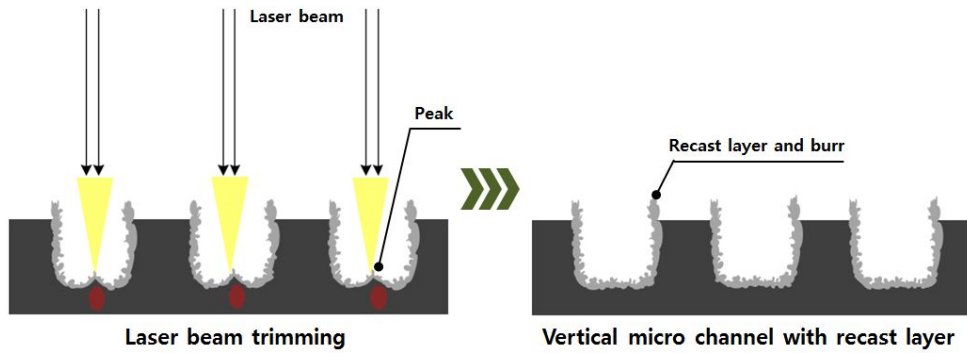
Figure 4.30 Principle of trimming process to remove peak on the middle of the micro channel

Figure 4.31 shows the results after eliminating peak on the middle of micro channel by using trimming process. As positioning of pre-textured workpiece is important, careless trimming causes poor quality of vertical side wall micro channel. Figure 4.31 (a) shows fabricated vertical micro channel after precise trimming process. After trimming process, recast layer and burr were generated by laser beam machining, were attached on the both side of wall, and thus precise cutting edged line was not observed in this figure. Though the large sized peak on the middle of w-shaped micro channel was eliminated by trimming process, the small peak and recast layer were still remained, and thus additional removing

process is needed. Figure 4.31 (b) illustrates failed shape of micro channel with imbalanced trimming process, and thus right side on bottom was collapsed due to imbalanced laser beam trimming. In this section, to eliminate peak structure between both side wall, laser beam trimming was implemented with small number of laser scanning path without tilting motion. Though the peak was nearly eliminated by trimming, generated thick recast layer and burr was still remained, and thus post process for removing recast layer and burr should be carried out for precise vertical micro channel array.
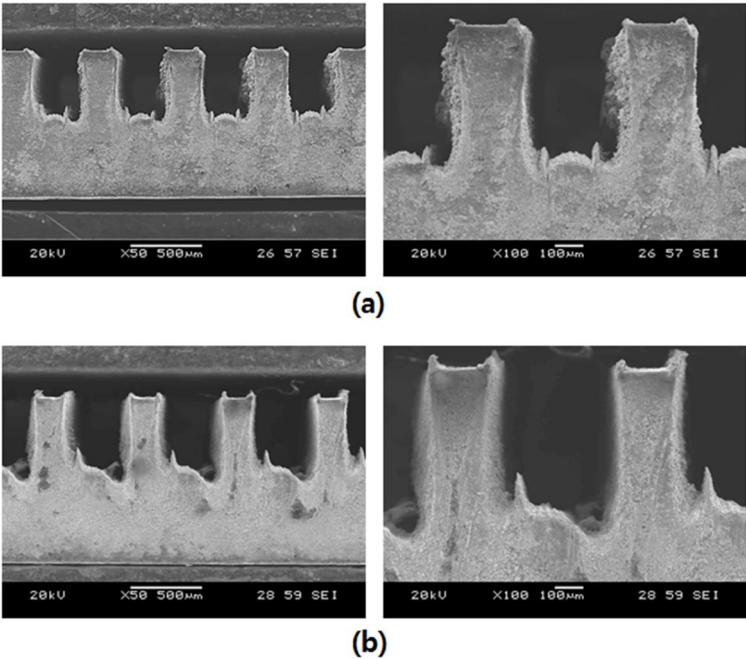
Figure 4.31 Fabricated vertical channel after trimming process, (a) precisely trimmed, (b) imbalanced trimmed micro channel

In this section, to fabricate vertical micro channel, multi−step laser beam machining was carried out. The tendency of resulted channel according to changing laser scanning path parameters was observed. Table 4.1 shows this tendency and guide line to fabricate micro channel and to control laser scanning path parameters.

Table 4.1 Tendency and guide line to fabricate micro channel and relation between laser scanning path parameters and geometric parameters
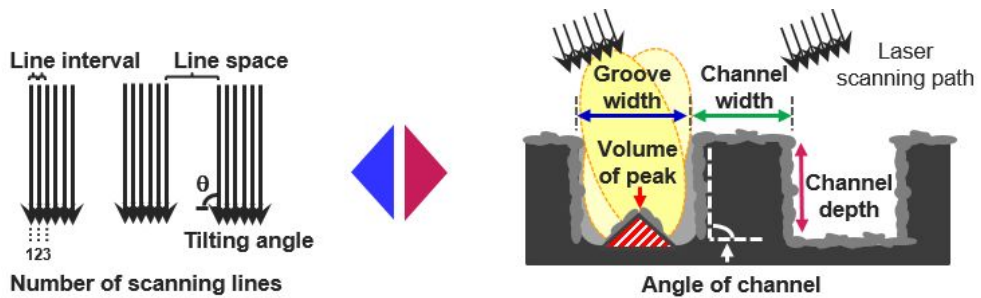
	Number of scanning lines (M) [lines]	Line interval (l) [μm]	Line space [μm]	Tilting angle (θ) [˚]
Control	Groove width Channel depth	Groove width Volume of peak	Channel width	Angle of channel
Detail	• $M\uparrow$ → Enlarged width → Converged depth (320 μm) • Recommend narrow bottom width → Efficient tilt process • To achieve large channel → Large powered LBM condition	• $l < 20$ μm → Steep slope (↑ θ for vertical wall) • $l = 20$ μm → Gradual slope (↓ θ for vertical wall) • $l > 20$mm → Failed overlap		• Angle of channel (90˚) → Tilting angle θ =15 ˚
Condition for vertical channel	16 (tilt) 11 (reverse tilt) 6 (trim)	20	200 (tilt) 350 (reverse tilt) 650 (trim)	15 ˚

Electrochemical etching

In previous sections, to fabricate vertical micro channel, sequential laser beam machining was carried out as combining varied laser scanning path and machining conditions such as tilting motion and trimming process. As implementing these sequential processes, the micro channel with vertical angle α, rough surface was textured by using pre-laser beam machining. The generated recast layer and burr could be problems for precision vertical micro channel machining, and thus these by-products should be eliminated to complete structuring. In this section, electrochemical etching was carried out to removing recast layer and burr. Electrochemical etching was generally used to treating surface quality as post treatment process as mentioned previous chapter 2. This process was implemented in atomic scale, which achieved smooth surface roughness and sharp cutting edge for precision machining. In case of electrochemical etching, there are various control parameters for achieving complete surface quality such as concentration of electrolyte, etch time, current density and gab between tool and workpiece. In this section, the etching machining time was chosen to observe tendencies of electrochemical etching process for post

treatment on resulted tungsten vertical wall micro channel after laser machining. Figure 4.32 illustrates the principle of eliminating process by using electrochemical etching. As shown in this figure, the generated recast layer was melted into electrolyte with atomic scale, and then hydrogen gas was generated on platinum electrode, and thus the vertical micro channel with smooth shape and sharp cutting edge was finally textured on tungsten.
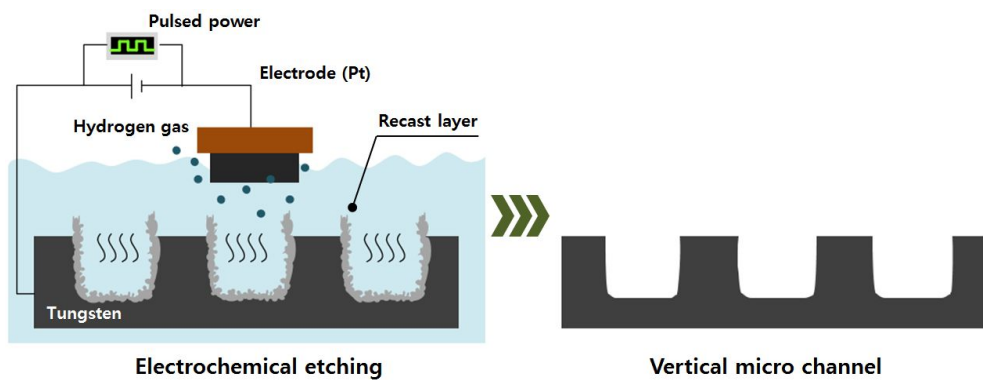
Figure 4.32 Electrochemical etching to eliminate generated recast layer and burr

In case of electrochemical etching, there are some parameters for affecting to machining quality such as gap between tool and workpiece, etching time, current density or applied potential and

duty ratio. In this research, electrochemical etching time was chosen to observe tendency of etching process. Figure 4.33 shows the results as changing electrochemical etching from 0 to 270 seconds. Figure 4.33 (a) shows the vertical micro channel after laser beam machining without electrochemical etching, the generated recast layer and burr were much pilled at side wall and little at top plane. Figure 4.33 (b) illustrates the result after electrochemical etching with 90 seconds, though recast layer and burr at top plane were almost eliminated, were not removed at side wall. Electrochemical etching has a tendency, active reaction at sharp tip or edge, and thus recast layer of edge region was eluted actively than plane side wall region. Figure 4.33 (c) shows the resulted vertical micro channel with appropriate etching time condition. The generated recast layer and burr at top plane and side wall was ideally eliminate. On the other hand, excessive electrochemical etching time caused collapsed structure. As shown in figure 4.33 (d) and (e), the edge was stubby and width of channel was narrow compared to previous etching conditions. For this reason, selection of appropriate etching time is very important for precision machining in electrochemical etching process.
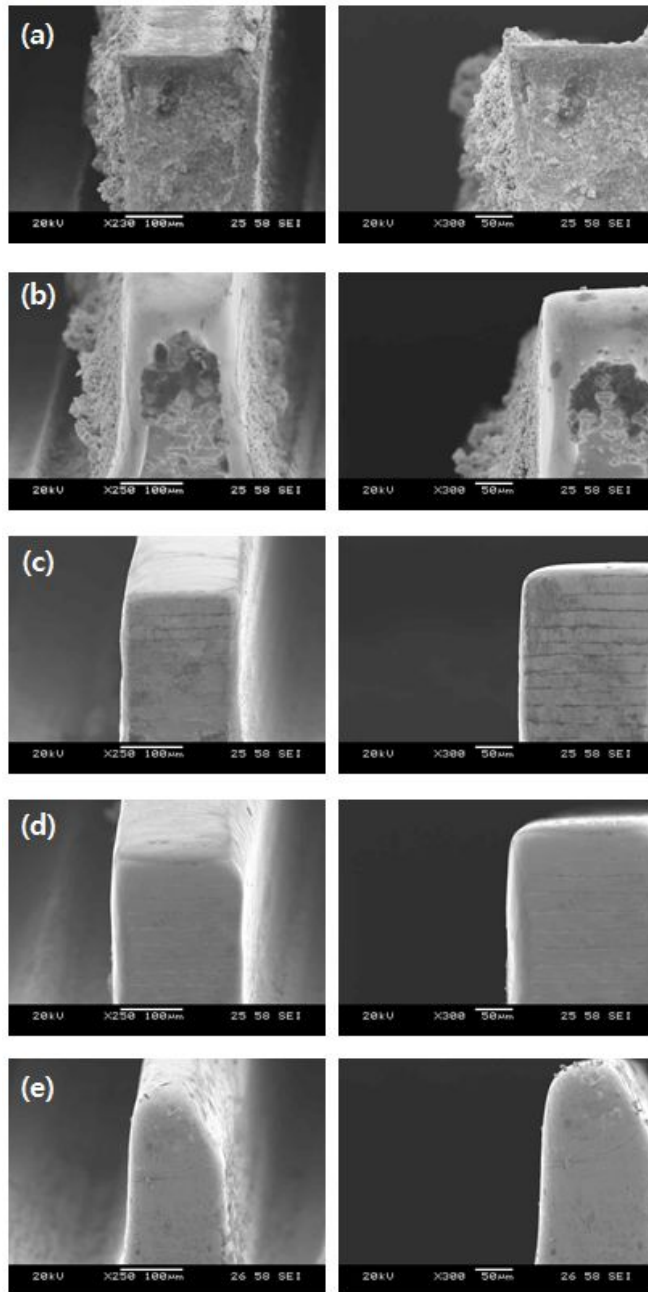
Figure 4.33 Electrochemical etching results as changing etching time, (a) only laser beam machined, (b) 90 s, (c) 150 s, (d) 210 s, (e) 270s

Figure 4.34 (a) illustrates finally finished shape of vertical micro channel as measuring SEM images. As shown in this figure, both side wall had vertical angle α and generated recast layer and burr were eliminated during electrochemical etching. Moreover, sharp cutting edge at vertical angle and uniform surface roughness quality on the top of micro channel could be observed. Different shape of channel with various width and depth also textured additionally. Figure 4.34 (b) shows the resulted anisotropic channel, which was fabricated by tilting process in laser beam machining and electrochemical etching. This directional textured surface can be used to specific function such as locking mechanism application. This locking application will be mentioned later chapter 5. Moreover, as using this newly suggested fabrication method, various shaped micro patterns were also textured on tungsten. Figure 4.34 (c) shows the female channel and male pin for directional locking which were fabricated by anisotropic structuring. Figure 4.34 (d) is textured micro dimple array which can be used as a lens mold. Figure 4.34 (e) and (f) show the resulted anisotropic micro channels which were textured with different laser scanning path.
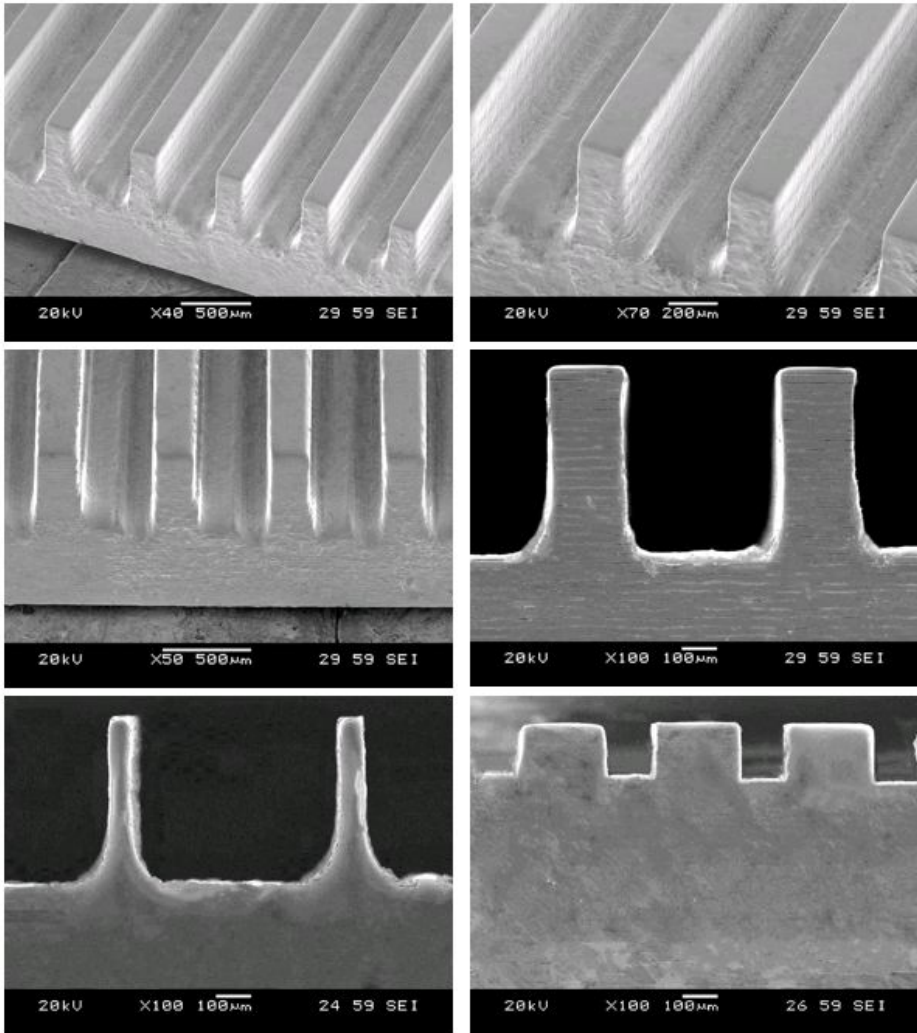
(a) Vertical channel

(b) Anisotropic channel

(c) Female/ male locking channel

(d) Micro dimple

(e) Wedged channel
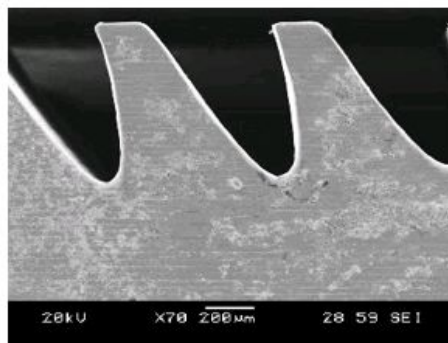
(f) Waved channel
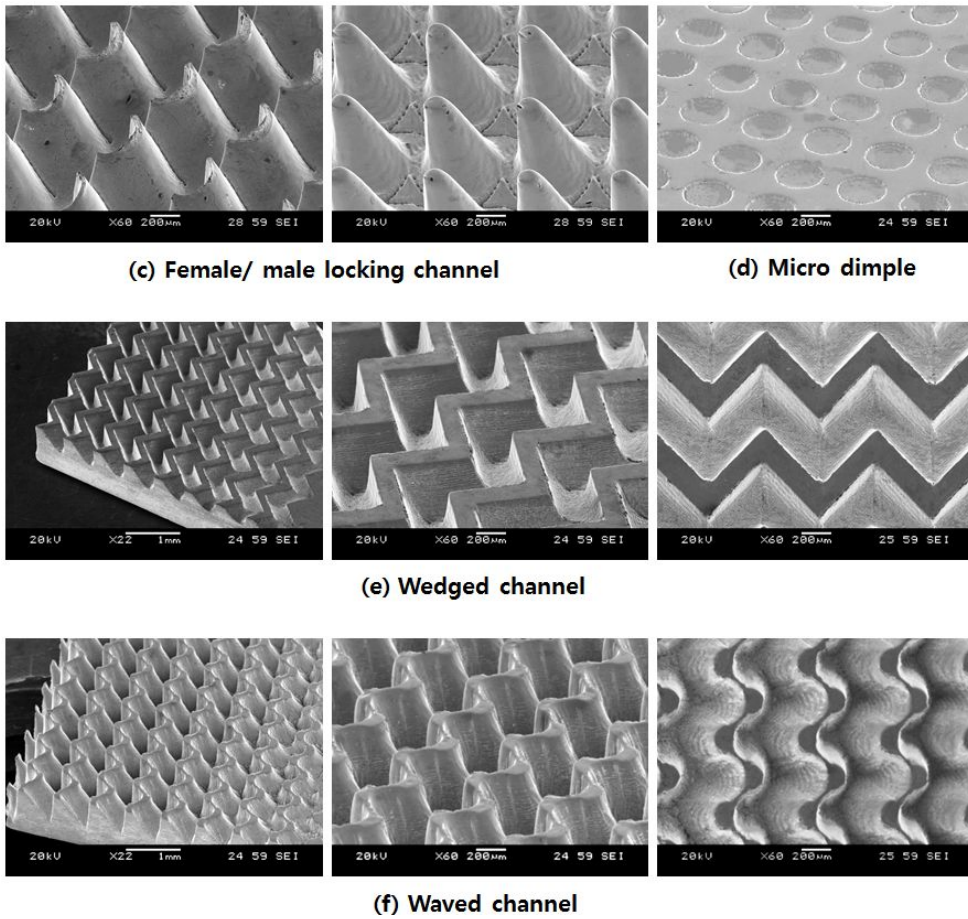
Figure 4.34 Final resulted vertical, anisotropic micro channel and other various shaped micro textured structures with different view

Electrochemical etching was carried out as a final step for vertical micro channel, however, the principle about elution process which was mentioned before chapter 2 should be verified. The recast layer of tungsten which was covered on original vertical micro

channel shape was known for tungsten oxide [21]. The distribution between original shape and tungsten oxide should be checked. Energy dispersive-spectroscopy (EDS) analysis was implemented to verify an atomic distribution between tungsten and its oxide recast layer. This analysis method can check out the atomic quantity percentage and atomic weight percentage, and thus a boundary line between fabricated original micro channel with pure tungsten material and generated tungsten oxide recast layer by laser beam machining can be observed. The mechanical polishing was carried out before implementing EDS due to precision cross sectional view demanding for precision analysis. Moreover, the metallographic etching should additionally be implemented, because the mechanical polished surface is not proper to precision analyze for EDS. In this research, the Murakami's reagent was used as etchant on tungsten surface to carrying out metallographic etching, which the components of the reagent are noted in formula 4.13 [37].

Murakami's reagent

$$10 \text{ g K}_3\text{Fe(CN)}_6 + 10 \text{ g NaOH} + 200 \text{ ml H}_2\text{O} \quad (4.13)$$

The metallographic etching was carried out at room temperature for 15 s. Figure 4.35 (a) shows the polished tungsten surface immediately after mechanical polishing, and the tungsten surface after metallographic etching is shown to figure 4.35 (b).

(a) Polished tungsten

(b) Metallographic etched tungsten (Murakami's reagent)
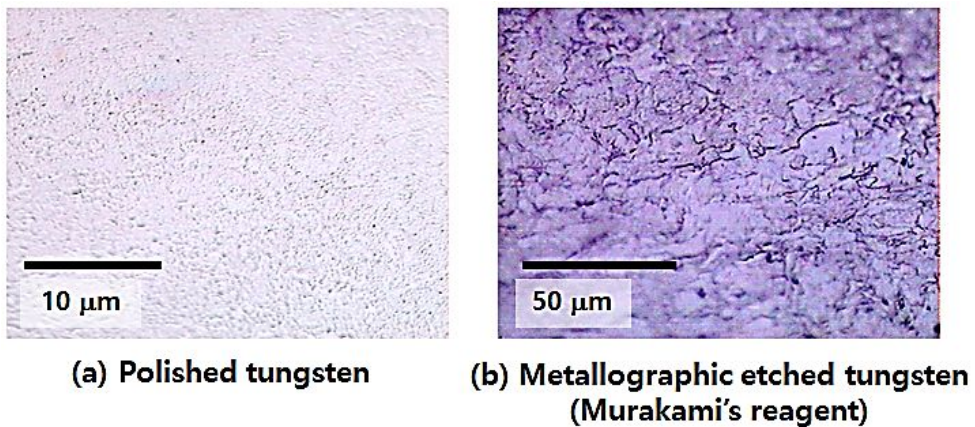
Figure 4.35 Optical images of the tungsten surface after the mechanical polishing and metallographic etching process, (a) polished tungsten surface, (b) tungsten surface after metallographic etching with Murakami's reagent

EDS analysis was carried out on metallographic etching tungsten micro channel surface. Figure 4.36 illustrates the resulted EDS and measured surface with cross sectional view. Figure 4.36 (a) shows

the experimental result from the vertical micro channel structuring process. The oxygen EDS map indicates that the cross-section of micro channel is distinguished into three areas with significant differences in atomic percentage distributions of oxygen and tungsten. While the original shaped area (blue-colored) had 0-20 at % of oxygen, the circumference (red-colored) and the outer area (green-colored) had 21-40 at % and 41-60 at % of oxygen, respectively. As for tungsten, the atomic percentage distribution has shown the opposite result of oxygen at each area (81-100 at % W in the original shaped section, 61-80 at % W in the circumference, and 41-60 % in the outer). The EDS analysis results imply that the recast layer of tungsten oxide had been generated from laser beam machining and then piled on the outer surface of the micro channel. Towards the inner area of core vertical channel structure, the rate of pure tungsten increased whereas the oxygen rate decreased. The atomic distribution maps for the anisotropic shaped micro channel structures (figure 4.36 (b)) fabricated from different scanning paths of laser beam and tilting motion showed similar appearance with that of the vertical micro channel structure.

Table 4.2 details the average atomic percentages of tungsten and oxygen for each cross section area illustrated in figure 4.36. Each average atomic percentage value was measured at the points marked with arrows in figure 4.36 (b). In the core area, the average oxygen atomic percentage was below the minimum 10 at % while tungsten was higher than 90 at %. The average oxygen atomic percentage at the circumference was found to be 30-36 at % and tungsten was 64-70 at %. In the outer area, the average oxygen atomic percentage was found to be 54-56% and tungsten was 44-46%. From those results, it can be concluded that the core of the micro channel structure in original shape had been covered with a recast layer of tungsten oxide, as previously illustrated in figure 2.9. This study has specialty in the point that the tungsten core structures and the recast layer of tungsten oxide were distinguished clearly by implementing EDS mapping analysis of atomic distribution. Furthermore, we could achieve shape-controlling micro channel by revealing the tungsten core structures.
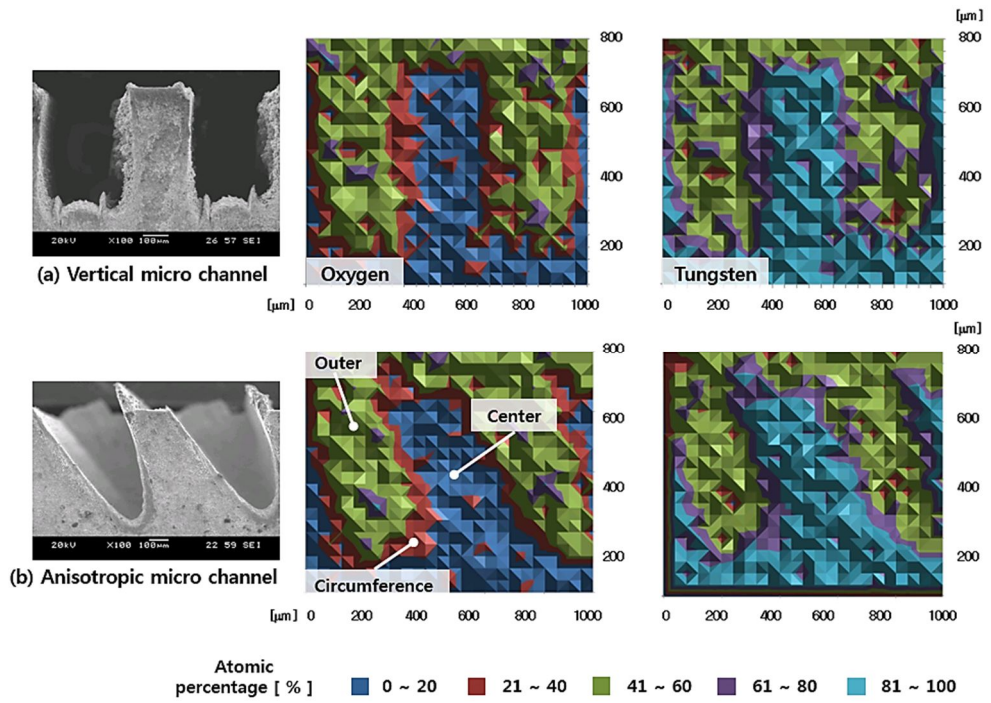
Figure 4.36 EDS mapping result with atomic distribution process of textured micro channel, (a) vertical shaped, (b) anisotropic shaped micro channel

Table 4.2 Average atomic percentage on the cross sectional surface of each micro channel

Atom	Vertical		Anisotropic	
	Oxygen	Tungsten	Oxygen	Tungsten
Center	9.205	90.795	9.855	90.145
Circumference	36.112	63.888	33.719	66.281
Outer	54.683	45.317	56.426	43.574

4.3 Micro pin

Near-pin shaped micro metal structures have been used in a wide range of applications, which require executing-specialized functions. A micro pyramidal structure can increase light extraction to improve the efficiency of LED flux utilization [38], and a metal micro pin is used during an electroencephalogram to measure brain and neural system signals [39]. A nano scale surface structuring study was carried out to assess anti-reflective functionality [40], and a micro pin-shaped structure was fabricated to separate oil from water [41]. In spite of their versatility, however, most of micro pin structures suffer from relatively low material stiffness and poor mechanical strength, which generally result from inherent material properties and structural weakness [42]. The use of high strength metallic materials such as tungsten, titanium and stainless steel can be considered as an alternative to improve those drawbacks. It will promise the high durability and reliability of micro pin structures so that they can withstand harsh environments.

In this paper, we propose a hybrid micro structuring technology to precisely control the shape of a tungsten micro pin array. The problems due to the limitation of material were resolved by using

high strength tungsten as workpiece material. As mentioned in previous chapter 2, which consists of two successive steps as follows: (a) rough−shaping of a micro pin structure via laser beam machining with pre−defined scanning path, and (b) electrochemical etching to reveal the original micro pin structure. Laser beam machining enabled to fabricate various shapes of micro pin arrays with high throughput. Subsequently electrochemical etching was carried out for removing generated recast layer to achieve micro structure with sharp cutting edges. This new method is thought to be a solution to improve surface quality problem that was caused by laser beam machining. In addition, shape control of tungsten micro pin structure was investigated depending on the scanning path of laser beam and electrochemical etching condition. The formation of recast layer during the process was characterized by EDS analysis.

Laser beam machining

In this section, the technology for structuring various size and polygonal shaped micro pin will be suggested. As shown in previous section, the original shape of core was defined by pre-determined laser scanning path. The generated recast layer during laser beam machining, however, covered the original shape that was impossible to observed precision structure. For this reason, electrochemical etching was carried out for eliminating covered recast layer. In this section, micro pin array was fabricated by using similar machining process, and thus various shape of micro pin was textured and controlled.

Number of lines

The number of lines was chosen as a parameter for shape control of micro pin structure. As mentioned in previous, the number of lines is related to thermal energy aggregation, heat overlapping and thermal absorption rate. For this reason, to fabricate various shape of micro pin, this parameter tendency test should be implemented. Figure 4.37 shows the controlled parameters during laser beam

machining for structuring micro pin array. Basic parameters are same to micro channel cases, however, group of lines was crossed with grid pattern due to separating each micro pin. In case of structuring micro pin array, the line space was set to 50 μm gap between each group of lines as reflecting the result of figure 4.24 (a) due to its sharp tip for pin.
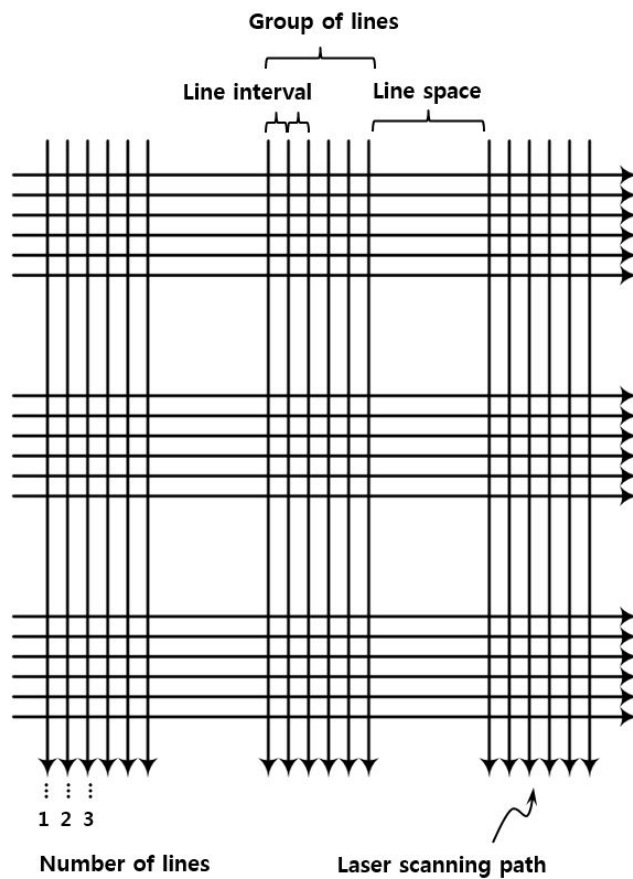
Figure 4.37 Parameters during laser beam machining for structuring micro pin array

Figure 4.38 illustrates the resulted micro pin array with varied number of line condition during laser beam machining. As increasing number of scanning path, base width of micro structure was wider due to increase of thermal energy aggregation and absorption, and the resulted depth was also deeper as same thermal ablation theory. The resulted depth, however, was deeper than micro channel case due to crossed area to separate each micro pin array. In this crossed region, thermal absorption was the most highest in laser scanned area.

(a) 6 lines   (b) 11 lines

(c) 16 lines   (d) 21 lines
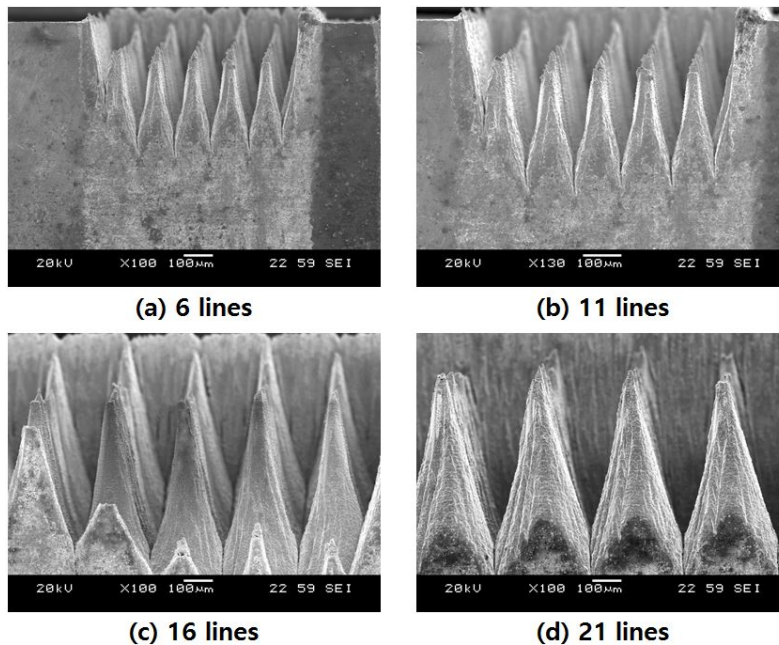
Figure 4.38 Textured micro pin array as changing number of laser line scanning path

Line interval

In case of micro channel, line interval was related to width and depth of textured structure, and shape of the textured slope also was controlled. The value of width is important parameter to decide efficiency of micro channel and micro pin application. For example, the gap between each channel is related to performance of micro fin channel for heat transfer. Moreover, the width between each micro needle affects to efficient skin penetration with low pressing force. Resulted gap between each micro pin was measured as changing line interval in this section. Figure 4.39 shows the textured micro pin array by using laser beam machining with varied value of line interval. As increasing line interval value, the resulted width was wider. However, in case of 30 μm (figure 4.39 (c)), though the value was highest, result was not micro pin but micro conical shape due to lack of overlapping between laser beam scanning path. For this reason, thermal energy aggregation and absorption was also insufficient. The resulted slope angle was not much different between 10 μm and 20 μm line interval as compared with micro channel case.
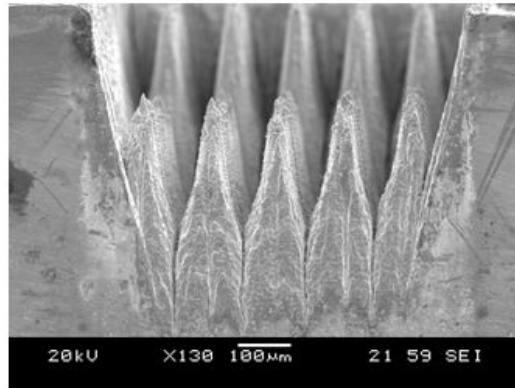
(a) 10 μm line interval
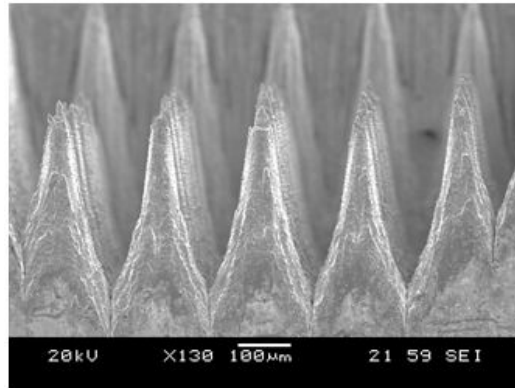
(b) 20 μm line interval
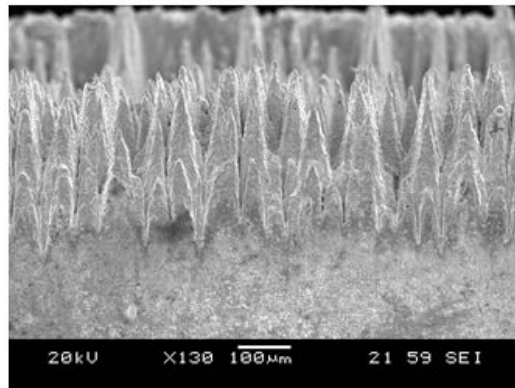
(c) 30 μm line interval

Figure 4.39 Textured micro pin array as changing line interval value

Laser scanning path for various pin shape

In previous section, we studied the structural tendencies of micro pin array as changing defined parameter of laser beam scanning path. In this process, a micro pin array was fabricated on a 1-mm thick tungsten plate using laser beam machining. Figure 4.40 illustrates the formation of micro pin array in a specific shape by controlling a scan path. When a focused laser beam is applied along a pre-defined path, the material on the scanned region (Zone A) would be removed by thermal ablation. The Gaussian-mode laser beam generally causes a tapered slope on the workpiece in ablation-dominated material removal process, and thus the remained part (Zone B) has sharp edge around the structure. In this principle of micro-structuring by laser beam machining, micro pin arrays with sharp tips can be fabricated from a crisscrossed laser scanning path. Moreover, proper-controlling of the scanning path enables to achieve micro pin structures in a variety of shapes such as such rectangle, triangle and hexagon. Nevertheless, it was expected from our previous study [21] that the micro pin array would have conical shape of structures due to a recast layer on the surface, which is inevitably produced during the laser beam

machining process. Hence a proper eliminating process to achieve the original shape of micro pin structures is required, and it will be detailed in the following section.
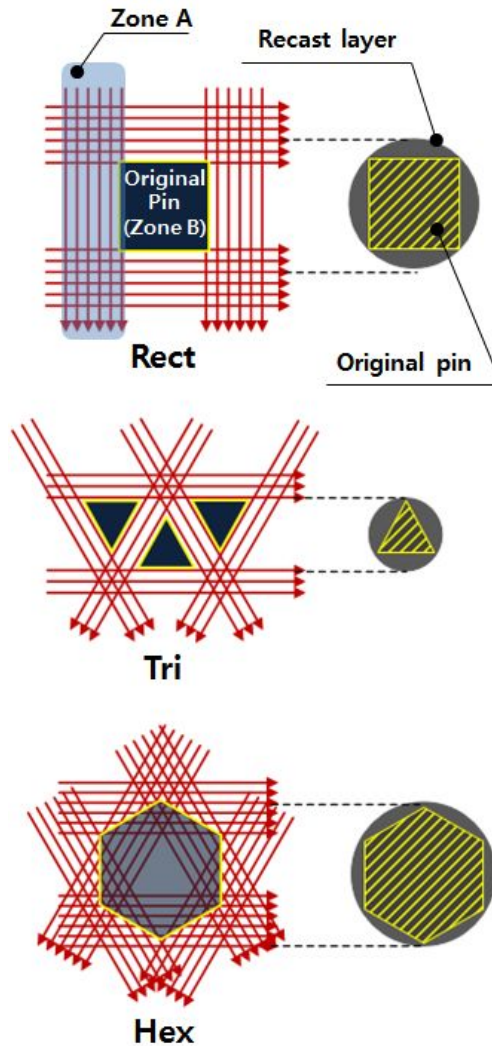
Figure 4.40 Fabrication of tungsten micro pin arrays in different shapes using laser beam machining with scanning path control

As using this pre-determined laser scanning path, the conical micro pin array was textured on tungsten. Figure 4.41 shows this textured result that conical micro pin array was laser machined by using rectangular pre-determined laser scanning path. . The fabricated micro pin on 1 mm thickness of tungsten was found to be 200 μm in diameter and 550 μm in height. The SEM images show that laser beam machining resulted in the formation of conical shape of micro pin structures with rough surfaces rather than polypyramidal shape of ones that were originally intended. This phenomenon is thought to be due to the recast layer concealing the core tungsten structures with sharp edges, which has commonly occurred in laser beam machining process based on thermal ablation. At this point, it is considerable that the tungsten micro pin structure had a significantly different shape than the stainless steel one which had been reported in our previous study [14]. Because stainless steel had as connatural characteristics of pilling chromium recast layer and dross during laser beam machining process, micro pin structures with rounded tips were formed over the workpiece surface. On the other hand, the connatural characteristic of tungsten was found to drive a different shape of structure after laser beam

115

machining. Thermal ablation had mostly melted and evaporated the tungsten exposed to laser beam, and the remained recast layer was accumulated on the bottom side of the workpiece. As a consequence, micro pin structures with sharp tips were formed below the workpiece surface. Such characteristic of tungsten in laser beam machining indicates that it can be the better solution to achieve micro pin structures with sharp tips as compared to stainless steel, even not considering the existence of recast layer on the surface.
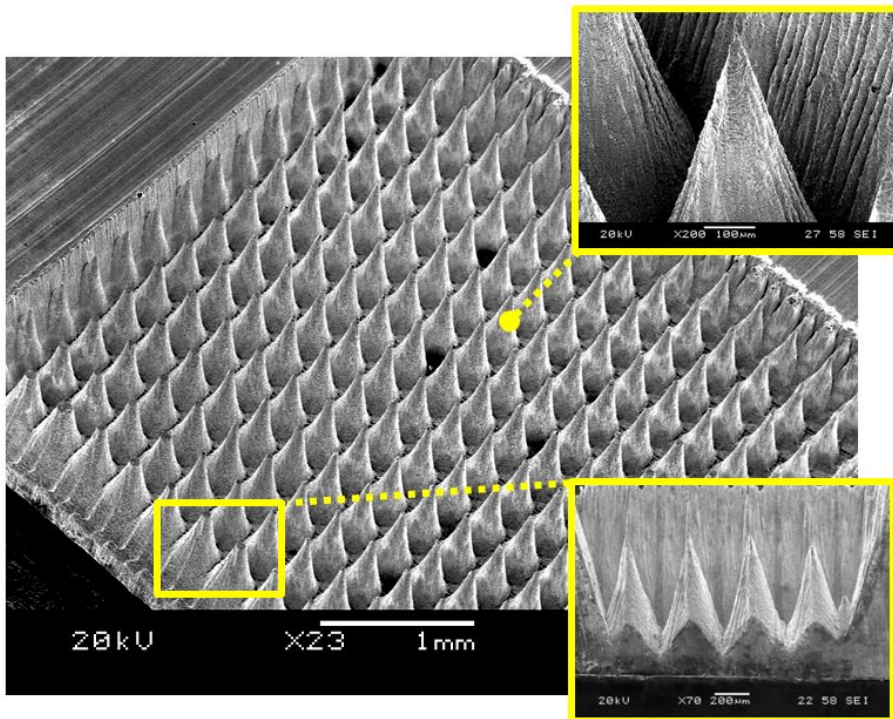
Figure 4.41 SEM images of the fabricated conical micro pin array after laser beam machining process

116

Electrochemical etching

In this study, electrochemical etching was used to remove the recast layer and burr on the tungsten micro pin structures after laser beam machining process as same to micro channel case. Electrochemical etching which is widely used to post treatment of surface also promises high throughput process as it can be simultaneously implemented on the entire substrate immersed into electrolyte. Moreover, it is beneficial for achieving sharp edge on the tip and symmetric cone shape that pursues feature of micro pin array as its isotropic dissolution characteristic [43].

As shown in figure 2.9 (a), the micro pin structure was made up of a tungsten core in an original shape and a recast layer generated by laser beam machining. At this stage, the tungsten pin core was completely concealed by the recast layer, and thus the original shape of micro structure could not be observed. When electrochemical etching was carried out, as illustrated in figure 2.9 (b), the recast layer would be eluted into the electrolyte so that the original core could be revealed. In this study, pulsed potential was applied between the anode connected to the workpiece and the cathode of platinum electrode to elute as same to micro channel

case. The accumulated tungsten oxide recast layer would be eluted when pulsed potential was applied. As a result, the original shape of the pure tungsten pin fabricated from the laser scanning path could be observed.

To characterize electrochemical etching to pre-textured micro pin array, parameter test as changing etching time was implemented. Figure 4.42 illustrates the electrochemical etching results of shape of micro pin that was laser machined with square laser scanning path. As shown in figure 4.42 (a) only laser beam machined micro pin without electrochemical etching process had rough conical shaped surface with sharp tip, and relatively high height of micro pin. On the other hand, electrochemical etched micro pin arrays were gradually stubby and smooth as increasing etching time (figure 4.42 (b, 15 S), (c, 30 s)). In case of 45 s etching time (figure 4.42 (d)), though increasing electrochemical etching time, the resulted micro pin had sharp edge on tip as well as around an each pin, and thus polygonal square micro pin array (original core shape) which was pre-determined in laser beam machining step was finally exposed from recast layer and burr. The resulted in figure 4.42 (e) had still sharp edge on tip and around the pin,

118

however, symmetry of structure was collapsed due to excessive electrochemical reaction. In case of 75 s etching time (figure 4.42 (f)), the edge of square shaped of micro was entirely collapsed and had stubby shape again, and wave line due to elution process on surface was also observed. For this reason, proper etching time should be applied for precision electrochemical etching.
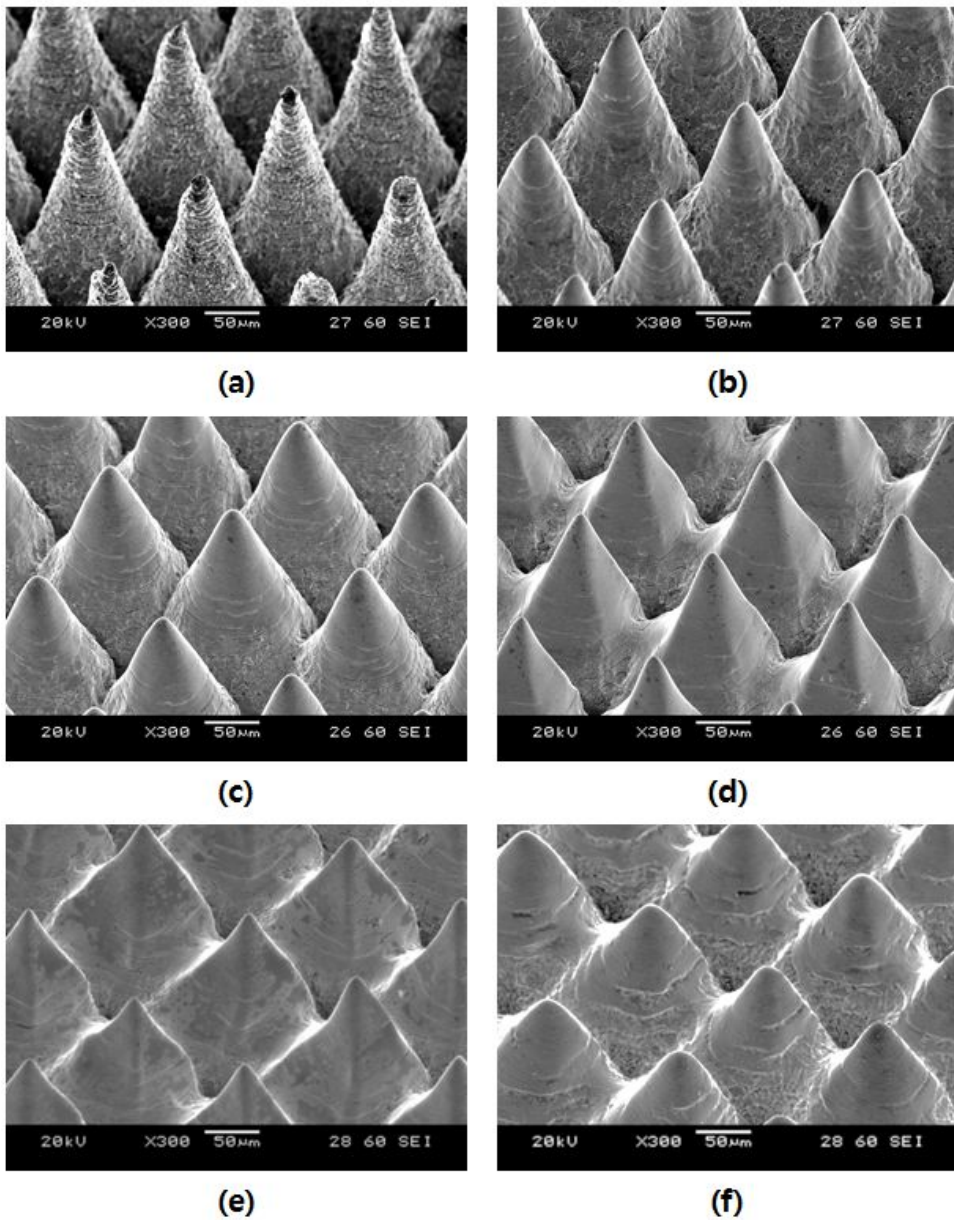
Figure 4.42 Electrochemical etched micro pin array as changing etching time, (a) no etched, (b) 15 s, (c) 30 s, (d) 45 s, (e) 60 s, (f) 75 s

Figure 4.43 shows the SEM images of micro pin arrays after the electrochemical etching process to remove the recast layer. As the recast layer had been eluted into electrolyte, the tungsten core structure with a sharp edge and smooth surface was revealed from the conical shape of micro pin structure with a rough surface by laser ablation. We consequently achieved various shapes of micro pin arrays such as square, triangle and hexagon, which had been pre-determined from the laser scanning path control. We also found that the rectangular and triangular shape of micro pin structures had sharp tips and cuttings edges while the hexagonal shape of ones had relatively stubby tips and edges. It implies that the micro pin structure in less-sided pyramidal shape would be more desirable for achieving sharper tips and cutting edges in comparison to the one in near-circular shape.

To sum up, the micro hybrid technology combining laser beam machining and electrochemical etching processes is highly beneficial for the fabrication of micro pin array with sharp cutting edges and tips using high strength tungsten material. We expect that it might offer an efficacious aid especially in the field of bio-medical industry. For example, a painless micro needle for an

intradermal injection which generally requires high sharpness and easy penetrativeness can be manufactured in a simple and fast way using the micro hybrid technology.
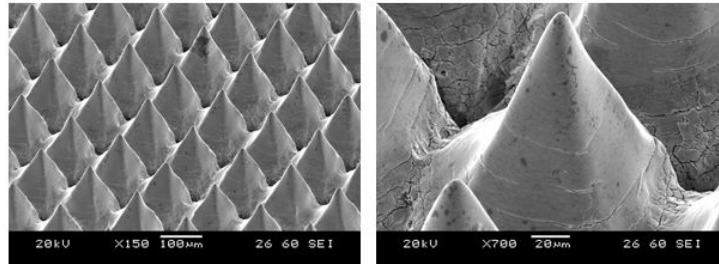
(a) Quadrangular micro-pin array
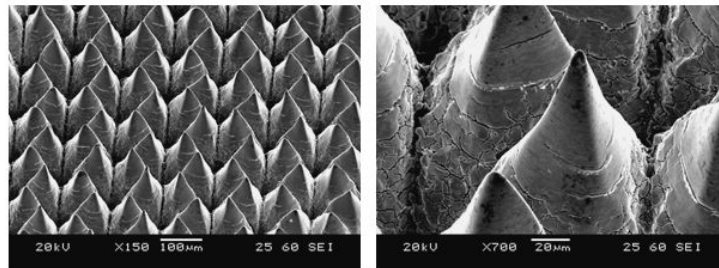
(b) Triangular micro-pin array
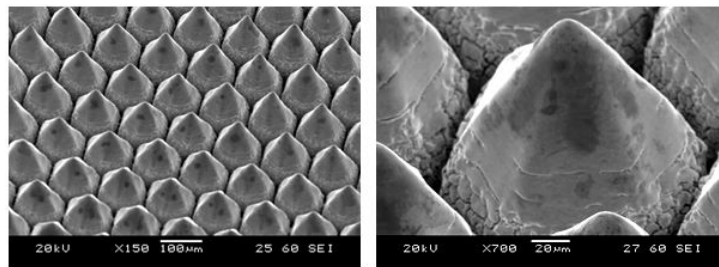
(c) Hexagonal micro-pin array

Figure 4.43 SEM images of fabricated micro pin arrays in various shapes using laser beam machining and electrochemical etching, (a) quadrangular, (b) triangular, and (c) hexagonal−pyramidal micro pin array

122

The formation of recast layer occurring in the laser beam machining process was characterized using EDS analysis. Prior to the EDS mapping process, the cross-sectional surface of micro pin structures in the normal direction was prepared from mechanical polishing process followed by metallographic etching with Murakami's reagent [37].

Figure 4.44 shows the cross-sectional view of SEM images and EDS mapping for different shapes of micro pin structures after mechanical polishing and metallographic etching. Figure 4.44 (a) illustrates the experimental result from the square scanning path of laser beam. The oxygen EDS mapping result indicates that the cross-section of micro pin is distinguished into three areas with significant differences in atomic percentage distributions of oxygen and tungsten. While the core area (blue-colored) had 0-20 at % of oxygen, the circumference (red-colored) and the outer area (green-colored) had 21-40 at % and 41-60 at % of oxygen, respectively. As for tungsten, the atomic percentage distribution has shown the opposite result of oxygen at each area (81-100 at % W in the core, 61-80 at % W in the circumference, and 41-60 % in the outer). The EDS analysis results imply that the recast layer of

123

tungsten oxide had been generated from laser beam machining and then piled on the outer surface of the micro pins, mainly concentrated on the bottom of the micro pin structure. Towards the inner area of core pin structure, the rate of pure tungsten increased whereas the oxygen rate decreased. The atomic distribution maps for the triangular and hexagonal shaped micro pin structures fabricated from different scanning paths of laser beam showed similar appearance with that of the quadrangular−pyramidal structure (Figure 4.44 (b) and (c)).

Table 4.3 details the average atomic percentages of tungsten and oxygen for each cross section area illustrated in figure 4.44. Each average atomic percentage value was measured at the points marked with arrows in figure 4.44 (b). In the core area, the average oxygen atomic percentage was below the minimum 10 at % while tungsten was higher than 90 at %. The average oxygen atomic percentage at the circumference was found to be 30−35 at % and tungsten was 65−70 at %. In the outer area, the average oxygen atomic percentage was found to be 50−55% and tungsten was 45−50%. From those results, it can be concluded that the core of the micro pin structure in original polypyramidal shape had been

covered with a recast layer of tungsten oxide, as previously illustrated in figure 2.9. According to the research by Kawakami, Y. *et al.* [21], the atomic existence of tungsten and oxygen after laser beam machining process on a tungsten workpiece could be observed by Auger depth−profiling analysis. This study has specialty in the point that the tungsten core structures and the recast layer of tungsten oxide were distinguished clearly by implementing EDS mapping analysis of atomic distribution. Furthermore, we could achieve shape−controlling micro pin arrays by revealing the tungsten core structures. Figure 4.45 illustrates SEM images of the cross sections for micro pin array in each shape fabricated from the micro hybrid process. Figure 4.45 (a) shows the square micro pin array, (b) shows the triangle micro pin array, and (c) shows the hexagon micro pin array after laser beam machining followed by electrochemical etching. The EDS analysis results on these structures confirmed that the tungsten core pin structure in original shape had been revealed completely.
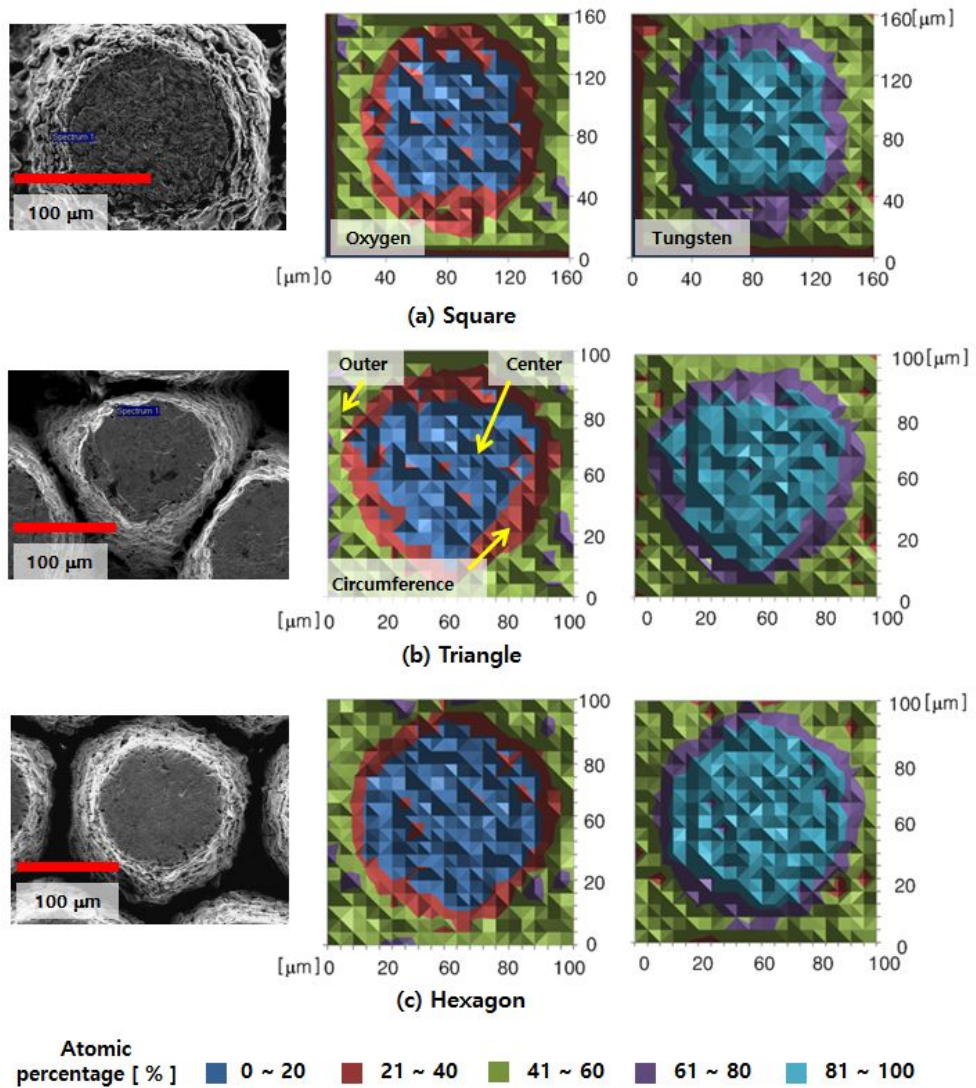
Figure 4.44 Atomic percentage EDS maps showing oxygen and tungsten rates on the cross sectional surfaces of micro pin structure fabricated with different scanning paths in laser beam machining, (a) micro pin array with a square scanning path, (b) a triangle scanning path, and (c) a hexagon scanning path.

Table 4.3 Average atomic percentage on the cross sectional surface of each micro pin array

Average Atomic Percentage

Atom	Square		Triangle		Hexagon	
	Oxygen	Tungsten	Oxygen	Tungsten	Oxygen	Tungsten
Center	9.210	90.790	9.023	90.977	8.761	91.239
Circumference	33.381	66.619	31.654	68.346	30.618	69.382
Outer	54.995	45.005	53.689	46.311	51.148	48.852
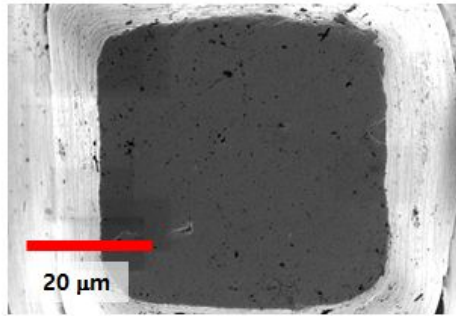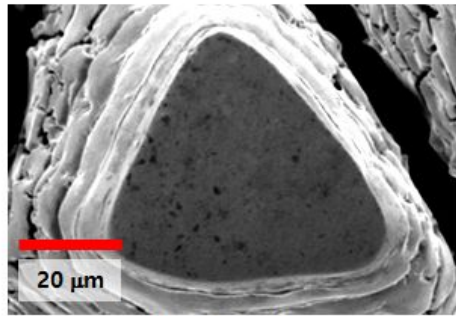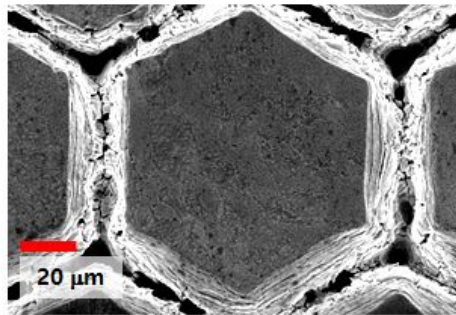
Figure 4.45 SEM images of the cross sectional view for micro pin structures in different shapes, (a) array with square scanning path, (b) array with triangle scanning path, and (c) array with hexagon scanning path.

A novel method to machine hard-to-cut metallic materials is demonstrated at the micro meter scale. Micro hybrid technology that combines laser beam machining and electrochemical etching processes is capable of fabricating different shapes of tungsten micro pin arrays with sharp cutting edges. The original shape of each pin was pre-determined by the designated laser scanning path. And the various micro pin shapes were revealed using electrochemical etching. During this process, the recast layer on each micro pin was eluted into electrolyte to reveal the square, triangle and hexagon micro pins. The EDS analysis verified that the recast layer was tungsten oxide and each original pin was tungsten. The fabricated tungsten micro pin arrays with various shape of laser scanning path were polished and metallographic chemical etching was carried out on the polished micro pin surfaces. The EDS atomic distribution analysis of cross section of each array confirmed the relative arrangement of tungsten and oxygen, reflecting the shape of the laser scanning path. Moreover, the shape controlled pins were polished to allow cross-sectional observation of the shapes.

In comparison with the existing methods for micro machining which

129

include EDM, ECM, LBM as well as MEMS process, the micro hybrid technology promises structural stability as using tungsten hard−to−cut material. The shape of fabricated micro pin is easily controlled by using this new technology. It improves the cost and time consuming problem of the previous method for shape control. The proposed combined manufacturing process has much potential for many applications. With regard to these advantages, we believe that shape controlled micro pin can meet broad applications in automotive [44], aerospace [45], medical [46] and nuclear industries [7].

Chapter 5

Application of textured surface

In this chapter, the textured tungsten surface by using suggested micro hybrid machining was used to specific function such as locking and micro needle. As implementing functional test for application, the versatility of textured tungsten surface can be verified. Moreover, the tendencies about each application as changing the textured structure were observed, and thus these studies will make indicator for achieving micro locking and needle applications.

5.1 Locking

Though application of tungsten is various, it is still not used actively due to difficulty to machine. For this reason, joining process between tungsten and other material is on the rise issue due to

difficulty of machining. Tungsten could be welded to itself or other material. Welding is a relative simple method in comparison to other joining process, however, the resulted welded region is always recrystallized, and thus it has brittle property. Even though the use of a filler rod such as W－Re, it cannot eliminate the brittle property of the tungsten due to heat affected zone [47]. Brazing is other method for joining tungsten to itself and other materials. Tungsten and other materials can be joined as melted bonding material in high temperature condition. It has some limitations that brazing should be done in a strictly controlled temperature condition due to preventing oxidation and its bonding efficiency. Brazing process is used to joining between tungsten monoblock and CuCrZr tube in plasma facing component (PFC) for ITER nuclear fusion reactor. The PFC, facing to high temperature on plasma state, suffers from crack and torsion as difference of thermal expansion rate between tungsten and CuCrZr [48]. This problems need to be surely resolved to achieving efficient nuclear fusion power generation. Diffusion bonding can be other solution for tungsten joining. This process uses atomic diffusion joining between tungsten to itself and other material under near－melting point temperature and pressure. It has

advantages that are relatively low thermal stress and deformation. Nevertheless, the interfacial contact region cannot be precisely controlled, generated porous structure that makes bonding strength weaken [49]. As considering various feature of tungsten joining method, mechanical locking can be a best solution for joining tungsten. Tungsten could also be textured to mate to itself and specific function as fastening mechanism.

In this dissertation, we suggested mechanical locking micro sized tungsten surface as using hybrid machining. In terms of tungsten joining, the suggested new technology can achieve mechanical locking by structuring grooved micro structure on surface. This convenient approach resolves the previous thermal defects such as torsion between materials and weaken bonding strength due to porosity. Moreover, as carrying out electrochemical etching in suggested new machining method, recrystallized brittle region can be strengthen due to thermal process. In addition, relative compact new machining system can be an advantage in comparison to previous complex system with thermal and pressure control equipment.

Anisotropic locking surface

To verify locking functional application, anisotropic shaped micro channel array was fabricated. These anisotropic shaped channels with various slope angle of the channel were textured by using tilting process as previous mentioned process in chapter 4.2 micro channel section. Each textured micro channel was fabricated by using laser beam machining with tilting process and electrochemical etching. The textured micro channel was set on 1 mm thickness tungsten with 5x5 mm^2 width area. Figure 5.1 shows the resulted textured anisotropic micro channel arrays which were used during directional locking force measurement. The resulted slope angles α of anisotropic micro channel were from 100 ° to 132° . As using these anisotropic channels, directional locking forces were measured to achieving locking application.
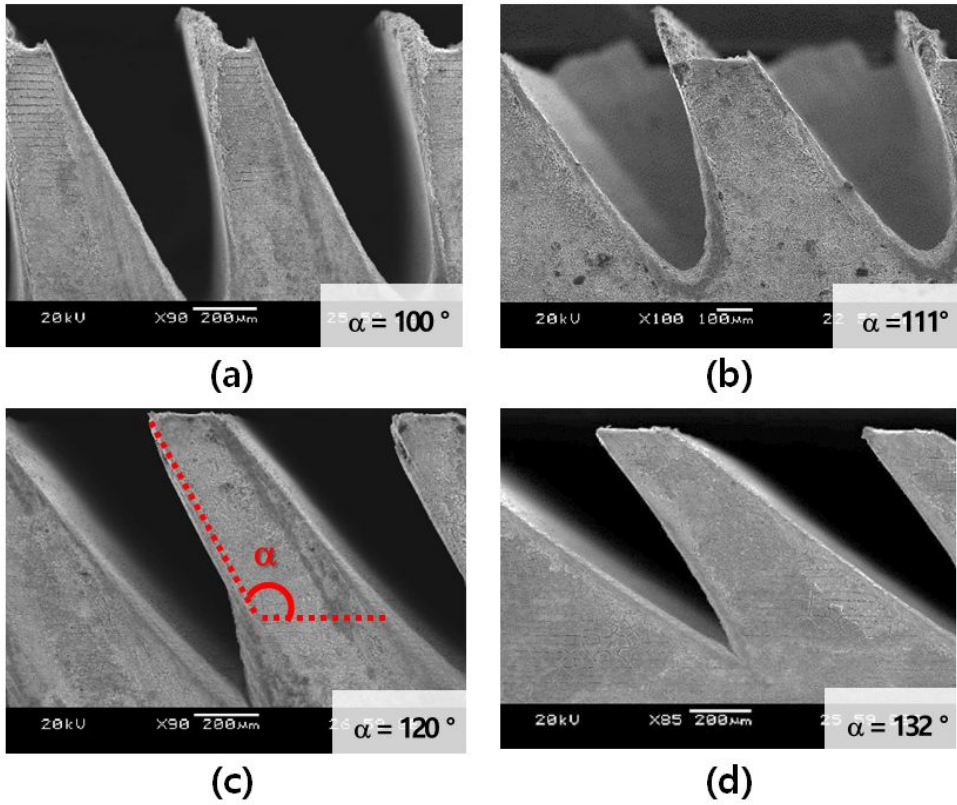
Figure 5.1 SEM images of textured anisotropic micro channel for locking with various slope angle of channel

Measurement system

Figure 5.2 illustrates analysis system for measuring directional locking force of each micro channel. Overall measuring system was set on X, Y, Z micro feed stage with 0.1 μm/count resolution. Anisotropic locking force was measured by using single point load cell (BCA 30 kgf, CAS korea) and amplifier (LCT−II, CAS korea). In this study, a pair of micro channel was used for measuring directional locking force, one micro channel was fixed to jig, another was anisotropic locked on fixed one. Figure 5.3 shows the principle of anisotropic locking. A micro channel that was posited on fixed one, was connected to load cell by wire, and thus directional locking force was applied by pulling the wire. Figure 5.4 shows the principle to measure directional locking force. In case of measuring horizontal directional locking force F_D (figure 5.4 (a)), a textured anisotropic micro channel was set to horizontal jig on base, and the load cell was set on the Z axis, and thus as moving Y directional stage, a pair of anisotropic locked micro channels was applied force until fracture. In case of measuring angled force, as shown in figure 5.4 (b), angled directional locking force F_D was applied to micro channel by using pulley. The height of pulley can be controlled by

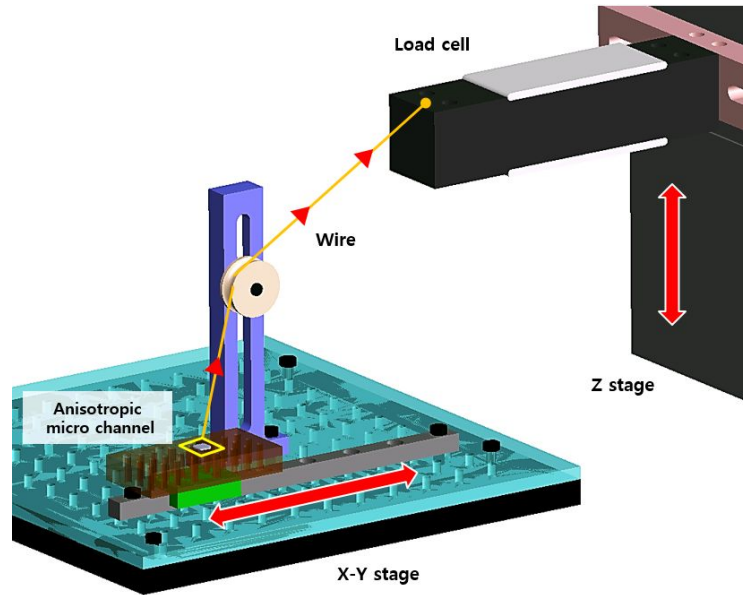vertical jig, and thus directional force applying angle β also can be controlled.

Figure 5.2 Measurement system for directional locking force

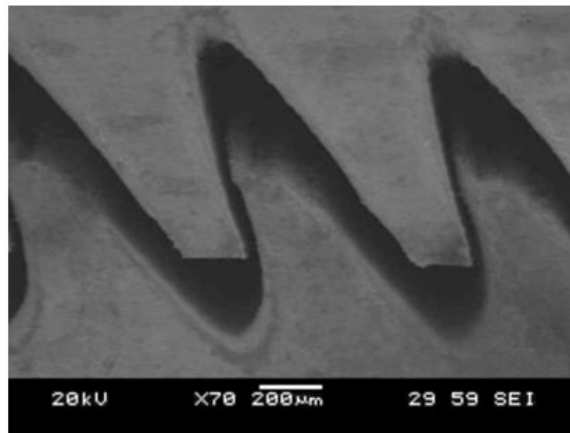Figure 5.3 Principle of directional locking as using a pair of anisotropic micro channel
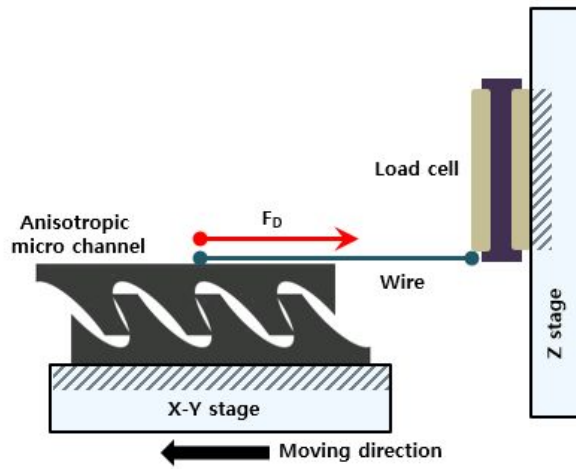
Figure 5.4 Principle to measure directional locking force until fracture of anisotropic micro channel, (a) horizontal, (b) angled directional locking measurement

Measured locking force

As using the prepared system (Figure 5.2), directional locking force was measured as various slope angles of micro channel and changing applied pull force. Figure 5.5 shows the measured results about directional locking force on horizontal plane without angled pull ($\beta=0°$). The directional locking force until fracture had difference between the slope angled shapes of micro channels. In case of anisotropic channel, especially $100°$ slope angle α of anisotropic channel the directional locking force until fracture was higher than isotropic micro channel due to a tendency to deliver main locking force to base of micro channel. For this reason, overall locking force applied to base of channel due to its anisotropic characteristic, and thus fracture was occurred to base of anisotropic channel. Figure 5.6 (b) illustrates this phenomenon. On the other hand, the fracture result of isotropic micro channel (figure 5.6 (a)) was differ, the fracture point was posited to middle of channel, and thus measured directional locking force was lower than anisotropic case.

Figure 5.7 shows the measured directional locking forces of opposite pull direction without angled pull ($\beta=0°$). Red line of

graph means the resulted locking force in unlocking direction. In this unlocking case, a pair of slope was contacted and slide to unlocking direction when the force was applied to opposite direction, and thus locking phenomenon was not occurred. For this reason, measured force in unlocking direction (7.4 N) was lower than locking direction force case (blue line graph, 133.4 N).
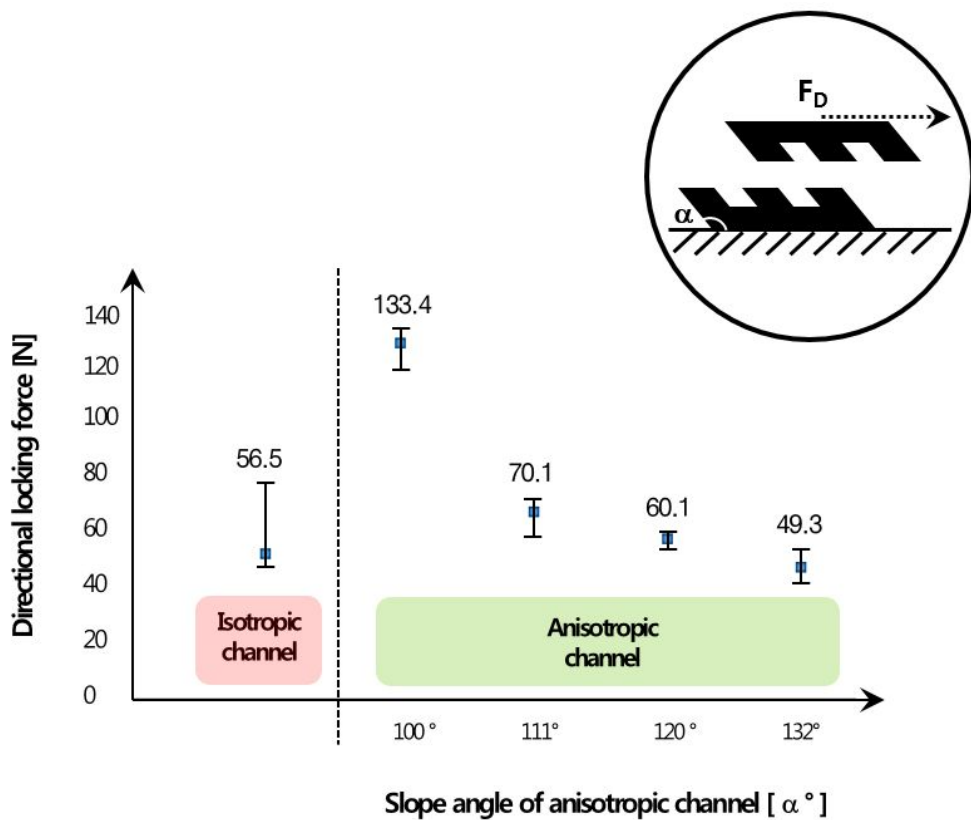
Figure 5.5 Measured directional locking force F_D on horizontal plane ($\beta=0°$)
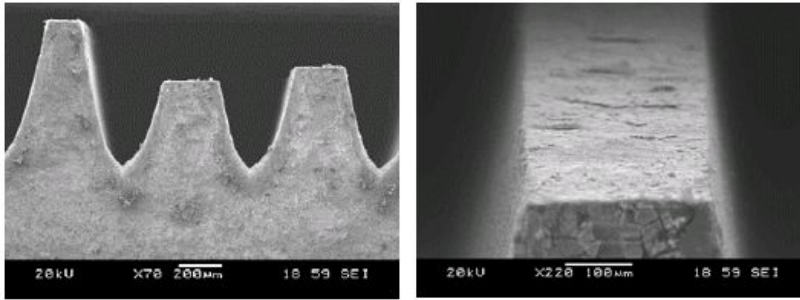
(a) Isotropic micro channel
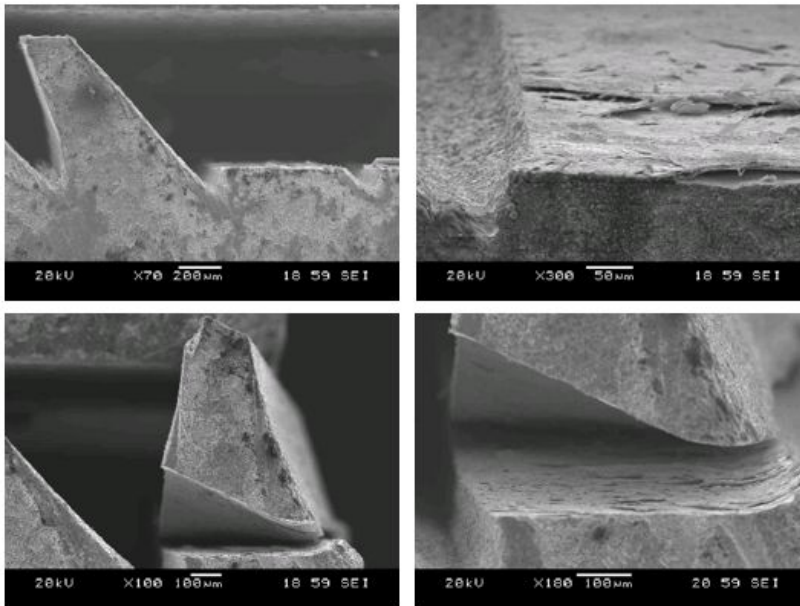
(b) Anisotropic micro channel

Figure 5.6 Fracture tendencies during directional locking force measurement, (a) isotropic, (b) anisotropic micro channel
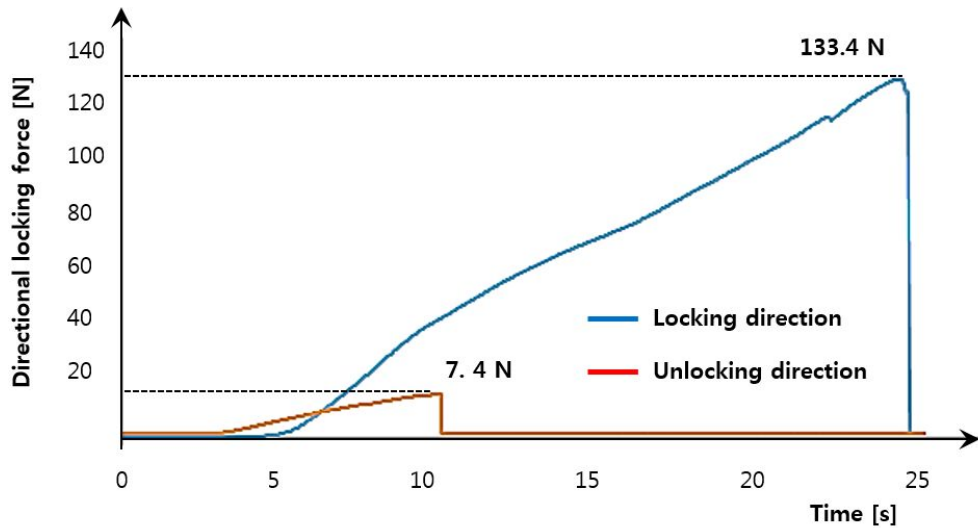
Figure 5.7 Directional locking forces until fracture and derailed in case of opposite directional force application

Directional locking forces F_D of varied slope α angle of channel were measured as changing pulling angle β. As increasing the pulling angle β, directional locking force was divided to normal and shear components. The resulted shear component of F_D was directly related to locking efficiency, however, the normal component was related to detachment of channel. Figure 5.8 shows the resulted directional locking force versus applied pulling angle. The resulted directional locking force F_D until fracture was gradually small as increasing the pulling angle β, because the

resulted normal component of F_D, was related to detachment of channel, was high also. For this reason, though the slope angles α of micro channel were differ, on all occasion($\alpha=100\sim132°$), directional locking forces in horizontal case ($\beta=0°$) was the highest due to the maximum shear component of F_D. As increasing the resulted slope angles α of micro channel, measured directional locking force was small, because locking force was relatively applied on high position of channel.

Figure 5.9 illustrates an example of anisotropic micro channel for vertical anisotropic locking application. As shown in previous results, a pair of anisotropic micro channel can generate maximum 133.4 N directional locking force, and thus it can endure about 13.6 kg of mass. This locking application with micro sized tungsten textured surface can be used to various joint and attachment area, and give a versatile potential to micro mechanical engineering.
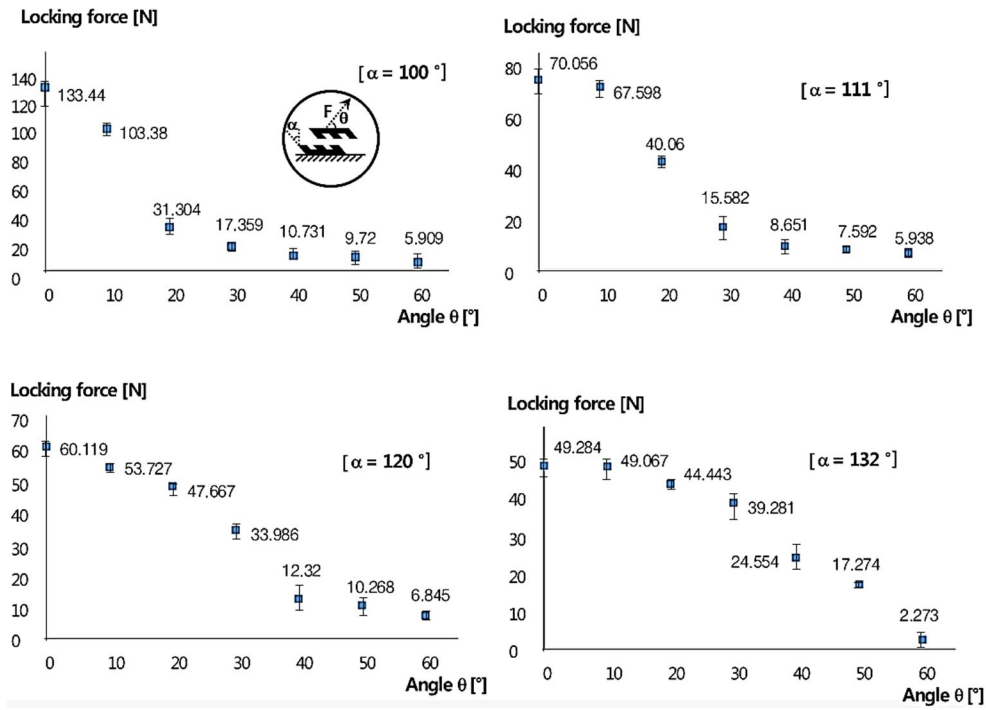
Figure 5.8 Measured directional locking force F_D versus pulling angle β from 0° to 60°, (a) α=100°, (b) 111°, (c) 120°, (d) 132°
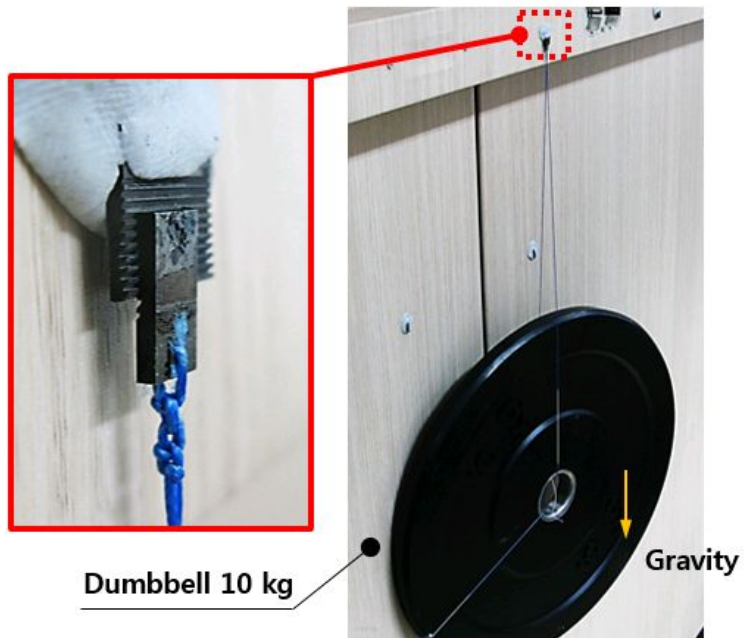
Figure 5.9 Directional locking application example on vertical wall

5.2 Needle

Recently, a tendency, applies micro precision machining to medical area, is on the rise issue. In this area, there is micro needle technology as an application which is delivery drug to transdermal. There are some method to administer drug such as oral dose and injection. In case of direct injection method, effect of drug is faster than oral dose, however, it causes pain for penetration during injection as stimulating pain nerve, and thus it is not proper to apply to a person who has needle phobia. A micro needle technology using micro manufacturing process resolves the problem of previous drug delivery method as using micro sized needle which does not stimulate pain nerve due to its small size. To fabricated micro needle, polymer mold replication method as using mostly photolithography and deep reactive ion etching, sputtering metal ion to near-needle structure were used, however, brittle characteristic of silicon which is used mostly to micro needle can be a problem due to remaining fractured piece of silicon needle into human skin. In case of polymer micro needle, durability under harsh circumstance such as high temperature can be a problem also. Moreover, these MEMS process has a problem to productivity as

long machining time [4].

In this dissertation, micro needle array using laser beam machining and electrochemical etching was fabricated on tungsten surface. Tungsten micro needle can resolve the problems of previous method. In this section, penetration force was measured to verify performance of the fabricated tungsten micro needle, and thus possibility of needle or electrode for medical application was verified.

Measurement system

Figure 5.10 shows the experimental set up for measuring penetration force of textured tungsten micro needle. To measure the penetration force, load cell (BCA 300 gf, CAS korea) was used, and it was set on Z axis micro positioning stage with 0.1 μm/count resolution. The textured micro needle array was set under the load cell. Tilting stage was used to uniform measurement during penetration to meat and gelatin. Tilting stage and meat/gelatin dummy moved by using X, Y micro positioning stage with 0.1 μm/count resolution also. All measuring process was observed by

using high speed video camera (ultima APX−RS, Photron). In this study, two types of example dummy were used. Gelatin and thick pork skin was used as dummy mimicking human skin. The gelatin was treated under 5 wt%, 5 ℃, 1 hour solidify condition.
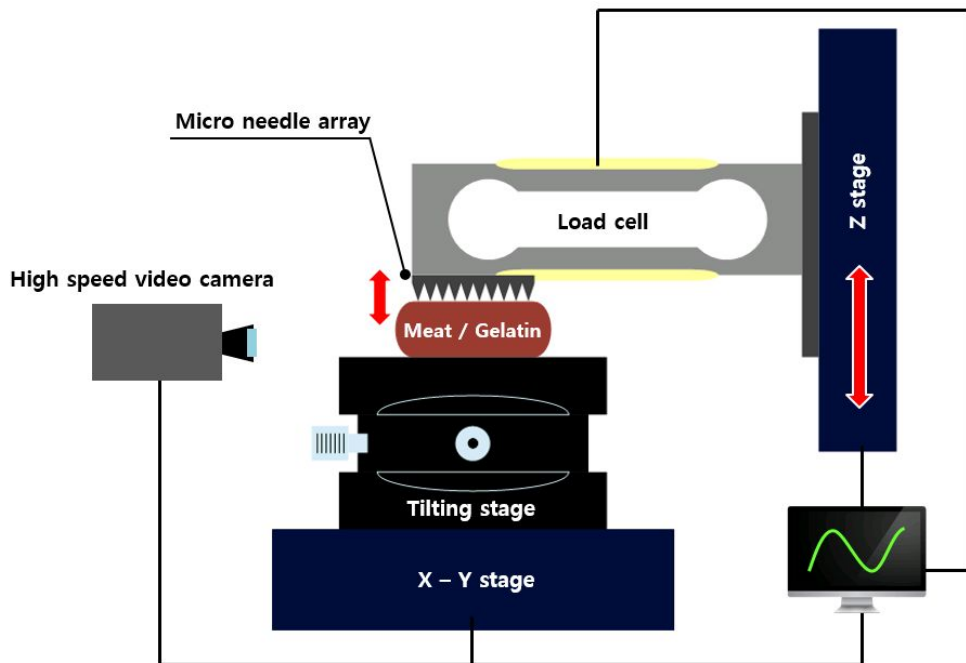
Figure 5.10 Experimental set up for measuring penetration force of tungsten micro needle

Measured penetration force

Figure 5.11 shows the measured penetrating force into gelatin by using textured tungsten micro needle array. In this section, the used micro needle was same to micro pin array in figure 4.27. Penetrated area was same to width (5x5 mm^2) of micro needle array. As going down Z axis with load cell positioning system, penetration force was measure, and all the procedure was observed by using high speed video camera. The gelatin was not penetrated but pressed as its elasticity until 130 μm moving distances, however, as reaching 130 μm (region (a)) immediately, penetration phenomenon was occurred into gelatin. The penetration force at this point was 0.094 N. In region (a), the penetration force increased rapidly due to resistance tendency of gelatin to penetrate. On the other hand, distance region (b) from 130 μm to 330 μm, penetration force decreased with a gradual slope as surficial friction between micro needle and gelatin, however, the resulted penetration force was still higher than resistant friction force. In case of distance

region (c) (over 330 μm), the resulted penetration force gradually converged to about 0.07 N as equilibrium between penetration and resistant friction force. Figure 5.12 illustrates the difference of penetration force between gelatin and thick pork skin cases. Overall penetration force distribution was similar as increasing moving distance, however, the peak penetration force (0.107 N) of pork skin case was higher than gelatin, and the penetration distance (170μm) was also higher as high solidity and elasticity of pork skin and inner dermal.
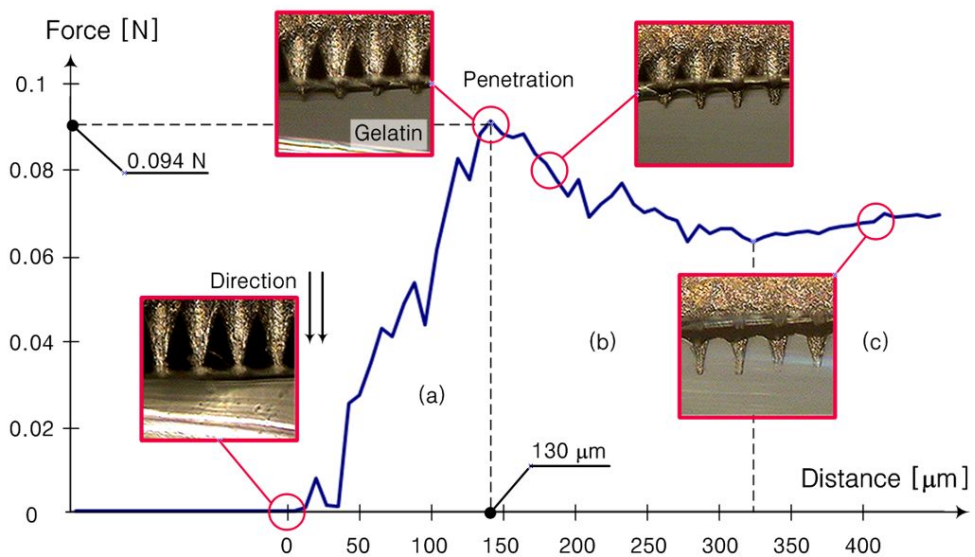
Figure 5.11 Measured penetrating force into gelatin by using textured tungsten micro needle
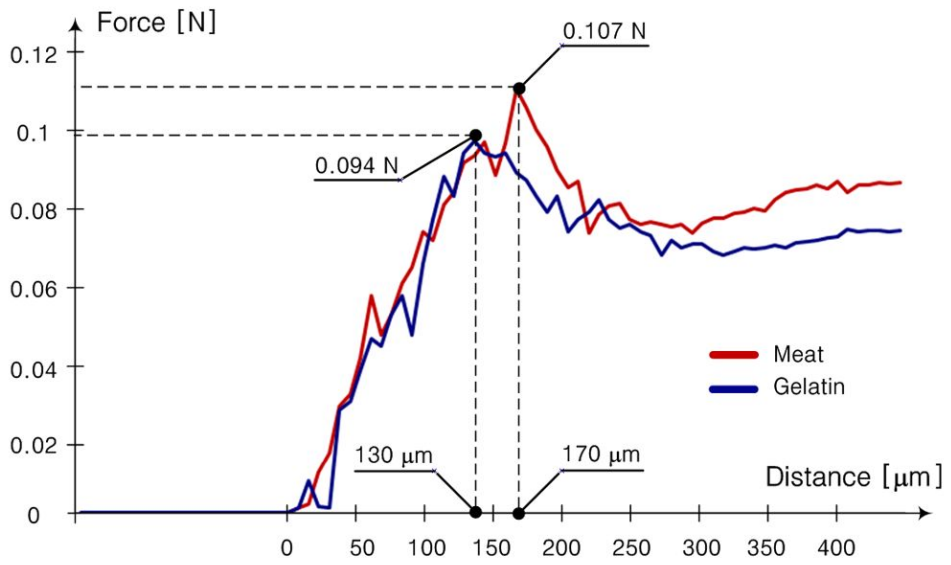
Figure 5.12 Measured penetrating force into gelatin and thick pork skin by using textured tungsten micro needle array

Chapter 6

Conclusion

Tungsten has various advantages such as high thermal melting temperature, mechanical stiffness and density. Though its versatility, tungsten structuring at the micro meter scale has problems such as time consuming, costal limitation and precision machining due to difficult-to-cut and high melting temperature characteristic of tungsten. In this dissertation, a novel method to machine tungsten was demonstrated at the micro meter scale. The suggested hybrid technology that combines laser beam machining and electrochemical etching is capable of fabricating various shapes of tungsten micro channel and micro pin arrays with smooth surface quality and sharp cutting edge. As using laser beam machining process, the original core was defined as pre-determined laser scanning path, and thus various shape of structure was textured on tungsten. In this step, by products such as recast layer, burr and recrystallized region that should be eliminated for precision fabrication were generated. The generated recast layer covered the original textured core during laser beam machining, and thus

152

electrochemical etching was implemented to revealing the original textured core structure. As carrying out electrochemical etching, generated recast layer on original core was eluted into electrolyte, and thus various shape of structure such as vertical, anisotropic micro channel, and rectangular, triangular, hexagonal micro pin array was finally textured.

In structuring micro channel and micro pin by using pre−determined laser scanning path, laser parameters of scanning path tests were carried out, because laser beam follows Gaussian power intensity distribution, and thus combination of laser scanning path with various parameters should be implemented previously. To fabricate vertical or anisotropic micro channel, tilting process and trimming process were carried out, because the tapered groove result was textured by using laser beam due to Gaussian distribution. Electrochemical etching was implemented as eliminating generated recast layer after laser beam machining, and thus various shape of micro channel such as vertical and anisotropic structure were finally textured. Moreover, EDS analysis was carried out to verify the principle of suggested shape control and structuring technology. As implementing atomic percentage mapping analysis between tungsten

and oxygen, existence of the pre-determined pure tungsten core which was covered into tungsten oxide recast layer was verified.

Various shape of micro pin array was fabricated by using hybrid structuring technology. Though the various shape of pre-determined laser scanning path during machining was changed, all the resulted shapes of micro pins were still conical shape, because original shape of pin was covered with tungsten oxide recast layer symmetrically. As carrying out electrochemical etching, original shapes of micro pins such as rectangular, triangular and hexagonal pin were revealed. Textured micro pin was also analyzed by EDS, and thus distribution in micro pin with cross sectional view was observed.

An application of textured micro channel and pin was studied also. In case of micro channel, locking application was verified by using textured anisotropic micro channel. Textured anisotropic tungsten micro channel generated directional locking force about 133.4 N. Moreover, the directional locking force was measured as changing the slope angle of the channel and angle of applying force. In case of micro pin, an application about micro needle in medical area was studied. As using textured micro pin array, the penetration force

154

into gelatin and thick pork skin were measured, and thus the effect of textured tungsten micro pin array in needle application was verified.

Reference

Primary Sources

Secondary Sources

Uncategorized References

1.   Zhao, H., et al., *Pressure drop and friction factor of a rectangular channel with staggered mini pin fins of different shapes.* Experimental Thermal and Fluid Science, 2016. **71**: p. 57-69.

2.   Mei, H., et al., *Multi-level micro-/nanostructures of butterfly wings adapt at low temperature to water repellency.* Soft Matter, 2011. **7**(22): p. 10569-10573.

3.   Pang, C., et al., *Analysis of Preload-Dependent Reversible Mechanical Interlocking Using Beetle-Inspired Wing Locking Device.* Langmuir, 2012. **28**(4): p. 2181-2186.

4.   McAllister, D.V., et al., *Microfabricated needles for transdermal delivery of macromolecules and nanoparticles: Fabrication methods and transport studies.* Proceedings of the National Academy of Sciences, 2003. **100**(24): p. 13755-13760.

5.   Leffler, P.E. and G. Kazantzis, *Chapter 58 - Tungsten A2 - Nordberg, Gunnar F. NordbergBruce A. FowlerMonica*, in *Handbook on the Toxicology of Metals (Fourth Edition)*. 2015, Academic Press: San Diego. p. 1297-1306.

6.   W. H. Yih, C.T.W., *Tungsten: Sources, metallurgy, properties, and applications*. 1979, New York: Plenum.

7.   Merola, M., et al., *Engineering challenges and development of the ITER Blanket System and Divertor.* Fusion Engineering and Design, 2015. **96–**

97: p. 34-41.

8.   Hirai, T., et al., *ITER tungsten divertor design development and qualification program.* Fusion Engineering and Design, 2013. **88**(9–10): p. 1798-1801.

9.   Yang, G., J.A. Gaines, and B.J. Nelson, *A Supervisory Wafer-Level 3D Microassembly System for Hybrid MEMS Fabrication.* Journal of Intelligent and Robotic Systems. **37**(1): p. 43-68.

10.   Zhang, J., et al., *Investigation of Micro Square Structure Fabrication by Applying Textured Cutting Tool in WEDM.* Micromachines, 2015. **6**(10): p. 1427.

11.   Song, K.Y., et al., *Electrical discharge machining using a strip electrode.* Precision Engineering, 2013. **37**(3): p. 738-745.

12.   Shin, H.S., M.S. Park, and C.N. Chu, *Electrochemical etching using laser masking for multilayered structures on stainless steel.* CIRP Annals - Manufacturing Technology, 2010. **59**(1): p. 585-588.

13.   Davim, J.P., *Machining Fundamentals and Recent Advances*. 2008: British Library Cataloguing in Publication Data.

14.   Lee, S.W., H.S. Shin, and C.N. Chu, *Fabrication of micro-pin array with high aspect ratio on stainless steel using nanosecond laser beam machining.* Applied Surface Science, 2013. **264**: p. 653-663.

15.   Dubey, A.K. and V. Yadava, *Laser beam machining—A review.* International Journal of Machine Tools and Manufacture, 2008. **48**(6): p. 609-628.

16.   Muthuraja, A. and S. Senthilvelan, *Abrasive wear performance of tungsten carbide based self-lubricant cutting tool material.* International Journal of Refractory Metals and Hard Materials, 2015. **51**: p. 91-101.

17.   Randall, M., *Powder metallurgy and particulate materials processing : the processes, materials, products, properties and applications*. 2005, German: Princeton, N.J. : Metal Powder Industries Federation.

18.   Li, X., J. Wang, and W. Li. *Current State and Prospect of Micro-Machining*. in *Automation and Logistics, 2007 IEEE International Conference on*. 2007.

19.   Kim, D.H., *Laser Processing*. 2005, Seoul: Kyungmoonsa.

20. William M. Steen, J.M., *Laser Material Processing*. 4 ed. 2010, New York: Springer London Dordrecht Heidelberg.

21. Kawakami, Y. and E. Ozawa, *Tungsten microcone growth by laser irradiation.* Applied Surface Science, 2003. **218**(1–4): p. 176-188.

22. Sano, T., et al., *Femtosecond laser fabrication of microspike-arrays on tungsten surface.* Applied Surface Science, 2005. **247**(1–4): p. 340-346.

23. Madou, J.M., *Fundamentals of microfabrication: the science of miniaturization.* 2 ed. 2002: CRC Press.

24. Schuster, R., et al., *Electrochemical Micromachining.* Science, 2000. **289**(5476): p. 98-101.

25. Kock, M., V. Kirchner, and R. Schuster, *Electrochemical micromachining with ultrashort voltage pulses–a versatile method with lithographical precision.* Electrochimica Acta, 2003. **48**(20–22): p. 3213-3219.

26. A. J. Bard, S.M.P., *Electrochemical Methods: Fundamentals and Applications.* 2 ed. 2001, New York: John Wiley & Sons.

27. Tipton, H., *Principles of electrochemical machining.* Vol. 21. 1976, London: J.A. McGeough Chapman and Hall.

28. W. K. Paik, S.M.P., *Electrochemistry: Science and Technology of Electrode Process.* 2001, Seoul: CheongMoonGak.

29. Lee, W.Y., J.G. Kim, and C.N. Chu, *Micro fabrication of aluminum oxide patterns using local anodization.* International Journal of Precision Engineering and Manufacturing, 2015. **16**(13): p. 2623-2630.

30. Fan, Z.-W., L.-W. Hourng, and C.-Y. Wang, *Fabrication of tungsten microelectrodes using pulsed electrochemical machining.* Precision Engineering, 2010. **34**(3): p. 489-496.

31. Lim, Y.-M. and S.H. Kim, *An electrochemical fabrication method for extremely thin cylindrical micropin.* International Journal of Machine Tools and Manufacture, 2001. **41**(15): p. 2287-2296.

32. Tönshoff, H.K., D. Hesse, and J. Mommsen, *Micromachining Using Excimer Lasers.* CIRP Annals - Manufacturing Technology, 1993. **42**(1): p. 247-251.

33. Zhang, H., et al., *Mechanism of Recast Removal During Laser Drilling Underwater.* Advanced Science Letters, 2011. **4**(6-7): p. 2071-2075.

34.   Dobrev, T., D.T. Pham, and S.S. Dimov, *Techniques for improving surface quality after laser milling.* Proceedings of the Institution of Mechanical Engineers, Part B: Journal of Engineering Manufacture, 2008. **222**(1): p. 55-65.

35.   Kleine, K.F. and K.G. Watkins. *Pulse shaping for microcutting applications of metals with fiber lasers.* 2004.

36.   A. Yariv, P.Y., *Photonics : optical electronics in modern communication.* 6 ed. 2007, New York: Oxford University Press.

37.   Polini, R., et al., *Effect of substrate grain size and surface treatments on the cutting properties of diamond coated Co-cemented tungsten carbide tools.* Diamond and Related Materials, 2002. **11**(3–6): p. 726-730.

38.   Sun, C.C., S.Y. Tsai, and T.X. Lee, *Enhancement of Angular Flux Utilization Based on Implanted Micro Pyramid Array and Lens Encapsulation in GaN LEDs.* Journal of Display Technology, 2011. **7**(5): p. 289-294.

39.   Wang, L.-F., et al., *A MEMS-based pyramid micro-needle electrode for long-term EEG measurement.* Microsystem Technologies, 2012. **19**(2): p. 269-276.

40.   Cai, J. and L. Qi, *Recent advances in antireflective surfaces based on nanostructure arrays.* Materials Horizons, 2015. **2**(1): p. 37-53.

41.   Li, K., et al., *Structured cone arrays for continuous and effective collection of micron-sized oil droplets from water.* Nat Commun, 2013. **4**.

42.   Xie, J., Y.W. Zhuo, and T.W. Tan, *Experimental study on fabrication and evaluation of micro pyramid-structured silicon surface using a V-tip of diamond grinding wheel.* Precision Engineering, 2011. **35**(1): p. 173-182.

43.   In, C.H.K., Gyu Man; Chu, Chong Nam, *Fabrication of Tungsten Prove using Electro-Chemical Etching.* Journal of the Korean Society of Precision Engineering, 2001. **18**(2): p. 8.

44.   Kim, J.K., et al., *Intergranular corrosion of Ti-stabilized 11 wt% Cr ferritic stainless steel for automotive exhaust systems.* Corrosion Science, 2009. **51**(11): p. 2716-2723.

45.   Ezugwu, E.O., *Key improvements in the machining of difficult-to-cut aerospace superalloys.* International Journal of Machine Tools and Manufacture, 2005. **45**(12–13): p. 1353-1367.

46. Niinomi, M., *Mechanical properties of biomedical titanium alloys.* Materials Science and Engineering: A, 1998. **243**(1–2): p. 231-236.

47. COLE, N., R. GILLILAND, and G. SLAUGHTER, *WELDABILITY OF TUNGSTEN AND ITS ALLOYS.* 1971: Defense Technical Information Center.

48. Liu, X., et al., *Tungsten joining with copper alloy and its high heat load performance.* Journal of Nuclear Materials, 2014. **455**(1): p. 382-386.

49. Kazakov, N.F., *Diffusion bonding of materials.* 2013: Elsevier.

국문초록

본 논문에서는 레이저 가공 및 전해에칭을 수행한 복합 가공법을 이용하여 텅스텐에 다양한 기능을 갖는 표면 텍스쳐링에 대한 연구를 진행하였다. 본 연구에서 소개된 복합 텍스쳐링 공정은 다양한 응용분야가 존재하는 텅스텐을 손쉽게 가공할 수 있으며, 빠른 가공 시간으로 인한 높은 생산성, 고품질의 형상정밀도, 저비용 공정을 이룩함으로써, 기존 텅스텐 가공법들이 가지고 있던 문제점들을 해결하였다. 먼저, 레이저 가공을 이용하여 다양한 레이저 스캐닝 패스로 텅스텐 마이크로 패터닝을 함으로써 빠른 시간에 형상 조절을 하였다. 이 과정에서 발생한 재응고층은 가공하고자 하는 기존 형상 표면에 붙어 형성되기 때문에, 마이크로 패턴의 형상 정밀도를 떨어지게 한다. 따라서 고품질의 표면을 얻을 수 있는 전해에칭을 수행함으로써 형성된 재응고층을 NaOH 용액에 녹여내고, 원하는 마이크로 패턴 형상을 얻을 수 있었다.

본 연구에서는 개발된 텍스쳐링 공정을 이용하여 마이크로 채널 및 핀 형상의 가공 지침을 보인다. 레이저 가공 시, 다양한 레이저 스캐닝 패스를 조합함으로써 형성되는 마이크로 구조물의 양상을 분석함으로써, 가공 파라미터 연구를 수행하였다. 또한, 수직형상 및 비등방성 마이크로 채널을 텍스쳐링 하기위한 레이저 가공 방향 및 과정에 대해 고찰함으로써 기울기 90도 이상의 채널 가공 지침을 제시하였다. 전해 에칭 시, 에칭 시간을 조절함으로써 형성된 구조물의 표면 분석을 진행하였고, 재응고층을 효과적으로 제거 하기 위한 조건을 모색하였다. 또한, EDS 분석을 수행함으로써, 본 연구에서 소개된 복합 텍스쳐링 공정의 원리를 규명하였다.

텅스텐 표면에 텍스쳐링 된 마이크로 채널을 응용하여 기계적 결합(로킹)력을 측정하였다. 또한, 마이크로 핀 형상을 약물전달용 니들로 이용함으로써, 본 복합 가공기술로 텍스쳐링된 텅스텐 표면의 다양한 응용분야를 제시하였다.

주요어: 텅스텐, 정밀 가공, 레이저 빔 가공, 전해 에칭, 로킹, 니들, 표면 텍스쳐링

학번: 2010-23214